UC Riverside

UC Riverside Electronic Theses and Dissertations

Title

The Development and Application of Semi-Empirical Dispersion Models: Impact of Roadside Structures, Identifying Emission Sources, and Producing Concentration Maps at Different Temporal and Spatial Scales

Permalink

https://escholarship.org/uc/item/341700gm

Author

Enayati Ahangar, Faraz

Publication Date

2018

Copyright Information

This work is made available under the terms of a Creative Commons Attribution License, availalbe at https://creativecommons.org/licenses/by/4.0/

Peer reviewed|Thesis/dissertation

eScholarship.org Powered by the California Digital Library
University of California

UNIVERSITY OF CALIFORNIA
RIVERSIDE

The Development and Application of Semi-Empirical Dispersion Models: Impact of Roadside Structures, Identifying Emission Sources, and Constructing Concentration Maps at Different Temporal and Spatial Scales

A Dissertation submitted in partial satisfaction
of the requirements for the degree of

Doctor of Philosophy

in

Mechanical Engineering

by

Faraz Enayati Ahangar

December 2018

Dissertation Committee:
Dr. Akula Venkatram, Chairperson
Dr. Marko Princevac
Dr. Heejung Jung

Copyright by
Faraz Enayati Ahangar
2018

The Dissertation of Faraz Enayati Ahangar is approved:

_____

_____

_____

Committee Chairperson

University of California, Riverside

ACKNOWLEDGEMENTS

None of my accomplishments would be possible without the support and assistance of numerous individuals. First, I am grateful for the mentoring of my advisor, Dr. Akula Venkatram, without whose guidance and help, this dissertation would not have been possible. His vast knowledge of the field of air quality modeling and mechanical engineering has helped me at every step in my research career and education.

I thank my committee members, Dr. Marko Princevac and Dr. Heejung Jung, who not only taught me the fundamentals of turbulence, air quality measurement techniques and instrumentation, but also challenged me to improve my work.

I would like to express my utmost gratitude to my colleague and friend Dr. Seyedmorteza Amini. We spent numerous hours working together during field measurements, meetings, and conferences. I want to thank Dr. Nico Schulte, who helped me through my research and taught me data analysis and modeling techniques. I would like to extend my thanks to Dr. Si Tan who always answered my questions regarding the fundamentals of dispersion modeling.

Many thanks to Dr. David Heist and Dr. Steven Perry from the U.S. EPA for sharing valuable research data from wind tunnel measurement.

The research in chapter 3 and 4, supported by the California Air Resources Board under contract number 13-306. I was also supported by the National Center for Sustainable Transportation during my research.

I thank the CARB's Research Division staff, including Dr. Abhilash Vijayan, Mr. Steve Mara, and Dr. Toshihiro Kuwayama, for their support during the course of the project. I

also thank the UCLA professors Dr. Suzanne Paulson, Dr. Yifan Zhu, and our colleagues Dr. Eon S. Lee, and Dr. Dilhara Ranasinghe for their collaboration at every step of the project.

The text in chapter 2 of this dissertation is in part a reprint as it appears in Ahangar, F. E., Heist, D., Perry, S., & Venkatram, A. (2017). Reduction of air pollution levels downwind of a road with an upwind noise barrier. Atmospheric Environment, 155, 1-10.

The text in chapter 3 of this dissertation is in part a reprint as it appears in Amini, S., Ahangar, F. E., Schulte, N., & Venkatram, A. (2016). Using models to interpret the impact of roadside barriers on near-road air quality. *Atmospheric Environment*, *138*, 55-64 and in Paulson, S.E., Zhu, Y., Venkatram, A., Lee, E.S., Ranasinghe, D.R., Enayati Ahangar, F., Amini, S., Frausto-Vicencio, I., Choi, W., Sum, W., 2017. Effectiveness of sound wall-vegetation combination barriers as near-roadway pollutant mitigation strategies.

Chapter 4 of this dissertation is in part a reprint as it appears in Ahangar, F. E., Amini, S., & Venkatram, A. (2017, June). Using Vegetation to Enhance the Impact of Solid Barriers on Near-road Air Pollution. In A&WMA's 110th Annu. Conf. Exhib.

The research in chapter 5 was supported by funding provided by NASA Earth Sciences Division Applied Sciences Program. I would like to thank Dr. Frank Freedman, San Jose State University for his help in carrying out this research.

I would also like to thank Dr. Vahid Hosseini, my undergraduate advisor at the Sharif University of Technology. He introduced me to the research on air pollution and for that, I will be forever grateful.

ABSTRACT OF THE DISSERTATION

The Development and Application of Semi-Empirical Dispersion Models: Impact of Roadside Structures, Identifying Emission Sources, and Constructing Concentration Maps at Different Temporal and Spatial Scales

by

Faraz Enayati Ahangar

Doctor of Philosophy, Graduate Program in Mechanical Engineering
University of California, Riverside, December 2018
Dr. Akula Venkatram

Dispersion models play an essential role in understanding the impact of pollutant emissions on air quality. Once their results have been evaluated with observations, they are used by regulatory agencies and planning bodies to permit new sources and develop policies to mitigate the impact of emissions on air quality. In my research, I developed and applied a class of dispersion models referred to as semi-empirical models whose formulation depends on representing some of the governing processes with parameters whose values are obtained by fitting model estimates to corresponding observations.

In recent years, roadway design is suggested as a potential strategy to mitigate the impact of vehicular emissions on near-road air quality. In my research, I developed a dispersion model to estimate the impact of a solid noise barrier upwind of a highway on

concentrations downwind of the road. The results showed that an upwind barrier reduces the downwind concentration by enhancing turbulence and shifting the emissions upwind through the action of the recirculating zone formed behind the upwind barrier. I also propose a tentative model to estimate on-road concentrations within the recirculation zone..

The applicability of the downwind barrier dispersion models to real-world measurements was also explored in my research. First, a field study was conducted to measure ultra-fine particles (UFP) concentration and micrometeorology data near a roadside barrier in Riverside, California. Two models for downwind barriers were evaluated with data collected and emission factors were estimated for the fleet. The primary effect of a downwind barrier was equivalent to shifting the line sources on the road upwind by a distance of about $HU(H/2)/u_*$.

Next, UFP concentrations were measured downwind of a solid barrier and a solid barrier with vegetation simultaneously to estimate the incremental effect of tall vegetation on the mitigation caused by a solid barrier. The vegetation above the solid barrier reduced turbulence levels of the air passing through it and added to the concentration reduction induced by the solid barrier most of the time; however, this was not the case for all of the observed data.

I then apply dispersion models at regional scales by interpreting $PM_{2.5}$ concentrations measured by a network of 40 low-cost monitors located in the Imperial Valley of southern California. This valley is bordered by deserts on the east and the west, the Salton Sea on the North, and Mexico to the South. Particulate matter can be transport into the valley from across these borders, and be generated from within the valley itself

because of agricultural activity. These borders are represented by line sources and the valley by an area source. I estimate the emissions from these sources by fitting model estimates to daily and annually averaged measurements made at 40 monitors. Once these emissions are determined, I use them as inputs in the dispersion model to construct $PM_{2.5}$ maps at a much finer resolution than that provided by the monitors.

Table of Contents

List of Figures

List of Tables

1. Motivation, Objective, and Approach

1.1 Problem statement

Several studies show that living in the vicinity of major roads and traffic-related air pollution can lead to adverse health outcomes that include increased mortality, lung cancer, asthma, birth and development defects, lower life expectancy, lung function growth defects in children, and increased hospital admissions (Beelen et al., 2007; HEI, 2010; Hoek et al., 2002; James Gauderman et al., 2000; Khreis et al., 2017; Pope III, 2002; Pope III and Dockery, 2006). These health effects are correlated with exposure to elevated air pollutant concentrations of motor-vehicle emissions of carbon monoxide (CO); nitrogen oxides (NOx); fine particles, black carbon (BC), polycyclic aromatic hydrocarbons (PAHs), and benzene (Hitchins et al., 2000; Kim et al., 2002; Kittelson et al., 2004). In particular, short term or long term exposure to particulate matter (PM), have been found to be correlated strongly with cardiopulmonary mortality and asthma (Anderson et al., 2012; Brauer et al., 2002; Dockery et al., 1993; Gehring et al., 2010). Particulate matter is defined as any solid or liquid droplets released to the ambient atmosphere and can be further categorized based

on particle diameter into coarse ($PM_{10-2.5}$), fine ($PM_{2.5}$), and ultrafine particles or UFPs ($PM_{0.1}$) where the subscript refers to the aerodynamic diameter in μm.

The issue of air quality is also a matter of environmental justice since most of the people who primarily live or work near high traffic roads or polluted areas often have low incomes, and are therefore less able to control their living and working conditions, move away from the polluted areas, and are more at risk of the negative health outcomes associated with exposure to vehicle emissions (Houston et al., 2008; Mitchell and Dorling, 2003). On road air quality is also a matter of concern to people who spend long periods of time commuting (Li et al., 2006).

With the growing population in urban areas, it is crucial to develop air pollution control policies that mitigate the impact of vehicular emissions. An effective air quality management policy includes a thorough assessment of the processes that govern existing air quality and quantity. This includes identifying pollution sources, characterizing their emission rates in terms of strength and variability, estimating the effects of geographical and atmospheric conditions on the dispersion of pollutants at different locations, and an analysis of the effect of the pollutants on the environment. Dispersion models are critical tools used by city planners, policymakers, and researchers for this assessment. Dispersion models are mathematical descriptions of the processes that relate ambient concentration levels to the emission rate of the corresponding pollutants. These models allow us to compute the spatial and temporal distributions of pollutant concentrations given the

emission distribution. They can also be used to estimate emissions associated with measured concentration distributions.

My research mainly involves developing and modifying a class of dispersion models referred to as semi-empirical models. A semi-empirical model has a mechanistic framework that incorporates some of the governing processes in terms of parameters. The framework is designed to facilitate the determination of the values of these parameters by fitting model estimates to corresponding observations; the 'empiricism' of the model is related to this step in formulating the model. The most commonly used models, especially regulatory models, belong to this class. Examples are:

- AERMOD: a dispersion model that uses current understanding of the atmospheric boundary layer to estimate dispersion of releases from for point, area, and volume sources (Cimorelli et al., 2005); AERMOD does not include line sources directly but uses a string of volume sources or elongated area sources to describe line sources such as highways (US EPA, 2004).
- CALINE4 and CAL3QHC/ CAL3QHCR: these models represent a highway as a set of rectangles each of which is modeled as a finite line source perpendicular to the wind. estimates air quality levels using a Gaussian dispersion model (Benson, 1992; Chen et al., 2009).

- CTDMPLUS: a model which simulates the flow and dispersion of pollutants for a point source over a complex-terrain by applying flow-distortion corrections caused by structures (Perry, 1992).
- R-LINE: represents a highway with a set of finite line sources, along lanes, whose contributions are computed through numerical integration. Dispersion is modeled using plume spread formulations based on micrometeorological variables. The current version of the model is designed for flat roadways with no obstacle around them (Heist et al., 2013; M. G. Snyder et al., 2013).

These models, along with other regulatory or non-regulatory models, have been used by city planners, policymakers, and researchers to find alternative ways of improving air quality.

In recent years, roadway configuration has been suggested as an important mitigation strategy (Gallagher et al., 2015). Urban roadways come in a variety of configurations: elevated highways, depressed highways, highways with roadside barriers, and roads in the midst of tall buildings. These configurations have major effects on the dispersion of vehicle emissions and hence on air quality of the surrounding areas. However, most of the current semi-empirical models, including the models mentioned earlier, do not include the effect of roadside structures on the dispersion of pollutants.

Another application of air quality dispersion models is to provide an accurate spatial and temporal overview of air pollution levels and find the concentration patterns over populous regions. In recent years, low-cost sensors networks have been suggested to

provide a more accurate map of concentration in regions of interest and identify pollution hotspots (Kumar et al., 2015). These networks have usually higher density than conventional air quality monitoring systems and can provide real-time concentration data for a large region of interest (English et al., 2017). The data from these sensors combined with dispersion models can result in small-scale air quality maps. It can also provide information about the location and strength of pollution sources.

In this thesis, I mainly focus on modifying and developing dispersion models to include the effect of different roadside structures at different meteorological conditions. I also examine the applicability of semi-empirical dispersion models for identifying and quantifying emission sources while providing finer resolution concentration maps in different regions of interest.

1.2 Background

1.2.1 Roadside structure effect on the dispersion of pollutants

The mobile fleet is the primary means of transportation in the US because of its flexibility, adaptability, and low cost compared to other transportation systems. Sustainable transportation requires the reduction of the negative effects of traffic-produced pollution and improving the air quality in urban areas. The benefits of efficient transportation have to be examined in light of the health impacts associated with pollutant emissions from vehicles traveling on urban road; city planners and developers find a growing concern in

near-road air quality since exposure to common vehicle emissions has been linked to numerous health problems (Samet et al., 2000; World Health Organization, 2006).

The most common practice in traffic-related air pollution control is tailpipe emission reduction. This includes before-source emission reduction, like improving efficiency or modifying the fuels, as well as developing after-source emission control systems, like gaseous absorption systems or particulate filters (Alley et al., 1998). Another approach is applying traffic management policies which can also reduce fuel consumption and improve the air quality in urban areas (Huan and Kebin, 2012; Monzón de Cáceres, 1994).

With increasing population in urban areas, a need for alternative air pollution mitigation strategies is imminent. In recent years, roadway design and structures are being considered as one potential solution for mitigating the exposure to near road population (Baldauf et al., 2008; Steffens et al., 2014). Many of the structures that affect dispersion process near roadways are already in place for other purposes. Sound walls are usually placed next to the highways to reduce sound pollution, trees and vegetation are usually planted to beautify the landscape, and overpass or underpass roads are used to enhance transportation. Characterizing the effect of these structures on air quality is an important aspect of city planning. In this work, I focus on quantifying the effect of roadside solid and vegetative barriers.

Studies have found that roadside barriers can improve air quality in near-road locations. Roadside barriers include near road solid or vegetative structures (i.e. sound walls, trees, brushes) that are located at either side of the road.

A solid barrier at the downwind side of the road will push `the airflow and pollutants upward above the barrier. The barrier also acts as a source of turbulence and increases initial vertical mixing and dispersion. This effect will last for several barrier heights downwind of the barrier and result in reducing concentration levels (Pournazeri and Princevac, 2015).

Most of the field studies have shown that with the exception of a few meteorological conditions, solid barriers will reduce downstream pollution levels for different gaseous and particle pollutants (Richard Baldauf et al., 2008; Baldauf et al., 2016; Bowker et al., 2007; Hagler et al., 2012; Hooghwerff et al., 2010; Lee et al., 2018).

One of the comprehensive controlled field studies was conducted at Idaho National Laboratory to investigate the impact of a solid barrier under varying atmospheric conditions (Finn et al., 2010). The barrier, constructed with hay bales, was 90 m long and 6 m high placed next to a 54 m long line source releasing SF_6. Measurements were also made simultaneously next to another line source, identical to the other line source, with no barrier next to it. The study showed that the solid barrier reduced downwind concentrations relative to the no-barrier values over a wide range of atmospheric stabilities. The study also showed that solid barriers might trap the pollutants on the road and increase the on-road concentration in very stable and low wind cases.

Wind tunnel studies confirm the results from the field studies. A comprehensive wind tunnel study has been conducted by (Heist et al., 2009) to find the effects of different road configurations at the U.S. EPA's meteorological wind tunnel (Snyder, 1979). The concentration gradients were measured next to a six-lane 1:150 scale highway with 12 different roadway design. These configurations included upwind or downwind barriers with flat, depressed, or elevated highways. All of the configurations examined in the study resulted in lower ground level concentration compared to a flat, unobstructed roadway. In single barrier cases, a recirculation zone was observed behind the barrier with near-surface winds blowing in opposite direction towards the wall.

A variety of models have been used to describe the effect of downwind solid barriers. Hagler et al. (2011) and Steffens et al. (2014) used computational fluid dynamics (CFD) models to produce adequate descriptions of the data from the wind tunnel (Heist et al., 2009). These simulations were applied to different configurations including flat, depressed, and elevated roads in presence of barrier at different locations around the roadway. Bowker et al. (2007) used the Quick Urban & Industrial Complex (QUIC) flow model coupled with a Lagrangian particle dispersion model to produce concentration patterns that were roughly consistent with observations from Baldauf et al. (2008).

Schulte et al., 2014 developed two semi-empirical models to explain the effect of downwind solid barriers:

1- The mixed-wake model which considers an exponential concentration profile above the barrier height and a constant concentration below the barrier. This concentration distribution is consistent with wind tunnel observations. (Figure 1-1).

2- The source-shift model assumes that vertical plume spread at barrier location is proportional to barrier height. Similar concepts were explored by Heist et al., (2009) by considering a virtual source.

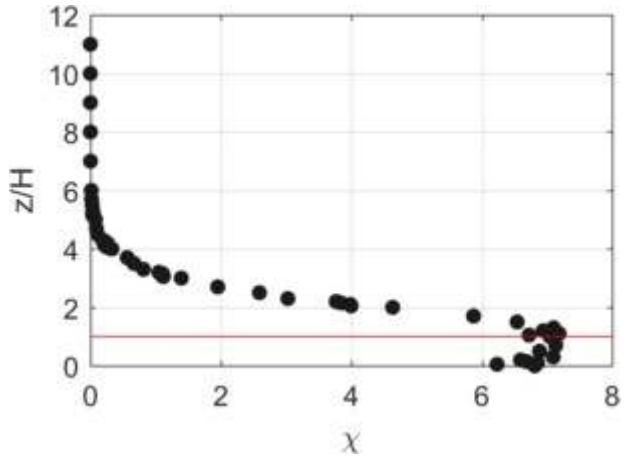

Figure 1-1- Normalized concentration (χ) profile to barrier height behind the downwind barrier case in the wind tunnel study (Heist et al., 2009). Red line represents the Barrier Height (H).

Amini et al., (2018) were able to explain the depressed roadway effect on dispersion by modifying the initial vertical plume spread and increasing the friction velocity due to the increased turbulence compared to flat terrain roadways.

Vegetative barriers also have been suggested as a potential method to decrease air pollution near roadways. However, the effects of these barriers on downwind air quality are uncertain. Despite numerous real-world measurements that have been devoted to

examining the effect of vegetative barriers on air quality near roadways, conclusions on their effects are not definitive. A field study was done in Finland by deploying passive and active samplers by Setala et al., (2013) under tree-canopies in tree-covered park areas and adjacent treeless areas in the vicinity of twenty sites in Helsinki and Lahti. Passive samplers showed insignificant decreases of NO_2, 19% reduction of VOC, and 35 – 40% reduction of the mass deposited. However, active samplers showed a 20% reduction of fine particles (20 – 1000 nm), and no difference for $PM_{2.5}$ and PM_{10} particles.

Several modeling and wind-tunnel studies have been carried out to describe the effects of vegetative barriers on urban air pollution. Steffens et al., (2012) incorporated particle aerodynamics and deposition mechanisms into the Comprehensive Turbulent Aerosol Dynamics and Gas Chemistry (CTAG) model to examine the effects of vegetative barriers on roadway-emitted pollutants. They modeled the results of the field experiment conducted in Chapel Hill, NC (Hagler et al., 2012). They assumed that vegetative barriers affect near-road air quality in the following ways: 1) particles are deposited on leaf surfaces, 2) downwind wind speed and turbulence levels in the flow passing through the barrier are decreased, and 3) a fraction of the flow carrying pollutants is forced to go over the barrier. The first and third effects mitigate air pollution, while the second effect leads to higher concentrations. Another Computation Fluid Dynamics model developed by (Vos et al., 2013) found that concentrations within street canyons are higher when trees are present. They found that the effect of vegetation in decreasing TKE and increasing local concentrations within street canyons. While denser vegetation can improve the air quality

by acting like a solid barrier, vegetation as a turbulence sink can result in higher near road concentration for certain porosities (Amini, 2018; Ghasemian et al., 2017).

So far, only a handful of field studies have been performed which explicitly investigate the effects of a combination of vegetation and a solid barrier on the air quality near roadways. Baldauf et al. (2008) conducted a comprehensive field study in Raleigh, NC where a stretch of a clearing, a solid barrier, and a vegetation-solid barrier combination was present. The results indicated that concentrations measured next to solid-vegetation barrier mitigated downwind concentrations more than the other two barriers. A CFD model based on Large Eddy Simulation (LES) examined the effects of common vegetative barrier configurations near roadways to find the most effective configuration (Tong et al., 2016). The results indicated that a wide vegetation barrier with high Leaf Area Density (LAD), and also a combination of vegetation and solid barrier work best as mitigation strategies.

The current semi-empirical models include only a handful of configurations. In chapter 2, I have developed a model to estimate the effect of upwind noise barriers. Moreover, these models have been tested only through wind tunnel experiments or controlled studies. In chapter 3, I explore the applicability of semi-empirical models for a real-world case study for solid noise barriers. In chapter 4, The models were extended to include the effect of vegetation behind a solid wall.

1.2.2 Using low-cost sensors for air quality an emission estimation

Air quality management policies are usually based on the analysis of long-term pollution data. Regulatory monitors are often used for this purpose because of their accurate and dependable observations. United States Environmental Protection Agency (EPA) uses a network of air pollution monitors operating federal reference methods (FRMs) or federal equivalent methods (FEM). The density of air pollution regulatory monitors is usually low because of their cost and they can only provide low spatial and temporal resolution. However, air quality can change rapidly over small scales because of the effects of local source and meteorology. The low resolution of data provided by regulatory sensors makes it difficult to use them for community-scale assessment and research. Low-cost environmental sensors networks can help us overcome this challenge (Kumar et al., 2015). These sensors can provide additional air pollution data to create finer resolution air quality maps. They also measure timely information about toxic gases and detect the local air pollution levels which can be used to detect hot spots (Jiao et al., 2016; Yi et al., 2015). The data collected by these sensors have become more reliable and accessible in recent years (Hagler et al., 2014; Wang et al., 2015) and can also provide initial data for planners to detect the communities most impacted by air pollution (CARB, 2018a; SCAQMD, 2018).

However, the use of low-cost sensor networks has some limitations. The sensors usually cannot be installed at every location of interest and they need constant servicing since they fail more frequently than regulatory monitors. To estimate concentration when

these data gaps happen, we can interpolate the observations at several monitoring sites. Geostatistical interpolation techniques like Kriging are commonly used to interpolate observations made at irregularly spaced location (Matheron, 1971). The results from interpolation models can be improved by using dispersion models to account for the local and potential pollution sources (Pournazeri et al., 2014; a Venkatram, 1988).

1.3 Objectives and approach

The objectives of my research program are to:

1- Understand the effects of road configurations and urban vegetation on the air quality impact of vehicle-related emissions through dispersion models that describe data from field studies and wind tunnel data.

2- Use dispersion models to interpret data from low-cost sensors by 1) identifying and quantifying pollution sources and 2) creating high-resolution concentration maps and.

The dispersion models that were investigated in this research are semi-empirical. These models estimate the dispersion process by using simple equations based on the main governing physical process. Then they add empirical parameters based the observations made in laboratory or field studies to fit these equations to measurements.

The approach that I took in my research is as follows:

1- The effect of upwind barriers on near-road air quality
    a- The data for upwind barrier effect on dispersion of pollutants were analyzed from a wind tunnel measurement conducted by (Heist et al., 2009)
    b- A model was developed based on the observation and previously developed dispersion models to explain the data.
    c- The sensitivity of the model was examined against different barrier heights and highway widths.
2- The effect of downwind barrier on near-road air quality
    a- A field study was conducted to examine the effect of downwind barrier in the near-road air quality next to a busy highway under different meteorological conditions.
    b- Two semi-empirical models were developed based on N. Schulte et al., (2014) models to explain the data collected during the field study.
    c- Emission factors were calculated for the fleet.
    d- A sensitivity study was conducted to find the effect of different barrier height on the dispersion process.
3- Using vegetation to enhance the impact of a solid barrier on near-road air pollution
    a- A field study was conducted to examine the effect of solid barrier and vegetation combination on near-road air quality.

b- The data collected for this field study was analyzed to examine the effect of added vegetation.

c- Previously developed modeled were modified to explain the vegetation effect based on the observation.

4- Using low-cost air quality sensor networks to estimate emissions and pollution concentration.

a- The data from low-cost sensor network was analyzed.

b- A multivariable regression approach was applied to find the emission rates for possible sources.

c- The predictions were combined with observations to produce accurate spatial and temporal maps of concentration field through kriging.

1.4 Structure of the dissertation

Chapter 2 explains the development of the model based on the estimates from wind tunnel study. Chapter 3 describes the field study conducted in Riverside, CA and the development of a model to find the effect of downwind wind barrier. Chapter 4 investigates the effect of added vegetation to a solid barrier on the dispersion of air pollutant. Chapter 5 analyzes the data from a low-cost sensor network and uses a method to find the emission rates and create fine resolution concentration maps based on observation and prediction.

2 The Effect of Upwind Barriers on Near-Road Air Quality

2.1 Introduction

Several field and laboratory studies have indicated that noise barriers next to roads reduce the near-road concentration of pollutants emitted by vehicles. Because these barriers are designed to reduce the impact of road noise on adjacent residential areas, they can be located on both sides of the road or only on one side. In this chapter, we refer to a barrier as "upwind" if the road is downwind of the barrier when the wind blows across the road. It is referred to as "downwind" otherwise.

A field study near interstate I-440, Raleigh, North Carolina, showed that the presence of a downwind noise barrier can reduce concentrations of CO and PM number by up to 50% downwind of the barrier (Richard Baldauf et al., 2008). A study at the Idaho National Laboratory that released a tracer gas, sulfur hexafluoride, from a line source upwind of a barrier showed similar reductions in tracer concentrations downwind of the barrier under all meteorological conditions (Finn et al., 2010). A wind tunnel study

examined the effect of different configurations including downwind solid barriers, upwind barriers, depressed highways, and elevated highways on near-road pollutant concentrations and found that all of these configurations result in reductions of near-road concentrations compared to those for a flat roadway with no barriers except for an elevated highway where the source is elevated on a sloped embankment (Heist et al., 2009).

These results from field and laboratory studies are supported by simulations using a Computational fluid dynamics (CFD) model, which shows that downwind roadside barriers result in reduced concentrations behind the barrier (Hagler et al., 2011). (Steffens et al., 2014) developed a CFD model based on Large-Eddy Simulation and found that roadside barriers, elevated highways, depressed highways, and combinations of these configurations reduced near-road concentrations. Schulte et al. (2014) developed a semi-empirical model to estimate concentrations in the presence of a downwind barrier and evaluated it with data from the Idaho Falls experiment (Finn et al., 2010) and wind tunnel data (Heist et al., 2009). However, none of these modeling studies examined the impact of single barriers upwind of the road or barriers on both sides of the road.

In this chapter, we propose a semi-empirical model to estimate the effects of upwind barriers on near-road pollutant concentrations. The impact of barriers on both sides of the highway is modeled using the upwind barrier model in combination with the mixed-wake model formulated to estimate the effect of a downwind barrier (Schulte et al., 2014). The models are evaluated using the data collected by Heist et al. (2009) in a wind tunnel

study. These semi-empirical models are useful because they capture the fundamental physics governing the effects of solid barriers on the dispersion of pollutants, and yet are anchored to observations through frameworks that facilitate application to real-world situations.

The results and the approach of this chapter are partly addressed in previous publications (Ahangar et al., 2017; Venkatram and Schulte, 2018).

2.2 Wind tunnel measurements

Heist et al. (2009) conducted a wind tunnel study to examine the near-road impact of emissions from a simulated six-lane divided highway modeled at 1:150 scale. They considered twelve roadway configurations (Table 2-1), including seven with solid noise barriers at different heights and locations, Five of the seven barrier cases are used in this examination of upwind barrier effects. The study was conducted in the meteorological wind tunnel at U.S. EPA's Fluid Modeling Facility (Snyder, 1979). The wind tunnel test section measures 370 cm wide by 210 cm high and 1830 cm long (Figure 2-1). The boundary layer wind profile was generated with a combination of Irwin spires (Irwin, 1981) at the inlet and roughness blocks arrayed on the floor to condition the flow to simulate a typical atmospheric boundary layer profile. The typical barrier height, *H*, at full scale was 6 m. Four cases, G, L, J, and K, involved only upwind barriers. Case I examined two 6 m barriers, one on each side of the highway. All of the cases used a neutral boundary layer with a surface roughness, $z_0 = 0.52\ cm$ (0.78 m full scale), and a friction velocity, $u_* =$

$0.3\frac{m}{s}$ and a displacement height $d = 5.4\ cm$ (8.1 m full scale). A near-neutrally-buoyant tracer gas (ethane) was released from six lines along the roadway, and downwind concentration samples were collected through tubes mounted on the wind tunnel carriage system. Tracer concentrations were measured using hydrocarbon analyzers (flame ionization detectors) to form concentration profiles. Velocity measurements were obtained with a two-component laser Doppler velocimetry (LDV) system.

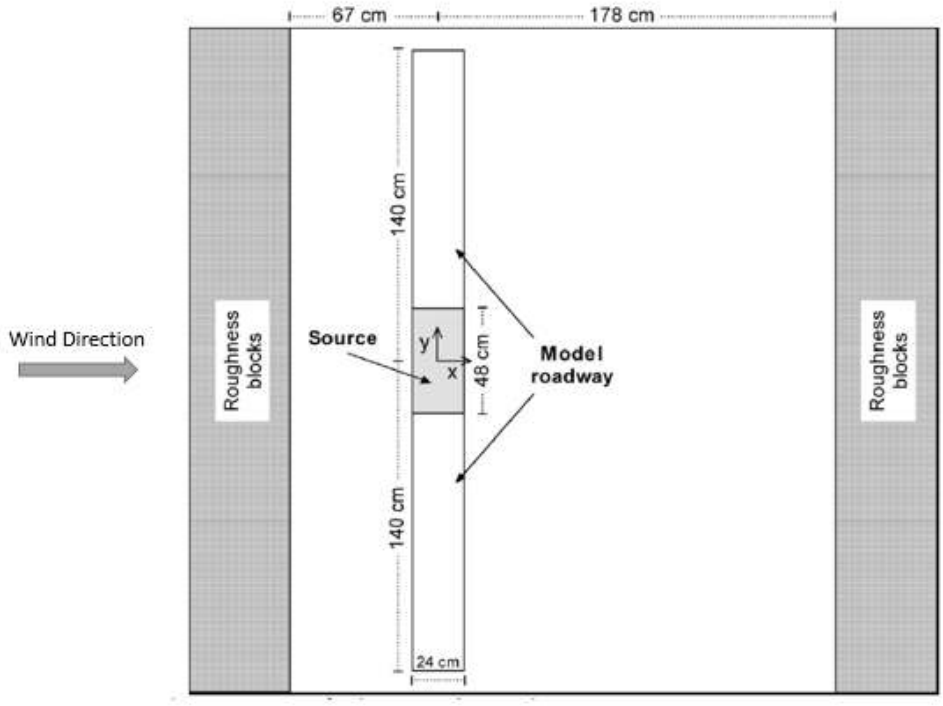

Figure 2-1- Layout of the wind tunnel study (Heist et al., 2009)

Table 2-1- Case descriptions in the wind tunnel study

Case	Description
A	Flat terrain
B	Elevated source, 1 H, 30° walls
C	Depressed source, 1 H, 90° walls
D	Depressed source, 1.5 H, 90° walls
E	Depressed source, 1 H, 30° walls
F	Depressed source, 1 H, 30° walls with noise barriers, 1 H tall, at upwind and downwind edges.
G	Noise barrier, 1 H tall, at upwind edge of the road
H	Noise barrier, 1 H tall, at downwind edge of the road
I	Noise barriers, 1 H tall, at upwind and downwind edges of the road
J	Noise barrier, 1.5 H tall, at upwind edge of the road
K	Noise barrier, 1 H tall, 1 H upwind of the upwind edge of the road
L	Noise barrier, 1 H tall, 2 H upwind of the upwind edge of the road

2.3 Upwind barrier cases

Figure 2-2 shows the configuration of each upwind barrier case modeled in Heist et al. (2009). Dimensions are in full scale.

a)

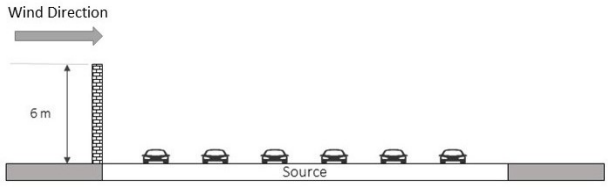

b)

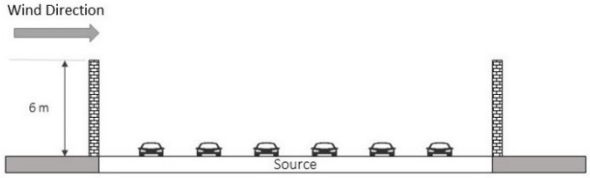

c)

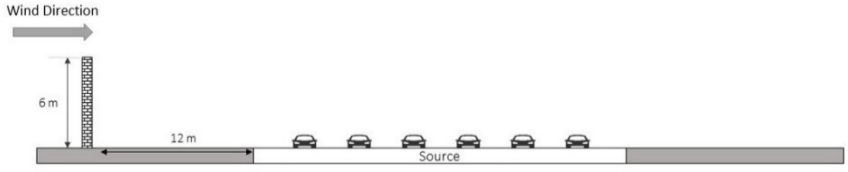

d)

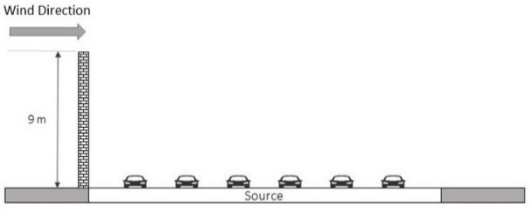

e)

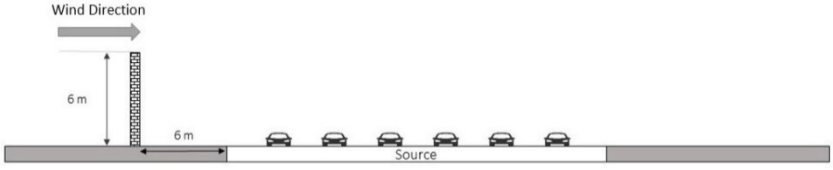

Figure 2-2- Different upwind barrier configurations, a) case G, b) case I, c) case L, d) case J, and e) case K.

Figure 2-3, which depicts the velocity profiles for the two single barrier cases, G and H, shows that the length of the recirculation zone behind the barrier is about 6 barrier heights. Note that H corresponds to a single barrier located downwind of the road. As expected, the velocity field around a single barrier does not depend on its location.

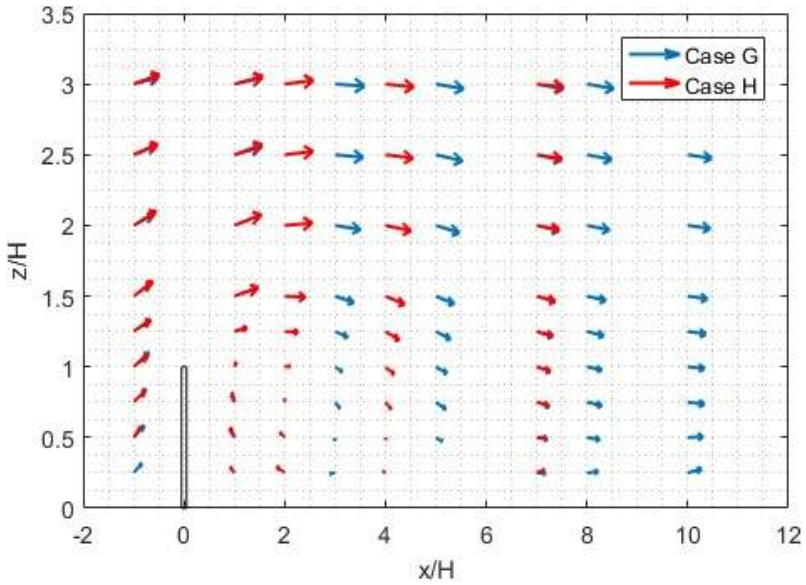

Figure 2-3- Wind velocity vectors in the presence of a solid barrier for case G and case H from the wind tunnel data. Dimensions are shown in barrier height (H) and the upwind barrier is located at x/H=0.

However, as Figure 2-4 shows, the recirculation zone extends 4 barrier heights behind the upwind barrier when there are two barriers on both sides of the highway. This observation is used in formulating the model for dispersion in the presence of two barriers. This is consistent with previous studies that show that the extent of the recirculation zone depends on the height of the barrier, the width of the road, the aspect ratio, and the type of boundary layer (Becker et al., 2002; Schulman et al., 2000).

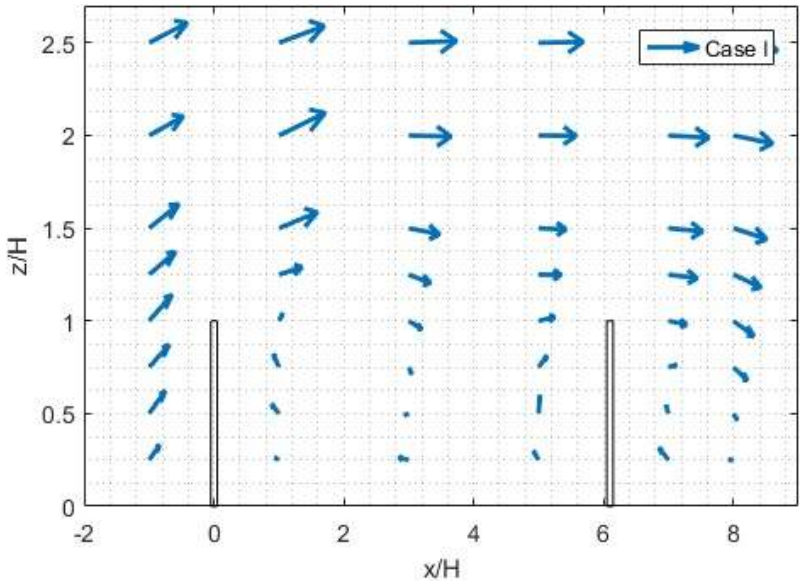

Figure 2-4- Wind velocity vectors in the presence of two solid barriers for case I from the wind tunnel data. Dimensions are shown in barrier height (H) and the upwind barrier is located at x/H=0.

Figure 2-5 shows the comparison of vertical velocity fluctuation, σ_w, at different downwind distances for the upwind barrier case. The barrier increases the initial mixing height and enhances the mixing. σ_w for the flat terrain case is 0.67 of its value at upwind barrier case at the edge of the highway. This effect will decrease at further downwind distances. At 20 barrier height distance, the fluctuation ratio is 0.87. The increase in the turbulence levels, especially close to the barrier, has been observed and implemented in the dispersion models in previous studies (Amini et al., 2018; Schulte et al., 2014).

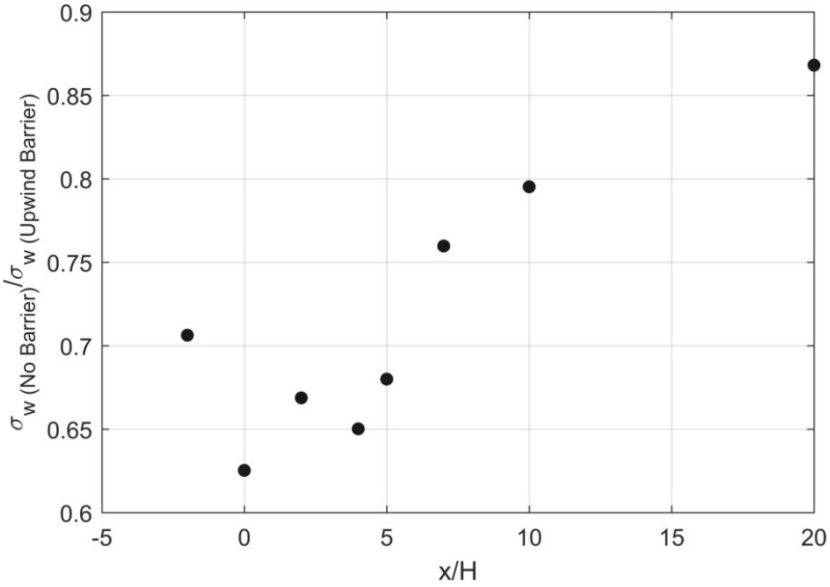

Figure 2-5- Ratio of observed vertical velocity fluctuations for no barrier case to upwind barrier at 1.5 barrier height.

2.4 Barrier models

2.4.1 Upwind barrier model

We see from the wind tunnel measurements, shown in Figures 2-3 and 2-4, that the flow in the recirculation zone is directed towards the upwind barrier close to the highway surface. This flow transports the pollutants emitted within the recirculation zone towards the barrier in the upwind direction. This feature is also observed in street canyons on the leeward side of the street and is incorporated in the Operational Street Pollution Model (Berkowicz, 2000). In the proposed model, we assume that the emissions on the highway that are covered by the recirculation zone originate from a line source located on the

upwind barrier at half the height of the barrier. The sources outside the recirculation zone contribute directly to the downwind receptors (See Figure 2-6).

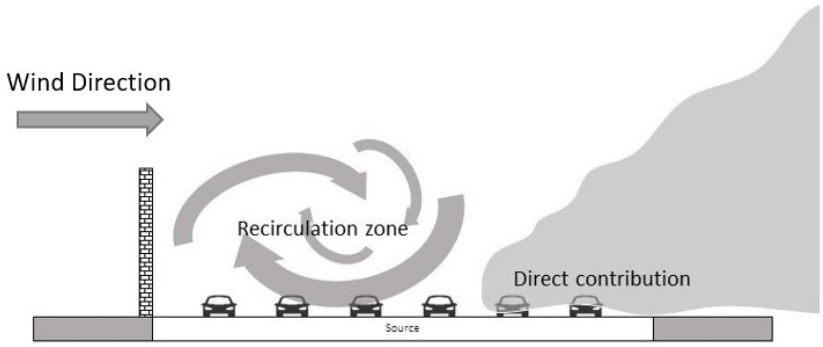

Figure 2-6-Recirculation zone and direct contribution in the upwind barrier model

We model the concentration associated with the line source using the approximation proposed by Venkatram and Horst (2006):

$$C(x,z) = \frac{q}{U(\bar{z})\cos\theta\sqrt{2\pi}\sigma_z(x/\cos\theta)}\left[exp\left(-\frac{(z_s-z)^2}{2\sigma_z(x)^2}\right) + exp\left(-\frac{(z_s+z)^2}{2\sigma_z(x)^2}\right)\right] \quad (2\text{-}1)$$

Where q is the emission rate per unit of length and θ is the angle of the wind direction perpendicular to the line source. In this equation, x is the downwind distance from the line source, z is the receptor height, z_s is the source height, σ_z is vertical plume spread, h is the source height, and $\mathrm{U}(\bar{z})$ is the wind speed evaluated at the effective plume centerline height, $\bar{z}$, defined by:

$$\bar{z} = \frac{\int_0^\infty z C^y(x,z)dz}{\int_0^\infty C^y(x,z)dz} \tag{2-2}$$

The height of this line source is taken to be half of the barrier height. The sources outside the recirculation are treated as line sources at ground-level at various distances from the receptor (Figure 2-6). The effect of the downwind barrier on these sources is described in Schulte et al. (2015). This model, referred to as the mixed-wake model, assumes that the concentration is uniform below barrier height, which results in the following expression for the near surface concentration, C_s,:

$$C_s = \frac{q}{U(\bar{z})cos\theta\sqrt{\frac{\pi}{2}}\sigma_z(x/cos\theta\ ) + U\left(\frac{H}{2}\right)Hcos\theta} \tag{2-3}$$

Where x is the downwind distance from the line source, H is the barrier height, and $U\left(\frac{H}{2}\right)$ is the wind speed at half of the barrier height. The model was evaluated using wind tunnel data (Heist et al., 2009) and tracer study data (Finn et al., 2010) , and showed good performance with measurements.

Plume spreads are calculated using the following equations:

$$\sigma_z = \sqrt{{\sigma_z}_p^2 + \sigma_{z_0}^2} \tag{2-4}$$

Where σ_{z_0} is the initial vertical plume spread and σ_{z_p} is calculated using the following equations (Akula Venkatram et al., 2013):

$$\sigma_{z_p} = \alpha * 0.57 \frac{u_*}{U(\bar{z})} x \frac{1}{1 + 3\frac{u_*}{U(\bar{z})}\left(\frac{x}{L}\right)^{2/3}}, L > 0 \quad (2\text{-}5)$$

$$\sigma_{z_p} = \alpha * 0.57 \frac{u_*}{U(\bar{z})} x \left(1 + 2\frac{u_*}{U(\bar{z})}\frac{x}{|L|}\right), L < 0$$

Here u_* is the surface friction velocity, L is the Monin-Obukhov length, and α accounts for increased rate of plume spread caused by the barrier. It has the following form of $\alpha = 1 + \frac{b(U(H)/u_*)^2}{1+\left(\frac{x}{20H}\right)^{1/2}}$ (Schulte et al., 2014).

The empirical constant b is set to 0.035 to fit with measurements. We assume that initial vertical spread of plume, σ_{z_0}, induced by the barrier is related to the barrier height through $\sigma_{z_0} = \beta H$ (Venkatram, 2013). $\beta = 0.25$ was selected to fit the measurements. The effects of two barriers, one upwind of the source and one downwind of the source, on dispersion is modeled by assuming that the effects from upwind and downwind models are independent and can be thus added linearly.

Part b of figures 2-7 to 2-10 compare ground-level concentrations measured in a wind tunnel study with corresponding model estimates. Model performance is measured using the following statistics of the ratios of the observed to measured concentrations: the geometric mean (m_g), the standard deviation (s_g), the fraction between 0.5 and 2 (fac2)

(Venkatram, 2008). We also calculate the correlation coefficient (r^2) between model estimates and corresponding measurements of ground-level concentrations. Observed concentrations are normalized to yield non-dimensional concentrations $\chi = \frac{CU_r}{\frac{Q}{L_x L_y}}$, where C is the concentration with background subtracted, U_r is reference wind speed, Q is the volumetric flow rate, L_x is the along wind dimension of the roadway segment, and L_y is the lateral length of the source segment.

We see that the simple model provides an excellent description of both the magnitudes as well as the spatial distributions of the measured concentrations.

a) Case G (Noise barrier, 1 H tall, at the upwind edge of the road)

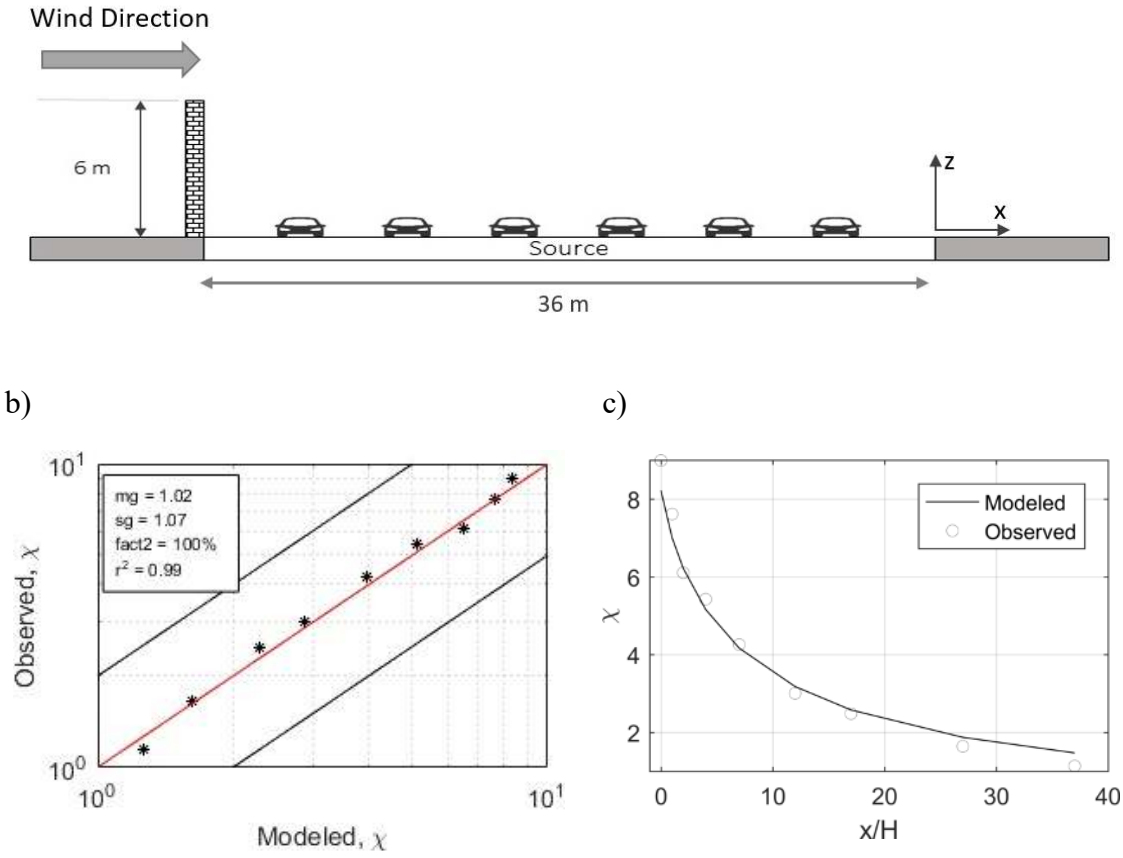

Figure 2-7- a) Barrier configuration, b) comparison of model estimates with observed concentrations, c) performance of model in describing spatial gradients for case G.

a) Case L (Noise barrier, 1 H tall, 2 H upwind of the upwind edge of the road)

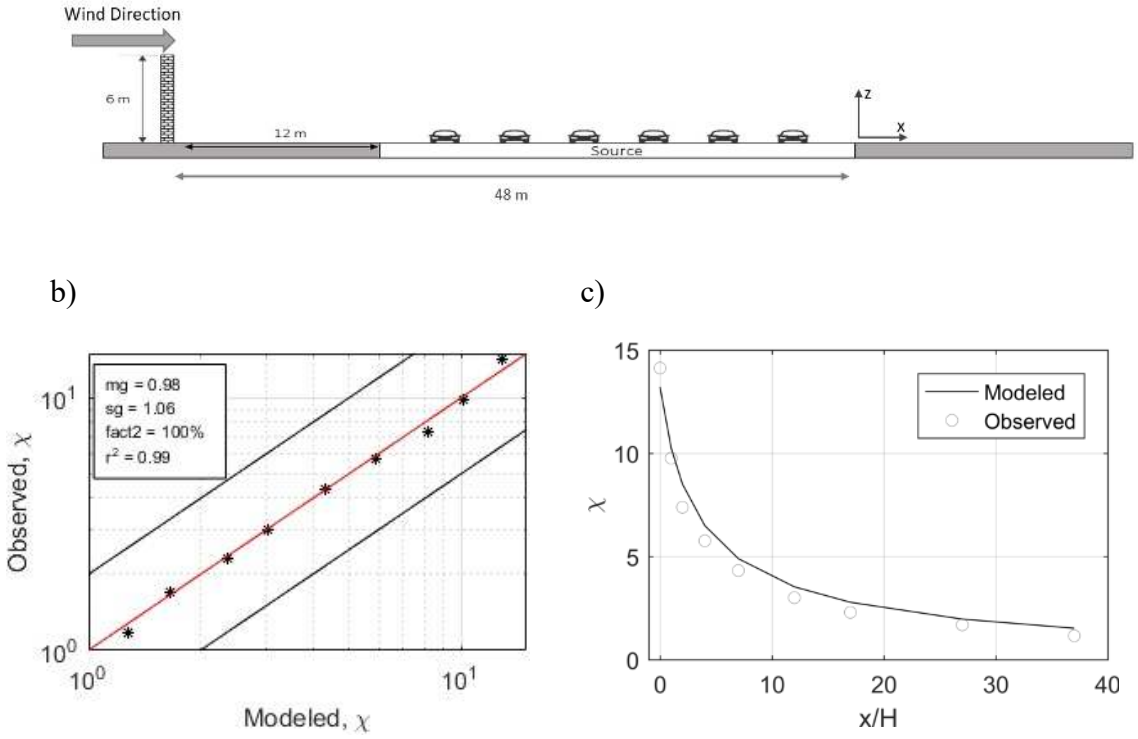

Figure 2-8- a) Barrier configuration, b) comparison of model estimates with observed concentrations, c) performance of the model in describing spatial gradients for case L.

a) **Case J (Noise barrier, 1.5 H tall, at the upwind edge of the road)**

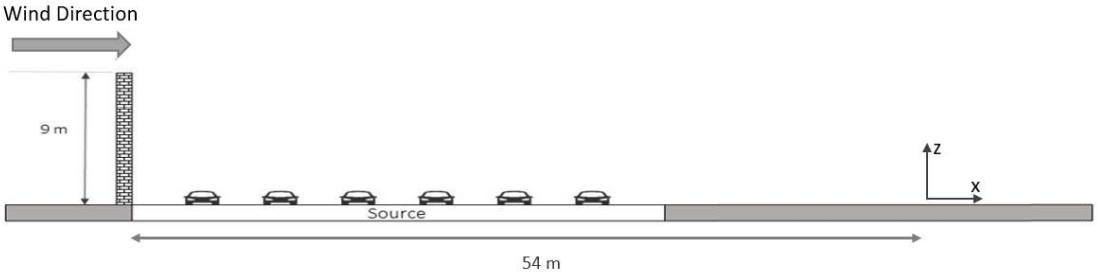

b)

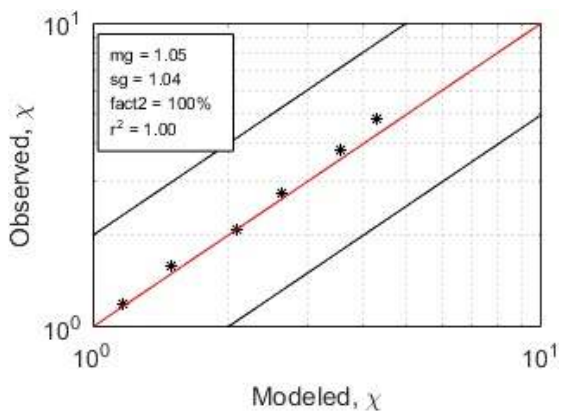

c)

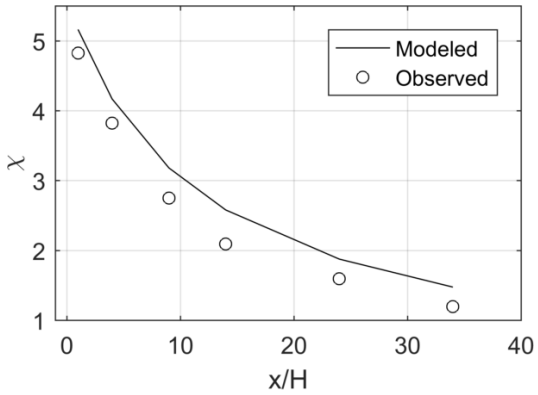

Figure 2-9- a) Barrier configuration, b) comparison of model estimates and observed concentration, c) performance of the model in describing spatial gradients for case J.

a) Case K (Noise barrier, 1 H tall, 1 H upwind of the upwind edge of the road)

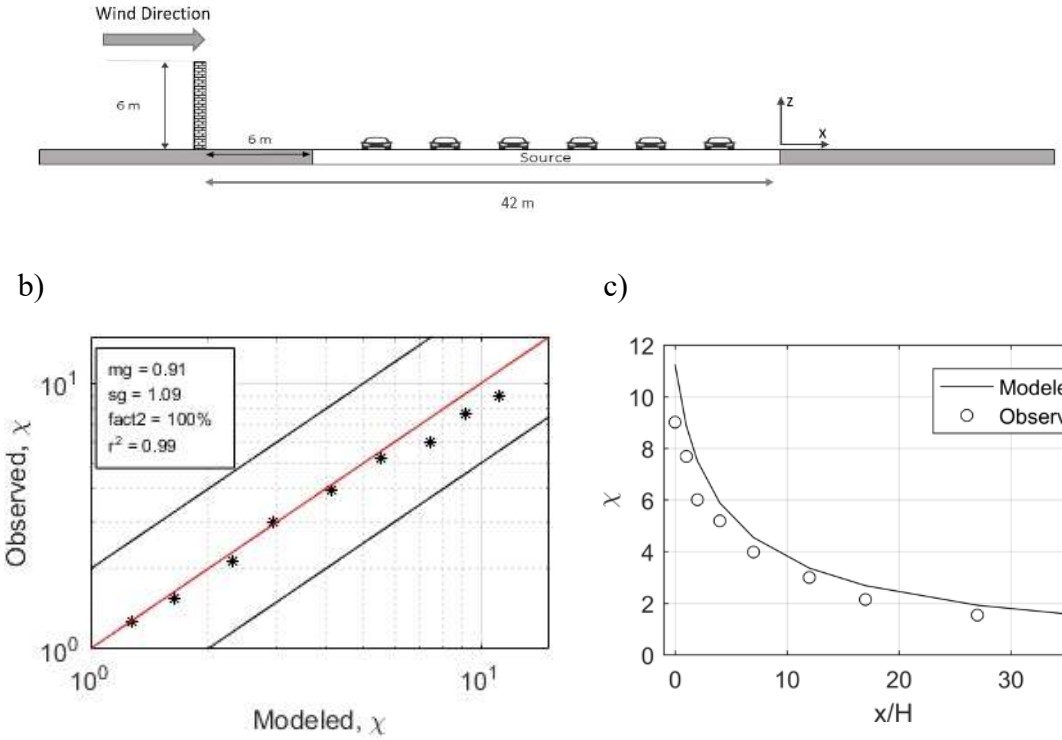

Figure 2-10- a) Barrier configuration, b) comparison of model estimates and observed concentration, c) performance of the model in describing spatial gradients for case K.

Part c of figures 2-7 to 2-10 compares concentrations measured at different downwind distances behind the barrier with corresponding model estimates. Since the pollutants coming from the recirculation zone are modeled as a single line source at the barrier location, the concentrations at the receptors within the recirculation zone are computed using a different model discussed later. Distances are measured from the edge of the highway for all the cases except case J which is from the end of recirculation zone at 9 barrier heights downwind of the upwind barrier. In case G, the model underestimates the concentration by 7 percent at the first receptor but shows better performance at further

downwind distances. For case L, the model also underestimates concentrations at the first receptor by about 8 percent and performs better for further downwind distances. In case J, the model underestimates concentration at the first receptor by 9 percent and shows good agreement at rest of downwind distances. On the other hand, for case K, the model overestimates concentrations at all of the downwind distances. The difference between the model estimate and the measured value is 18 percent at the first receptor and gradually becomes smaller at further downwind distances.

2.4.2 Barriers on both sides of the highway

Case I in the wind tunnel measurements has barriers at both sides of the highway. Wind profiles are shown in figure 2-4. The recirculation zone behind the upwind barrier extends for about 4 barrier heights, which is shorter than the previous case when only one barrier was present. The portion of the highway within this recirculation zone is modeled with the upwind barrier model and the rest of the highway is modeled using the mixed-wake model.

Figure 2-11 shows the model performance with two barriers. The model shows good performance in general.

a) Case I (Noise barriers, 1 H tall, at the upwind and downwind edges of the road)

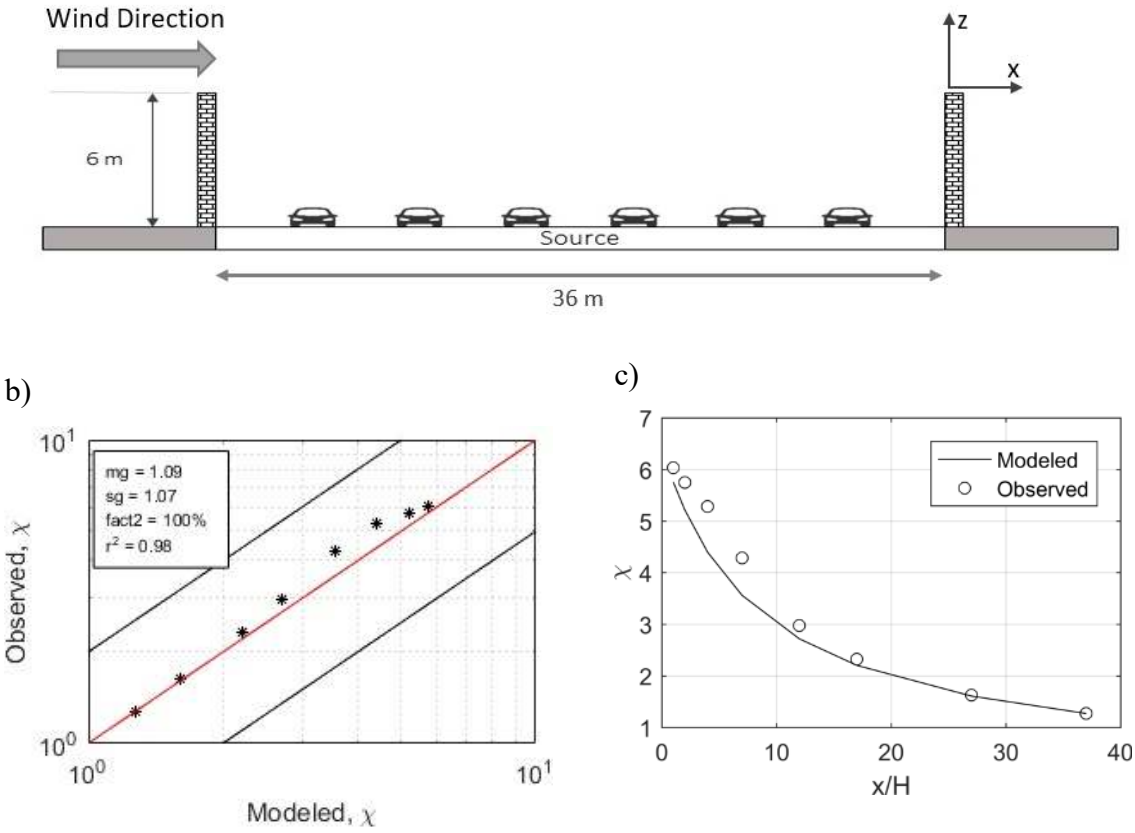

Figure 2-11- a) Barrier configuration, b) comparison of model estimates and observed concentration, c) performance of the model in describing spatial gradients for case I.

2.5 Sensitivity of the model to the height and road width

2.5.1 Upwind barrier

Here we estimate the effect of the upwind barrier in reducing near-road ground-level concentrations relative to the no barrier case. The barrier was located right at the upwind edge of the highway. Three barrier heights were selected, 3 m, 6 m, and 9 m, to represent the range of typical barrier heights.

Figure 2-12 shows the spatial concentration variation for the three barrier heights relative to the no barrier case as a function of x/H and x, the downwind distance to compare the effect of different heights, the concentration reduction was considered at two different distances. The first receptor was at $x = 60\ m$ to exclude the largest recirculation zone extending 54 m for the 9 m barrier. The reduction caused by the 3 m barrier is 26 percent. The 6 m barrier results in a reduction of 44 percent and the 9 m barrier results in a 60 percent reduction. For the 3 m barrier, the recirculation zone covers half of the highway and shifts the emitted pollutant to the barrier location. The emissions outside the recirculation zone have a direct effect on the near road concentrations. In the 6 m and 9 m barrier cases, the recirculation zone covers all of the highway and the difference between concentration gradients are only caused by different initial vertical plume spreads and source heights.

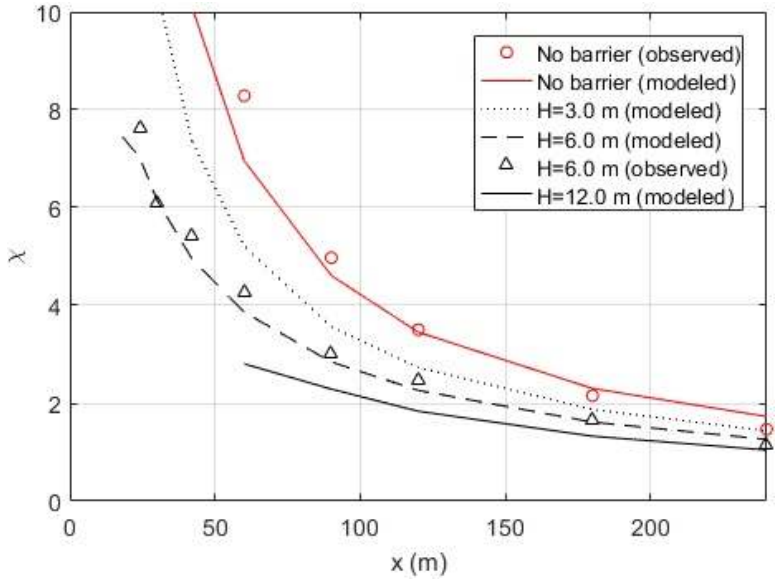

Figure 2-12- Model estimates of concentration profiles for upwind barrier with different heights and the comparison with observed measurements. Distances are from highway's median.

The other receptor is at $x = 240\ m$ or 40 barrier heights. The reduction for 3 m barrier is only 16 percent at this distance compared with the no barrier case. The reductions for the 6 m and 9 m barriers are 26 percent and 35 percent respectively. As expected, the effect of the barrier on reducing concentrations increases with barrier height, and weakens with downwind distance

Next, we examined the sensitivity of the model to increasing the highway width. If the recirculation zone covers the whole highway, we see a large reduction comparing to the no barrier case. Increasing the highway width results in reducing the upwind barrier effect because a greater fraction of the emissions lies outside the recirculation zone. Figure 2-13 shows the sensitivity of the model to increasing the highway width (W). The

concentrations are normalized with the no barrier concentration corresponding to the same highway width.

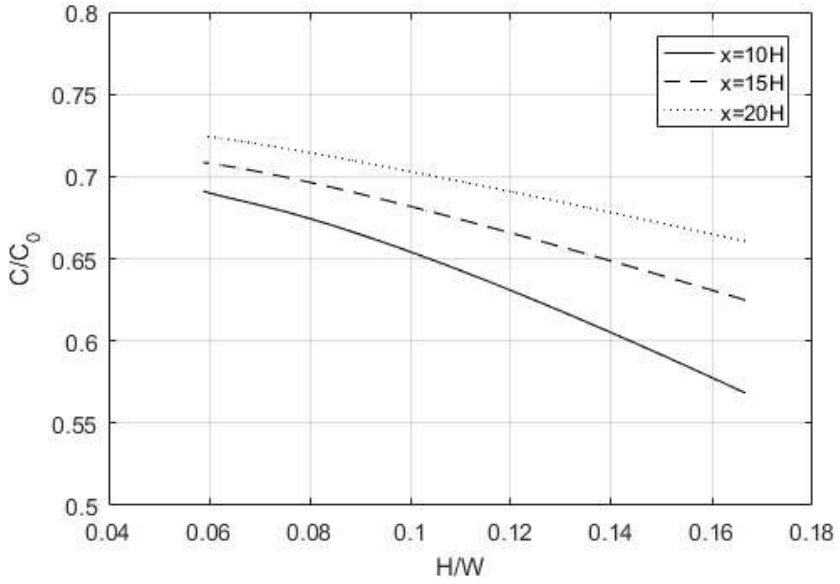

Figure 2-13- Sensitivity of the model to increasing the highway width. Concentrations are calculated at different distances of x=10H, x=15H, and x=20H from the center of highway where H=6m.

2.5.2 Barriers on both sides of the highway

Three different barrier heights are considered to estimate the sensitivity of the model in the presence of two barriers (Figure 2-14). The heights are 3 m, 6 m, and 9 m. The reductions caused by barriers are calculated at two different distances. At $x = 60\ m$, the 3 m barriers cause a 37 percent reduction, the 6 m barriers cause a 49 percent reduction, and the 9 m barriers cause a 66 percent reduction. At $x = 240\ m$, the 3 m barriers cause only a 17 percent reduction, the 6 m barriers cause a 27 percent reduction, and the 9 m barriers cause a 36% reduction. The effect of two 3 m barriers at both sides of the road is

larger than that for one upwind barrier case, while for the 6 m barriers, one or two barriers have almost the same effect.

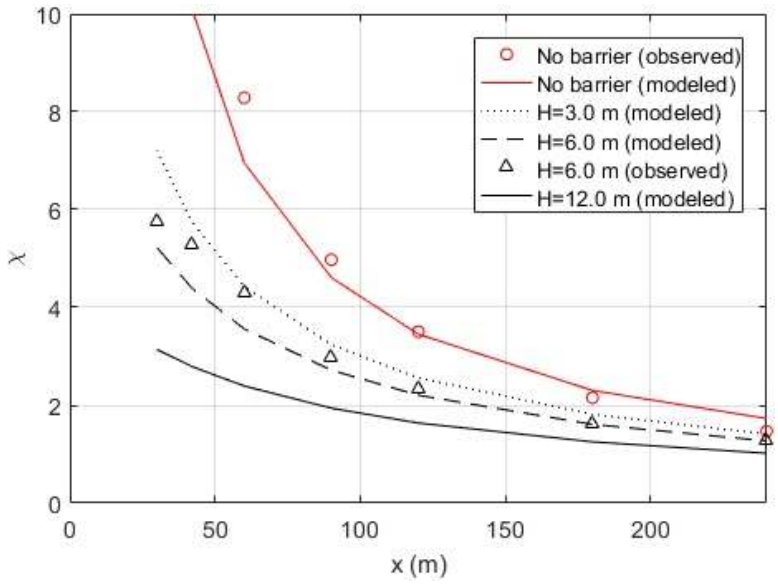

Figure 2-14- Model estimates of concentration profiles in presence of barrier on both side of the highway with different barrier heights and the comparison with observed measurements. Distances are from highway's median.

2.6 Comparison of upwind, downwind, and two barrier model

Here we compare the effects of different barrier configurations on concentrations downwind of the road. The first configuration is an upwind barrier, which is modeled using the proposed upwind barrier model. The second configuration is a downwind barrier, which is modeled using the mixed-wake model, and the last configuration considers barriers on both sides of the road.

Figure 2-15-a compares the measured surface concentration variations behind the barrier for three different configurations with those associated with the no barrier case. The

downwind edge of the highway is at $x = 18\ m$ (3 barrier heights), where the height of the barrier for all the cases is 6 m.

The presence of two barriers on both sides of the road causes a 76 percent reduction compared to the no barrier case at one barrier height downwind of the edge of the highway (4 barrier heights or 24 m downwind of the center of the highway). This reduction is 14 percent at 40 barrier heights (240 meters). The effects of either upwind or downwind barriers are similar. An upwind or downwind barrier results in about 70 percent reduction at $x = 24$ and around 20 percent at $x = 240\ m$. The concentrations are close to each other at downwind distances beyond 10 barrier heights for all three configurations.

Figure 2-15 indicates that the model yields the variation of concentrations similar to that of the measured concentrations. The largest concentration reductions occur for the two barrier case, and the reductions for the one barrier case, either upwind or downwind, are similar. The model predicts a 72 percent reduction for upwind or downwind barriers and a 78 percent reduction in presence of two barriers at both sides of the highway.

The effects of upwind and downwind barriers individually are very close to each other in the wind tunnel. The reason is that in an upwind barrier case, the most effective factor for concentration reduction is the length of the recirculation zone. If the recirculation zone covers all of the highway width, which was the case in the wind tunnel study, the barrier has a marked effect on concentration reductions. This is because all of the emissions from the highway are transported towards the upwind barrier. This effect not only shifts

the source further from the receptor but also results in more vertical mixing and pollution dilution.

a) b)

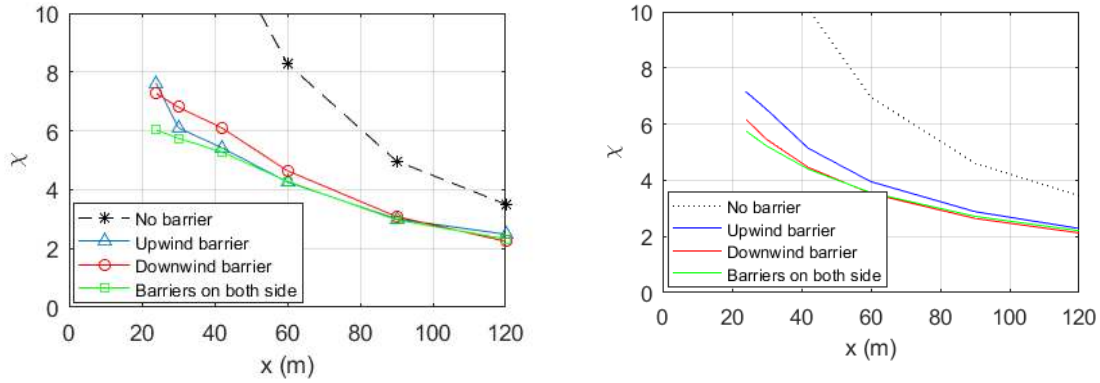

Figure 2-15- a) Observed and b) modeled concentration gradients for different barrier configurations. Distances are from highway's median.

2.7 Model for on-road concentrations

The upwind barrier model presented does not estimate concentrations within the recirculation zone where the near-surface flow is towards the upwind barrier. Here we present a tentative model to estimate concentrations within this region. Consider a road in which the upwind barrier induces a recirculation zone that extends a distance W_r from the upwind barrier.

We assume that the flow inside this zone carries pollutants towards the barrier in plumes originating from an area source of width W_r. Consider a section of the road with

width dp at a distance p from the upwind barrier. The surface concentration associated with this source at a receptor at a distance x from the barrier is (Akula Venkatram et al., 2013):

$$dC = \sqrt{\frac{2}{\pi}}\frac{q}{W}dp\frac{1}{\sigma_z U} \tag{2-6}$$

where σ_z is evaluated at a distance $(p - x)$ from the source. q is the emission rate per unit length of the road, and W is the total width of the road. The plume spread associated with atmospheric turbulence is given by the neutral expression: $\sqrt{\frac{\pi}{2}}u(\bar{z})\sigma_z = \alpha u_* x$ where $\alpha = 0.71$ (Venkatram et al., 2013). We then write

$$\sqrt{\frac{\pi}{2}}\sigma_z U = \alpha u_*(p - x) + h_0 U \tag{2-7}$$

Here h_0 is the initial plume spread induced by vehicle motion. Inserting Equation (2-7) into equation (2-6) and integrating between the limits x and W_r yields the expression for the surface concentration contributed by the emissions traveling towards the upwind barrier:

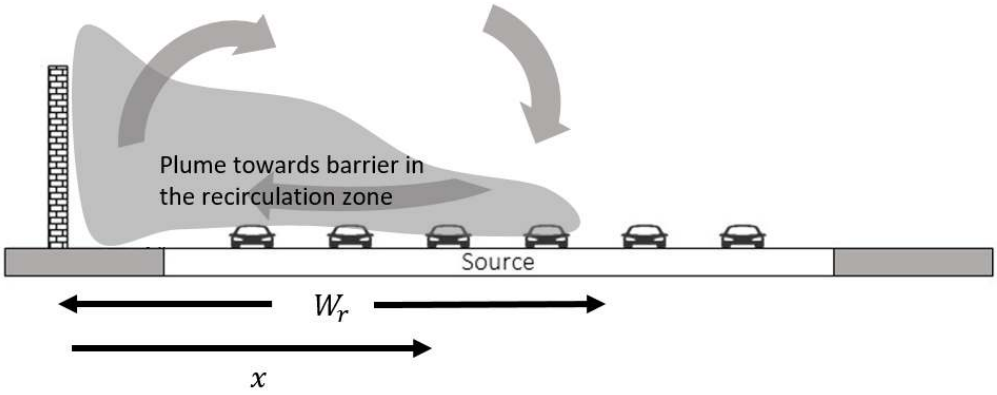

Figure 2-16- Schematic of the on-road barrier model.

$$C_d(x) = \frac{q}{W\alpha u_*} ln\left(1 + \frac{\alpha u_*(W_r - x)}{h_0 U}\right) \quad (2\text{-}8)$$

$when\ x \leq W_r$

The velocity, *U,* is evaluated at $h_0 = 1.5\ m$. The concentration estimate from Equation (2-8) is added to the contribution from equation (2-1), corresponding to the line source on the upwind barrier.

a) b)

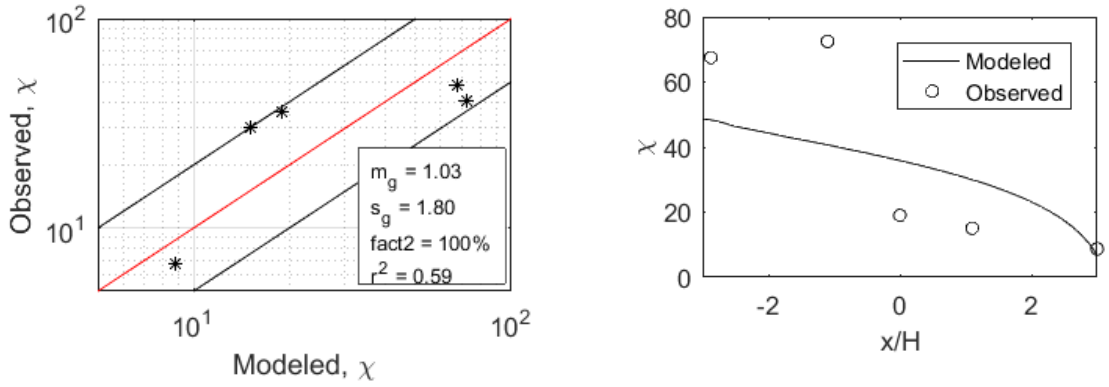

Figure 2-17- a) Comparison of the modeled and observed values and b) Modeled and observed concentration gradient in the roadway for case G.

Model estimates are compared with data from case G which simulated a six-lane highway using line sources consisting of small holes. Blocks with dimensions of $0.6 \times 0.6 \times 1.2\ cm$ ($0.7 \times 0.9 \times 1.8\ m$ in real scale) were placed in front of them to enhance near road turbulence. The first receptor in the roadway was at 0.3 times the barrier height above the surface. We assume that the surface concentration is the same as the concentration measured at 0.3 H in the turbulent recirculation zone.

Figure 2-17 compares the modeled surface concentrations and measurements at 0.3 H above the surface for Case G. The correlation between the modeled and observed values is clearly not as good as that for the estimates downwind of the road. However, the concentration estimates are reasonable, within a factor of two of the observations, considering the complexity of the dispersion processes within the cavity of the upwind barrier.

2.8 Summary and conclusions

A solid barrier at the upwind edge of a highway has significant effects on the dispersion of traffic produced emissions. It produces two effects that reinforce each other in reducing downwind concentrations relative to those in the absence of the barrier: it creates a recirculation zone behind the barrier that sweeps the emissions upwind towards the barrier, and at the same time enhances vertical dispersion. We have presented a model to account for these effects.

The model considers the emission sources within the recirculation zone as a single line source at the barrier location and assumes that the initial vertical plume spread is a fraction of the barrier height. By combining this model with the mixed-wake model for the downwind barrier, we are able to simulate the situation with two barriers on both sides of the highway. The models were evaluated with data from the EPA wind tunnel study data and showed generally good agreement with measured values.

The presence of an upwind barrier results in a reduction of downwind concentrations relative to the no barrier case. This reduction increases rapidly with barrier height especially when the height reaches the level at which the recirculation zone covers the entire width of the highway. These results suggest that an upwind barrier that results in a recirculation zone covering the width of a highway can be almost as effective as a downwind barrier. For a single, solid barrier, this width is 6 times the barrier height; for two barriers this width is 4 times the barrier height.

Barriers on both sides of the highway result in a larger concentration reduction than either an upwind or a downwind barrier. Beyond 10 barrier heights downwind of the two barriers, the reductions caused by the three configurations are similar.

Although the model presented here includes the effects of atmospheric stability and near-parallel wind directions, it has only been tested with data from the wind tunnel under neutral conditions when the wind direction is perpendicular to the road. Its applicability to other conditions requires further evaluation with field data.

3 The Effect of Downwind Barriers on Near-Road Air Quality

3.1 Introduction

Wind tunnel and tracer studies clearly show that downwind solid barriers lead to reductions in near-road concentrations of pollutants emitted by vehicles. Downwind barrier refers to a wall that is erected on the downwind side of the road. In the wind tunnel experiment by Heist et al. (2009), there were three cases with downwind barriers. These measurements demonstrated the physical mechanisms behind the mitigating impact of barriers: the plume from the road is lofted over the barrier and coupled with enhanced vertical dispersion results in the reduction of concentrations behind the barrier. Similar effects have been observed in other wind tunnel studies (Pournazeri and Princevac, 2015)

The results from the wind tunnel studies were confirmed and elaborated in a tracer study conducted by Finn et al. (2010). They studied the effects of a barrier by releasing SF_6 from two identical 54 m long line sources. One source was located 6 m upwind of a 90 m long, 6 m high solid barrier and the other had no structures next to it. Tracer concentrations

were measured simultaneously on identical sampling grids downwind of the sources. Six sonic anemometers measured turbulence around the barrier. Carefully controlled experiments showed that the barrier will increase the vertical mixing and reduced concentrations over a wide range of atmospheric stabilities.

Few field studies have been conducted near roadways to confirm these results in the real-world conditions. For example, Hagler et al. (2012) found that UFP concentrations at 10 m behind the 6 m barrier were about 50% less than those measured at this distance downwind of road sections without a barrier. Baldauf et al. (2008) found that CO and PM concentrations were reduced by 15% to 50% within 50 m of the 6 m barrier. The effect of the barrier persisted up to at least 20 times the barrier height in these studies, after which the concentration approached the value that would occur without a barrier. Hooghwerff et al. (2010) compared the effect of different types of downwind barriers on the dispersion of NOx and particulate matters, including a barrier with coating, porous barrier, barriers with different heights and design. The results showed that a downwind barrier reduces the concentration levels and the most effective parameter that decreases the concentration is the height of the barrier.

Variety of models have been used to describe the effect of downwind solid barriers. Hagler et al. (2011) and Steffens et al. (2014) used computational fluid dynamics (CFD) models to produce adequate descriptions of the data from the wind tunnel (Heist et al., 2009). Bowker et al. (2007) used the Quick Urban & Industrial Complex (QUIC) flow

model coupled with a Lagrangian particle dispersion model to produce concentration patterns that were roughly consistent with observations from Baldauf et al. (2008). Heist et al. (2009) used a virtual origin shift to explain the lower concentration values in presence of the barrier.

Schulte et al. (2014) developed a semi-empirical dispersion model that described data from the wind tunnel and the tracer studies. This model parameterizes the major features of the flow and dispersion effects induced by a barrier to avoid the computational burden of mechanistic CFD models (which have their own set of parameterizations). It is designed to be incorporated into routinely used models such as AERMOD (Cimorelli et al., 2005) or RLINE (M. G. Snyder et al., 2013). In this chapter, we evaluate the model with field data collected next to a real-world roadside barrier to answer the question: Can a model developed with data from controlled experiments describe observations made in the vicinity of an urban highway with a multitude of confounding factors?

The results and the approach of this chapter are partly addressed in previous publications (Amini et al., 2016; Paulson et al., 2017).

3.2 Field study

3.2.1 Site description

The study was conducted at the University of California, Riverside next to CA-60, U.S. Interstate 215 (I-215) highway. The highway has a barrier section located on the next

to the campus with an average traffic flow rate of 200000 vehicles/day. Meteorological data were collected from close meteorological station to plan the field study. Wind data collected from Riverside Municipal Airport, which is 5 km away from the barrier site, indicates a dominant wind from the west during the measurement period as shown in Figure 3-1. Strong western winds were blown during the day close to perpendicular to the freeway, which makes it convenient to study barrier effects during daytime unstable conditions. During the night, the low-velocity winds blow from the east, and the barrier is located upwind of the road.

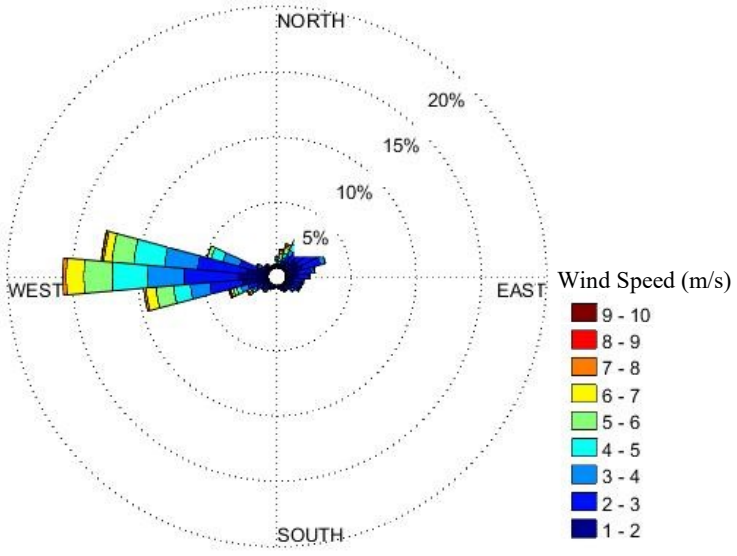

Figure 3-1- Wind rose from Riverside Municipal Airport meteorological station for 2017.

The barrier is 1 km long and 4.5 m height. The distance from the edge of the road to the barrier is 3 m. There are three lanes and one High Occupancy Vehicle (HOV) lane on the northbound side and four lanes and one HOV lane on the southbound side of the freeway. There is an entrance to the northbound lanes and an exit on the southbound side of the freeway. The lanes are 3.5 m wide and the median is 10 m across. The freeway is at the same level as the adjacent streets. There is no major source of pollution within a 3.5 km radius of the barrier site except the freeway. The heading of the freeway is 140°. Therefore, the wind direction perpendicular to the freeway is 230° true to the north. Two parking lots are located behind the barrier, which provides convenient locations for sampling.

The largest obstacles in the parking lots downwind of the barrier are widely scattered trees. There are no other major obstacles within 170 m of the barrier. A 2-lane street, West Campus Drive, runs parallel to the freeway between the parking lots. The street is mainly used to access the parking lots and the traffic is mainly passenger cars traveling during the morning hours, 8 A.M. to 10 A.M., and in the evening, 4 P.M. to 6 P.M. Another parking lot extends for 300 m west of the freeway. There is no major obstacle in this parking lot and trees are sparser and shorter than in the eastside parking lots.

3.2.2 Meteorology

Dispersion of air pollutant is governed by meteorology; so a comprehensive measurement of meteorological parameters is needed for any air quality and dispersion

field study. Campbell Scientific CSAT3 Three Dimensional Sonic Anemometers were used to measure flow properties. The measured data were stored on Campbell Scientific CR1000, CR3000, and CR5000 data loggers. Two 3-d sonic anemometers were employed to measure upwind and downwind flow characteristics at the rate of 10 HZ. A sonic anemometer was attached to a light post on the upwind side of the freeway (parking lot 30; assuming wind is westerly) at 4 m height above ground level (AGL) to capture upwind flow characteristics. The UC Riverside Community Garden is located on the west side of the anemometer, which ensured the absence of any major obstacle to upwind wind flow. Another sonic anemometer was attached to a light post within the wake region behind the barrier at 4 m AGL to record flow characteristics behind the barrier. Figure 3-2 shows the wind rose measured by the upwind anemometer in the second week of September 2014.

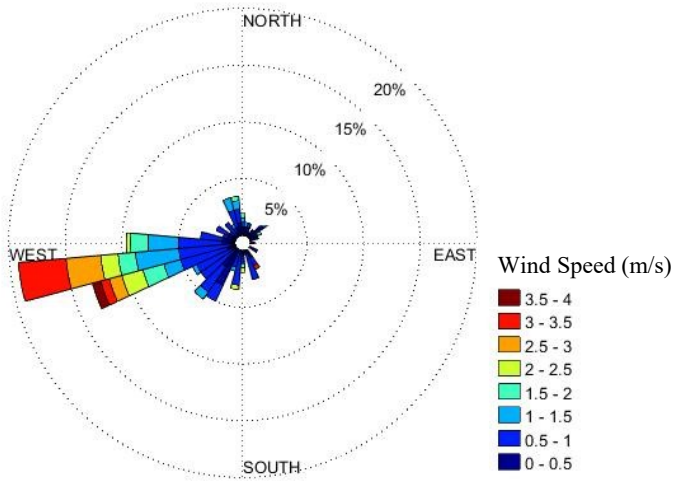

Figure 3-2- Wind rose measured by the upwind sonic anemometer during 9/4/2014 to 9/10/2014

The dominant wind during the day is blowing from the west/southwest direction. The meteorological data measured by the UCR meteorological station (Figure 3-1) were consistent with the onsite sonic data, which indicated that the upwind anemometer was not affected by local obstacles.

3.2.3 Air quality measurements

In this study, we used UFPs were as a tracer. UFPs are of public interest because they pose a great adverse health problem due to their large pulmonary deposition in areas with a high concentration (Oberdörster, 2000). UFP concentration next to major highways is often well above background levels and can be measured continuously with readily available instruments. Gidhagen et al. (2005) and Zhang et al. (2004) show that at the 100 m scale being considered here, deposition and coagulation play a minor role relative to turbulent dispersion in reducing particle number concentrations. Thus, UFP can be considered to be a passive tracer by using particle number concentration to characterize dispersion. One major problem with using UFP as a tracer is that UFP emission factors from vehicles are highly uncertain. Thus, it is necessary to treat the emission factor as an unknown which value is obtained by fitting model estimates to measurements. This process is discussed in more detail in a later section.

Fifteen tests were conducted on different days and at different times of day from July 2014 to May 2015 but due to the malfunction of instruments and unfavorable meteorological conditions, only six tests were selected for analysis.

Table 3-1 shows the dates and duration of measurements. The total duration of all 6 tests is 29 hours.

Table 3-1- Overview of dates and duration of measurements.

Test	UFP measurement dates	Time of Measurement
1	07/22/2014	12:00-18:30
2	08/11/2014-08/12/2014	20:30-00:30
3	08/18/2014-08/19/2014	20:00-00:30
4	08/19/2014-08/20/2014	20:00-01:00
5	04/07/2015	12:30-17:30
6	05/05/2015	14:00-18:30

UFP number concentrations were measured using the TSI Condensation Particle Counter (CPC) Model 3022A. The cutoff size of these CPCs is 7 nm. The measured concentration range was $5 \times 10^3 - 10^5$ particles/cm^3. According to the CPC manual, accuracy within this range of concentrations is $\pm 10\%$. The CPC concentrations were stored on a custom-designed data logger.

CPCs performance can be affected by ambient high temperatures that are common in California. To ensure the validity of the data measured by the CPCs, all of the instruments were calibrated against a reference CPC in the field. To do so, the instruments were co-located at one location and the data collected during this period was used to derive the instrument calibration factor. Calibration factors were used to adjust the concentrations measured during the experiment. Any instrument that showed weak correlation with the reference CPC was filtered out of the test. Figure 3-3-a shows a sample calibration factors for one the CPCs during Test 1.

a) b)

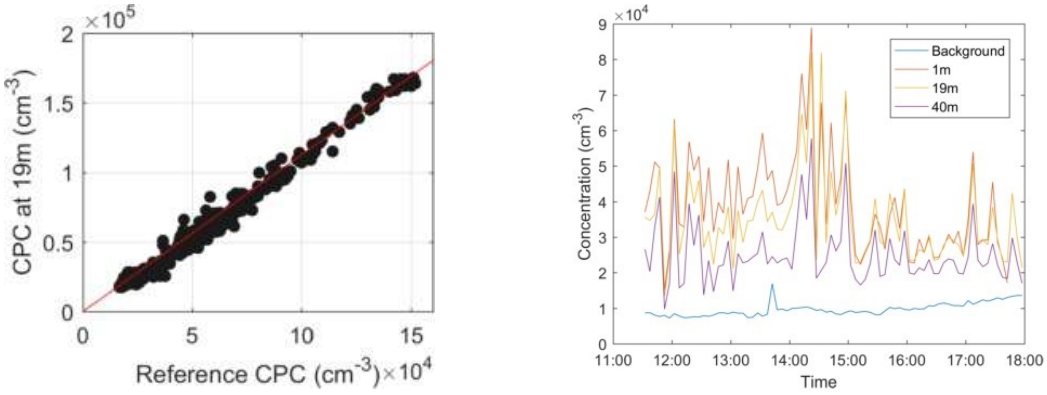

Figure 3-3- a) Calibration plot during Test 1 for the CPC at 19m distance behind the barrier ($Slope = 1.13$ and $r^2 = 0.99$). b) Five-minute average concentration measured at different locations during Test 1.

Several CPCs were used to measure background UFP concentrations and downwind UFP concentrations at several downwind distances. A CPC was placed at the upwind side of the freeway (assuming that the wind is blowing westerly) to measure background UFP number concentrations. The rest of the CPCs were deployed behind the

barrier (Figure 3-4). The downwind CPCs were placed at least 250 m away from the barrier edge to avoid barrier edge effects. CPC locations were changed from one test to another to avoid any systematic bias in measurements. The background concentrations were subtracted from the downwind concentrations to estimate contributions from vehicles on the highway. Figure 3-3-b shows the five-minute average concentration levels at different locations during Test 1. Background values were usually stable close to $10^4\ particles/cm^3$ for most of the observations which ensured that the background location is not affected by local emission sources and is reliable throughout the study.

Figure 3-4- Approximate location of instruments.

Perpendicular winds to the highway are ideal for the line source dispersion modeling since they mainly transfer traffic produced emission to the downwind sensors

and minimize the contribution of other surrounding sources. In this study, we analyzed only the data observed when the wind direction was within 45° of perpendicular to the freeway to avoid the confounding role of wind direction. The wind direction perpendicular to the freeway is 230° true to the north. The meteorological conditions used to analyze the data corresponding to the upwind 3-d sonic, which are shown in Table 3-2. The air quality data, micrometeorological data, and traffic data were averaged over 30-minute periods for analysis.

Table 3-2- Meteorological conditions.

Test	# of data points	Mean Monin-Obukhov Length (m)	Mean Wind Direction (deg true N)	Mean Wind Speed (ms^{-1})	Mean Friction Velocity (ms^{-1})	σ_θ	Cloud Cover
1	10	-11.51	254°	2.72	0.31	5.67°	Clear
2	7	-15.74	256°	1.37	0.17	8.21°	Clear
3	9	-9.06	238°	1.00	0.14	10.48	Clear
4	10	-5.78	254°	1.14	0.14	5.79°	Clear
5	9	-38.76	238°	2.45	0.44	13.35	Mostly Cloudy
6	9	-42.96	268°	2.83	0.47	2.81°	Partly Cloudy

Tests 1 through 4 were conducted in unstable conditions. Winds were moderate during test 1 and very light during tests 2, 3, and 4. No major variability in wind direction was observed during the first 4 tests and the wind directions were almost always favorable with respect to the freeway orientation. Skies were clear during all first 4 tests.

Tests 5 and 6 were conducted in near neutral conditions. Winds were moderate and the wind direction was steady. Wind directions were almost always favorable during these two tests. Skies were mostly cloudy in test 5 and partly cloudy in test 6.

To analyze the UFP concentrations, the background concentrations were subtracted from the downwind concentrations during all tests. The averages of observed concentration gradients for all six tests are shown in Figure 3-5. No concentration peak was observed behind the barrier as in the observations of Ning et al. (2010). The background concentration was almost always around 10^4 #/cm^3. We next examine whether these concentration measurements can be described with a dispersion model that was evaluated with data from controlled experiments conducted in the wind tunnel (Heist et al., 2009) and in the tracer field study (Finn et al., 2010).

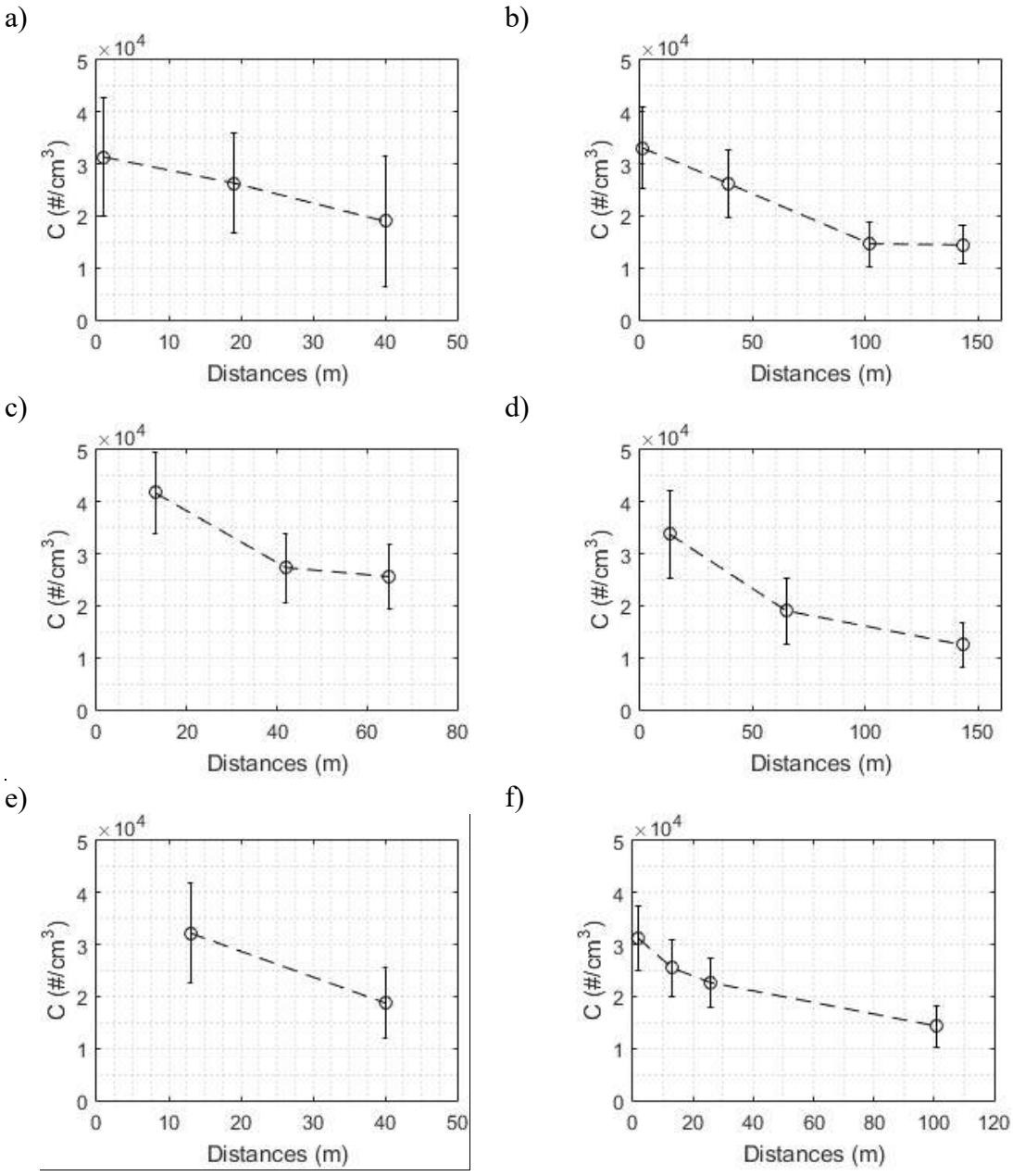

Figure 3-5- Averaged particle concentrations at different distances behind the barrier for a)Test 1, b)Test 2, c)Test 3, d)Test 4, e)Test 5, and f)Test 6.

3.2.4 Traffic activity

The number of vehicles passing each lane of the freeway was downloaded from the CalTrans Performance Measurement System which provides five-minute average historical data for highway (www.pems.dot.ca.gov). The detectors record the number of cars and trucks separately. Figure 3-6 shows the traffic activity during different days of measurement. Trucks consisted 6 percent of the fleet in total.

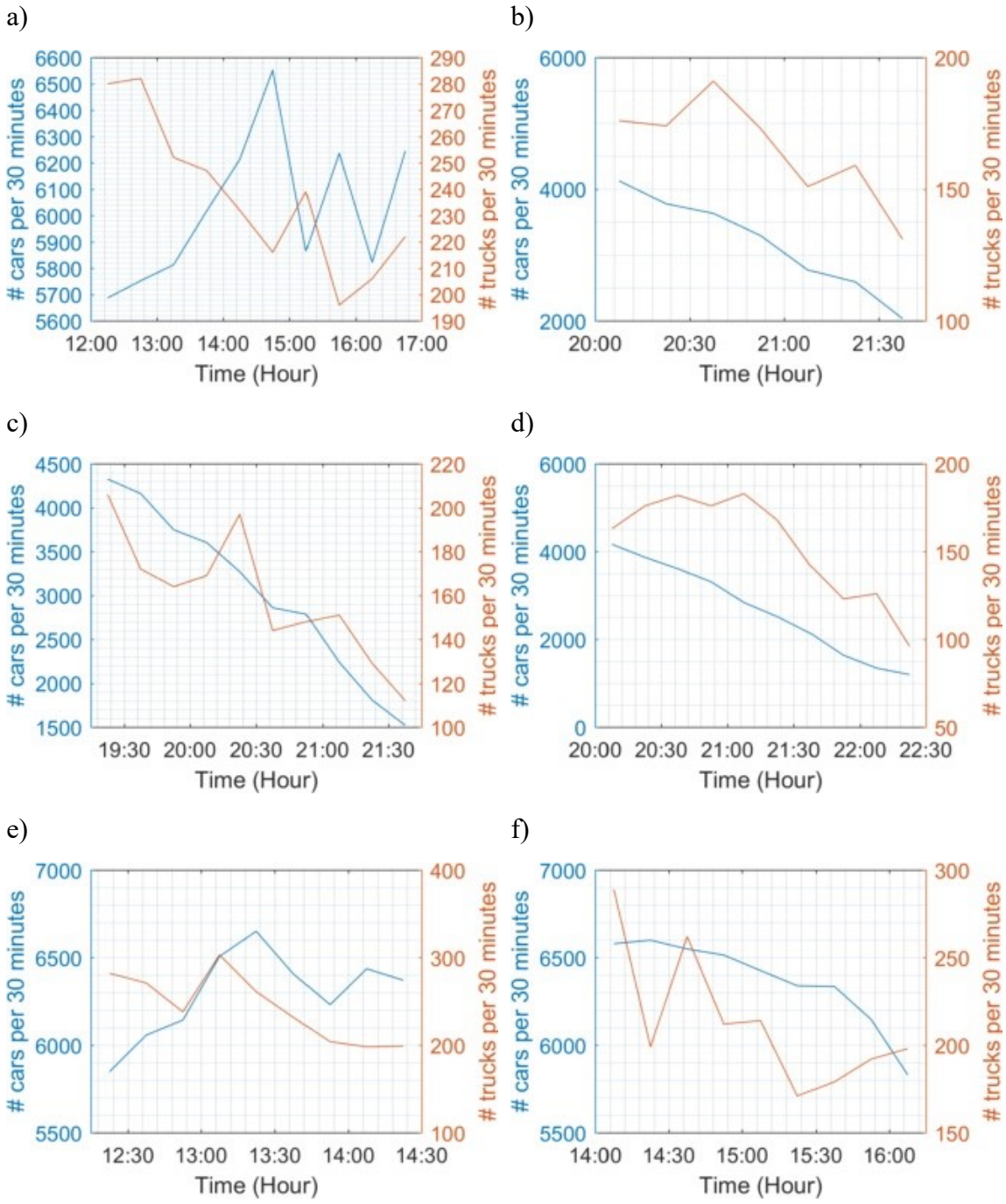

Figure 3-6- Traffic activity for a)Test 1, b)Test 2, c)Test 3, d)Test 4, e)Test 5, and f)Test 6.

3.3 Framework for the barrier models

The basis of modeling in this chapter is the mixed-wake model developed by Schulte et al., 2014. The model used to interpret the data assumes that the concentration is well-mixed from the surface to the barrier height, and the concentration profile follows a Gaussian distribution above the barrier height with the maximum concentration occurring at the barrier height, as shown in. We can then express the surface concentration associated with an infinitely long line source as:

$$C_s = \frac{q}{U\left(\frac{H}{2}\right)\cos\theta\, H + U(\bar{z})\cos\theta\sqrt{\frac{\pi}{2}}\sigma_z} \tag{3-1}$$

where q is the emission rate per length of the line source, C_s is the concentration at the surface, H is the barrier height, $U(\bar{z})$ is the wind speed at the effective centerline height of the plume above the barrier, and θ is the wind direction with respect to the perpendicular to the road. Vertical plume spread, σ_z, is calculated using equations used in R-LINE model from Venkatram et al. (2013).

3.3.1 Simple barrier model

We can derive a simplified version of Equation 3-1 by using the neutral expression

$$U(\bar{z})\sigma_z \propto u_* x \tag{3-2}$$

where u_* is the surface friction velocity. Equation 3-1 then becomes

$$C_s = \frac{q}{U\left(\frac{H}{2}\right)\cos\theta\, H + a u_* x} \tag{3-3}$$

where the empirical constant, a, is 1.

Since the width of the road is comparable to the downwind distances being considered here, we treat the road as an area source with width *W*. Then, the concentration at a downwind distance *x* from the barrier becomes:

$$C_s = \int_x^{x+W} \frac{\frac{q}{W}}{U\left(\frac{H}{2}\right)\cos\theta\, H + u_* x}\, dx = \frac{q}{u_* W} \ln\left(1 + \frac{W}{\frac{U\left(\frac{H}{2}\right)}{H\frac{u_*}{u_*}}\cos\theta + x}\right) \tag{3-4}$$

This simple model, which applies primarily to neutral conditions, serves as a reference model whose performance against observations will be compared with that of an improved version.

3.3.2 Modified mixed-wake model

The second model considered here modifies Equation 3-1 to improve its performance during unstable conditions when Equation 3-1 overestimates concentrations close to the source in the Idaho Falls tracer experiment (Finn et al., 2011). The modified model assumes that the maximum concentration occurs above barrier height to be consistent with the wind tunnel data (Heist et al., 2009). The second modification is an entrainment factor, f_m, that reduces entrainment into the barrier wake during unstable

conditions. This is an empirical modification to account for the overestimation of concentrations close to the source under the unstable conditions of the Idaho Falls experiment. The factor reduces entrainment behind the barrier as the absolute value of the Monin-Obukhov length decreases. It is also a function of downwind distance, starting at values below unity just downwind of the barrier and approaches unity at large downwind distances. f_m is taken to be:

$$f_m = f_c + (1 - f_c)\left(1 - \exp\left(-\frac{x}{L_s}\right)\right) \tag{3-5}$$

where f_c, the entrainment factor at $x = 0$, is taken to be:

$$f_c = \exp\left(-\frac{L_s}{|L_{MO}|}\right) \tag{3-6}$$

where $L_s = 10H$ and H is the barrier height. f_c decreases as the absolute value of Monin-Obukhov length decreases.

The third modification is the effect of barrier on surface friction velocity. Surface friction velocity is enhanced based on an empirical model for the development of a neutral boundary layer after a roughness change,

$$u_{*w} = u_*\left(\frac{z_{0w}}{z_0}\right)^{0.17} \tag{3-7}$$

where the effective roughness of the wall is taken to be $z_{0w} = H/9$.

Since Monin-Obukhov length is proportional to u_*^3, the Monin-Obukhov length behind the barrier is taken to be:

$$L_w = L\left(\frac{u_{*w}}{u_*}\right)^3 \tag{3-8}$$

The velocity below the barrier height is assumed to be uniform with height given by its value at $z = H$. With these parameterizations, the surface concentration can be expressed as

$$C_s = f_m C_{max}[\exp(-p_1^2) + \exp(-p_2^2)] \tag{3-9}$$

where C_{max} is the maximum concentration is

$$C_{max} = \frac{\frac{q}{\cos\theta}}{f_m U(H).H.[\exp(-p_1^2)+\exp(-p_2^2)]+U(\bar{z})\sqrt{\frac{\pi}{2}}\sigma_z.[2-\mathrm{erf}(p_1)-\mathrm{erf}(p_2)]} \tag{3-10}$$

In this equation, $U(H)$ is the velocity at barrier height, $p_1 = (H - H_p)/\sqrt{2}\sigma_z$, $p_2 = (H + H_p)/\sqrt{2}\sigma_z$, and H_p is the height of maximum concentration, taken to be:

$$H_p = H + \frac{\sigma_{z_B}}{2} \tag{3-11}$$

where σ_{z_B} is the vertical plume spread right behind the barrier. This model performs much better than the model presented in Schulte et al. (2014) in describing concentrations close

to the barrier in the Idaho Falls experiment (Finn et al., 2010) during unstable conditions, which correspond to those considered in the current field study.

3.4 Comparison with observations

As indicated earlier, the UFP number emission factor is highly uncertain. The literature reports a large range 10^{12}~10^{14}#/(veh.km) (Kumar et al., 2011; Morawska et al., 2008). In this study, we treat the emission factor as an unknown parameter whose value is obtained by fitting model estimates to measured UFP concentrations. Because we wanted to evaluate the performance of the model in describing the impact of the barrier on downwind concentrations, we fitted the model only to the data measured beyond 50 m from the barrier where barrier effects are expected to be small.

The ratio of UFP High Duty Vehicle (HDV) emission factor to that of Light Duty Vehicle (LDV) was taken to be 25. This ratio was found using $PM_{2.5}$ emissions from EMFAC Model inventory data (California Air Resources Board, 2011). Car and truck emission factors were averaged over mileage for the fleet operating in Riverside County.

The fitted emission factors were found to lie within $10.3 \pm 2.39 \times 10^{13}$ #/(veh.km) (95% confidence interval) range for simple barrier model and $7.04 \pm 1.49 \times 10^{13}$ #/(veh.km) (95%) range for the modified mixed-wake model for all of the six tests.

The performance of the models are evaluated using the geometric mean (m_g), standard deviation of the residuals between the observations and predictions (s_g), the fraction of data points that lie within a factor of two of the observations (fact2), and the

correlation coefficient between the observations and predictions (r^2). The geometric mean and standard deviation are defined as:

$$\ln m_g = \sum_i \frac{\epsilon_i}{N} \tag{3-12}$$

$$\ln s_g = \sqrt{\frac{\sum_i \left(\epsilon_i - \ln m_g\right)^2}{N-1}} \tag{3-13}$$

where $\epsilon = \ln C_{obs.} - \ln C_{pred.}$ is the residual between the observed concentration and the predicted one, and N is the number of data points. Both models show good correlation with observations.

The performance of the models using the average emission factor for all six tests is shown in Figure 3-7. The r^2 are similar for the two models using a barrier height of 4.5 m.

a) b)

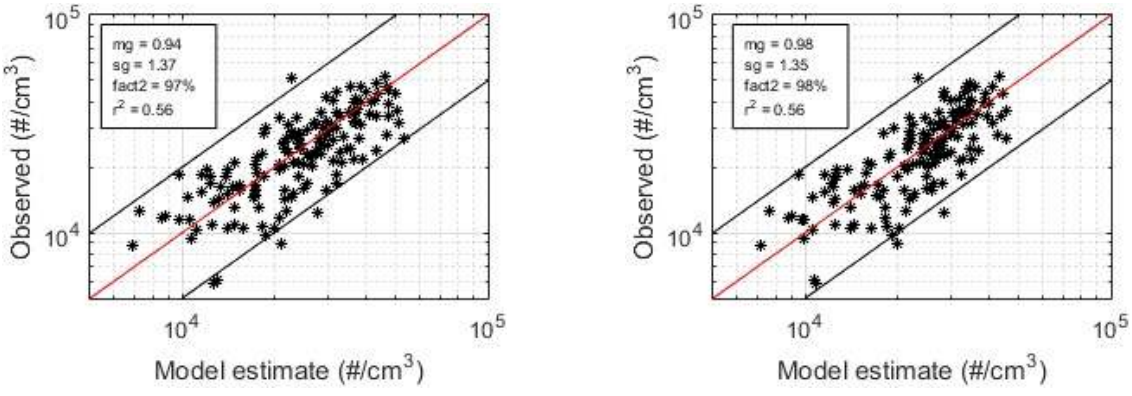

Figure 3-7- Comparison of observations and a) simple barrier model estimates and b) the modified mixed-wake model estimates.

To distinguish between the two models we investigated the sensitivity of model performance to different barrier heights using normalized bias (Chang and Hanna, 2004) to measure their relative performance.

Figure 3-8 shows the bias versus barrier heights for both models. The bias is zero for the barrier height of 4 m for the modified mixed-wake model, and is zero for the barrier height of 6.7 m for the simple barrier model. These results indicate that both models capture the essential effects of barriers on downwind concentrations. There is evidence that the modifications to the mixed-wake model improve model performance.

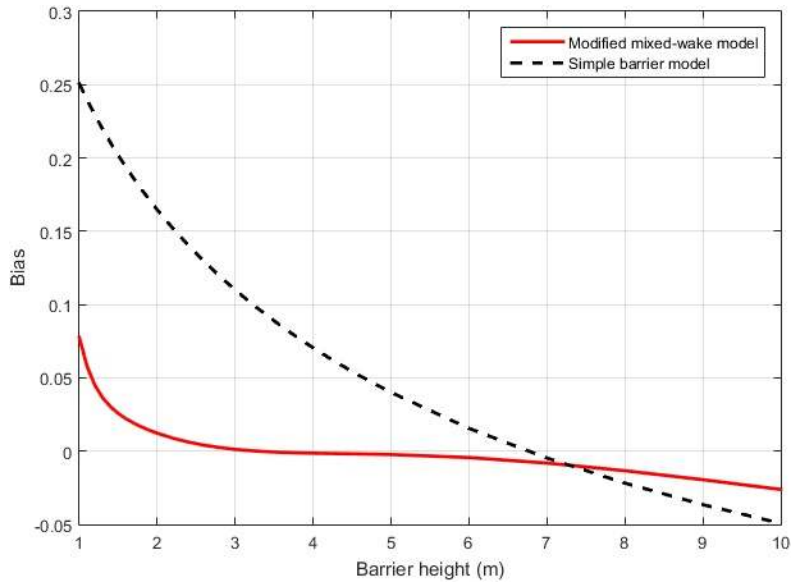

Figure 3-8- Bias versus barrier height for the modified mixed-wake model (red solid line) and for simple barrier model (black dashed line).

Figure 3-9, which compares the concentration gradients of the observations with those from tests 4 and 6, indicates that both models provide a realistic depiction of the gradients.

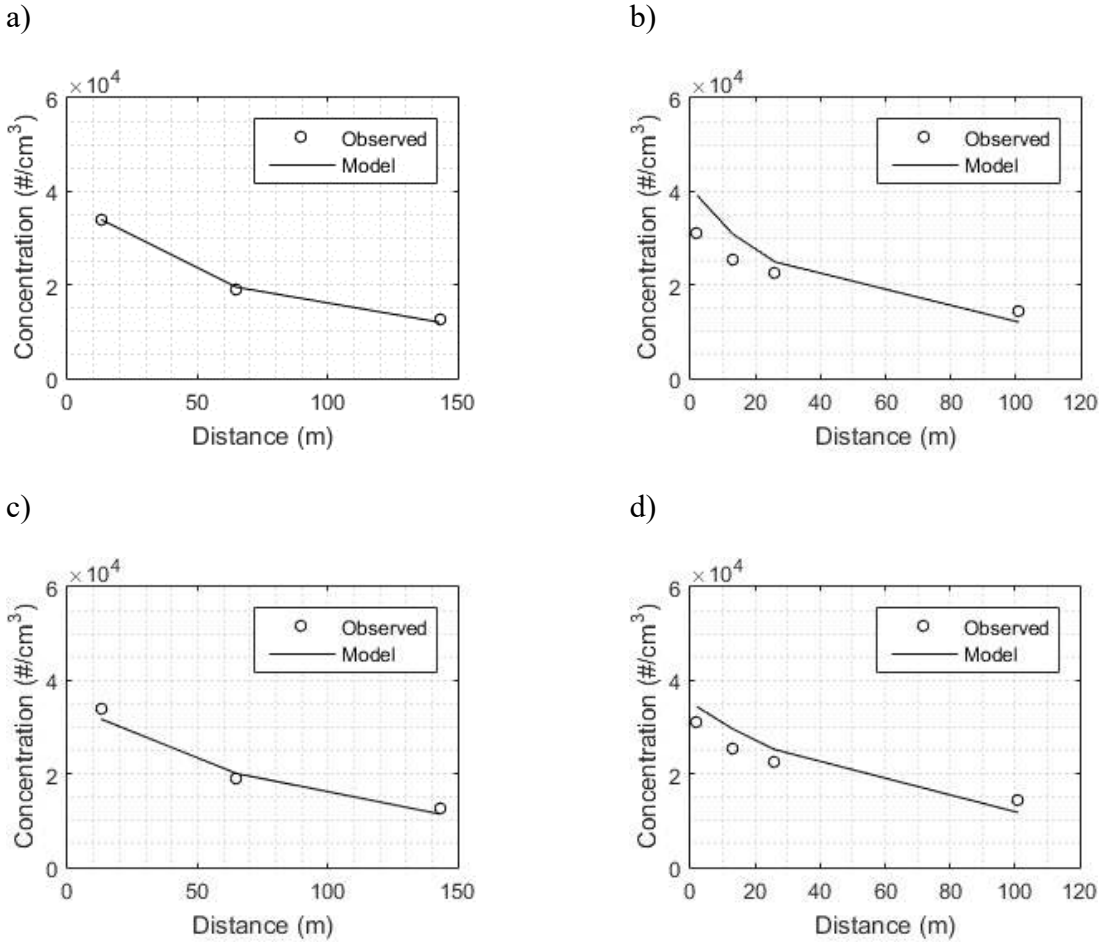

Figure 3-9- Concentration gradients for observations and a) simple barrier model for test 4, b) simple barrier model for test 6, c) the modified mixed-wake model for test 4, and d) the modified mixed-wake model for test 6. (Emission factors are calculated for each day using the data measured beyond 50 m from the barrier.)

3.5 Model sensitivity to the barrier height

The variation of UFP concentrations with distance in the first 100 m behind the barrier for different barrier heights, with micrometeorological inputs of test 6, are shown in Figure 3-10. The no-barrier case concentrations were estimated by assuming that the vehicles on the freeway induce an initial vertical spread of 1 m. The concentration reduction, relative to flat terrain, just next to the 2 m barrier is around 40%. This reduction increases to 55% by doubling the barrier height. The concentration reduction decreases with distance to about 10% at 40 m for the 2 m barrier. This reduction is 25% for a 4 m barrier. The average concentration reduction from 0-40 m is 13-20% for a 2 m barrier. This average reduction increases to 30-45% with a doubling of the barrier height to 4 m.

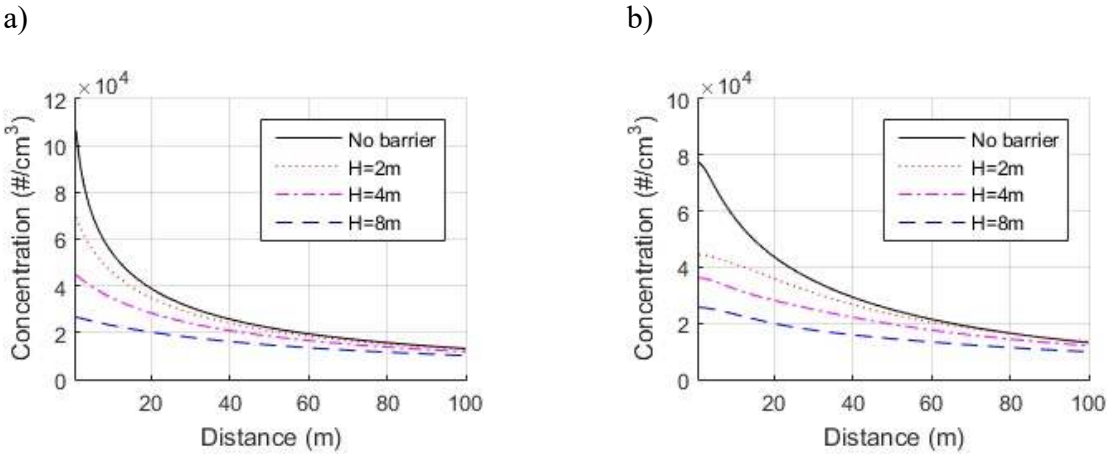

Figure 3-10- Comparison of estimated concentrations behind barriers with different heights and an open field for a) simple barrier model and b) the modified mixed-wake model.

3.6 Summary and conclusions

We used data from a field study to evaluate a dispersion model that parameterizes the effects of roadside barriers on dispersion. This model was developed using 1) data from experiments conducted in the wind tunnel and 2) measurements from a tracer study in which concentrations were sampled simultaneously downwind from two line sources, one behind a 6 m barrier and the other located in open terrain. The primary question this chapter addresses is whether a semi-empirical dispersion model based on data from controlled experiments can describe data collected downwind of a sound barrier next to a real-world urban highway with a multitude of confounding factors.

Six tests were conducted next to a congested freeway, which had several factors that aided the interpretation of the data: 1) absence of a major source of pollution, except the freeway, in the neighborhood, 2) absence of a major obstacles on the east and west sides of the freeway, except the noise barrier, 3) absence of a busy street behind the barrier, 4) presence of a single barrier downwind of the freeway, and 5) presence of parking lots on both sides of the freeway to provide the opportunity to place several CPCs to measure UFP concentrations.

Two models were evaluated with the data from the field study. The first is a simplified version of the model presented in Schulte et al. (2014), which we refer to as the Simple Barrier Model. The second is a modification of the model described in Schulte et al. (2014) to account for reduced entrainment in the immediate wake of the barrier during

unstable conditions. Both models performed well in estimating the pollutant concentrations. Because the emission factor for UFP is highly uncertain, we treated it as a model parameter whose value was obtained by fitting model estimates to observations of UFP concentrations measured at distances where the barrier impact is small. The emission factors resulting from the simple barrier model is $10.3 \pm 2.39 \times 10^{13}$ #/(veh.km) (95%) and that from the modified mixed wake model is $7.04 \pm 1.49 \times 10^{13}$ #/(veh.km) (95%). These values are well within the range reported in the literature (Kumar et al., 2011; Morawska et al., 2008).

Both models provide adequate estimates of the magnitude and the spatial variation of concentrations; the modified mixed wake model has a smaller bias. The models predict that a 4 m barrier results in a 30-45% reduction in average concentration within 40 m (10H) of the barrier, relative to the no-barrier site. This concentration reduction is 13-20% if the barrier height is halved. The good performance of the simple barrier model reinforces the conclusion from Schulte et al. (2014) that the presence of the barrier is equivalent to shifting the line sources on the road upwind by a distance of about $HU(H/2)/u_*$.

4 Using Vegetation to Enhance the Impact of Solid Barriers on Near-road Air Pollution

4.1 Introduction

Vegetative barriers have been suggested as a potential method to decrease air pollution near roadways. However, the effects of these barriers on downwind air quality are uncertain. Vegetative barriers affect air quality in two main ways: 1) they absorb particles through dry deposition and 2) they alter the flow fields by forcing the flow over the barrier and decreasing downwind turbulence level and wind speed (McNaughton, 1988; Petroff et al., 2008a; Steffens et al., 2012; Tong et al., 2015; Vos et al., 2013; Wang and Takle, 1995).

Despite the numerous real-world measurements that have been devoted to examine the effect of vegetative barriers on air quality near roadways, conclusions on their effects are not definitive. Field studies conducted on evergreen and deciduous trees in North Carolina, USA also concluded that vegetation can lead to higher, lower, or the same level

of concentrations as the clearing section (Hagler et al., 2012). Another field campaign was conducted in Queens, New York City and higher concentrations were measured behind the vegetation barrier because of the decreased values of Turbulent Kinetic Energy (TKE) behind the vegetative barrier (Tong et al., 2015).

So far, only a few studies have been performed which explicitly investigate the effects of a combination of vegetation and a solid barrier on the air quality near roadways. A comprehensive field study was conducted in Raleigh, NC where a stretch of a clearing, a solid barrier, and a vegetation-solid barrier combination was present (R. Baldauf et al., 2008). The results indicated that concentrations measured next to solid and vegetative barrier mitigated downwind concentrations more than the other two barriers. A CFD model examined the effects of common vegetative barrier configurations near roadways and found that a wide vegetation barrier with high Leaf Area Density (LAD), and also a combination of vegetation and solid barrier work best as mitigation strategies (Tong et al., 2016).

The study described in this chapter focuses on the impact of a barrier with tall vegetation behind it in mitigating the impact of vehicle emissions. A field campaign was conducted in Sacramento, CA. UFP number concentrations and turbulence levels were measured at a solid barrier section and a wall-vegetation barrier section at 4 m downwind of the barriers. The results indicated that the downwind concentrations of the wall-vegetation barrier combination are lower than that of the solid barrier and the turbulence

behind the wall-vegetation barrier is lower than that of the solid barrier. A semi-empirical model was developed to describe the collected data. The model assumes that adding vegetation results in a decrease in turbulence levels above the barrier and decreases the entrainment of particles into the wake of the barrier. This reduces the ground-level concentrations close to the barrier.

The results and the approach of this chapter are partly addressed in previous publications (Enayati Ahangar et al., 2017; Schulte et al., 2017).

4.2 Field study

A field study was conducted in Sacramento, California to examine the effect of tall vegetation behind a barrier on concentration levels in the vicinity of the highway. The study

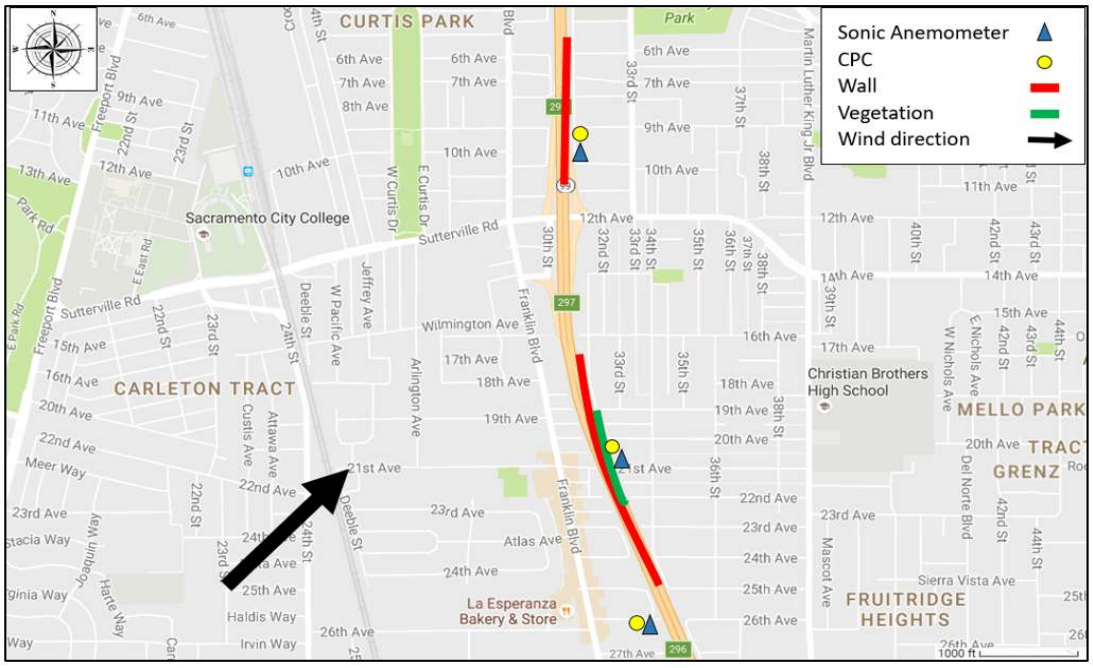

Figure 4-1- Location of instruments

was conducted next to CA-99 in Sacramento (Figure 4-1). The freeway, which has an average traffic flow rate of approximately 200,000 vehicles/day, is 42 m wide and has 10 lanes including 2 High Occupancy Vehicle (HOV) lanes. The barrier is 12 m from the edge of the highway, which is the only major source of pollution near the study area.

The wind rose (Figure 4-2) derived from winds measured at the Sacramento

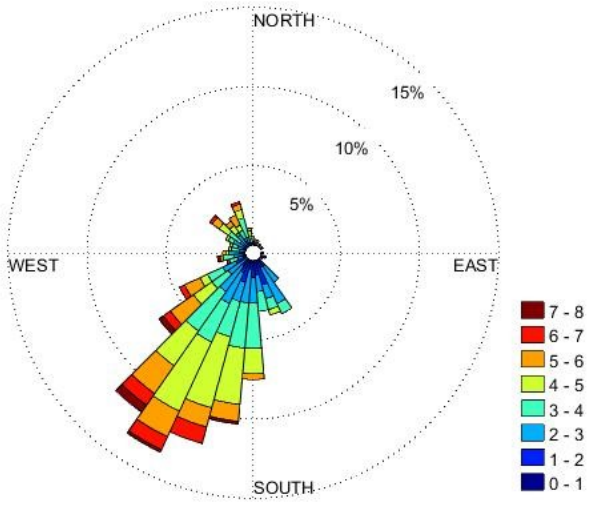

Figure 4-2- Wind rose from meteorological station during June 2016

Executive Airport shows that the dominant wind direction during the daytime is from the southwest. During the night, the winds are light from the north.

The field study was conducted at two barrier sites (Figure 4-3). The first site has a 5 m barrier extending over 500 m on the east side of the highway. The other site has a barrier of the same height with tall trees planted behind it. The vegetation is a row of pine

trees planted next to the barrier extending over 200 m along the highway. The height of the trees is 15-18 meters. The freeway is at the same level behind the barriers at both sites.

At both locations, the areas downwind of the barriers are residential with one story houses. There are also streets behind the barriers at both locations, which made it possible to make measurements within 10 m distance from the barriers.

The primary pollutant for this measurement was Ultrafine particles (UFPs). UFPs have high concentrations near the highway and major urban sectors comparing to background levels which make them good tracers for studying dispersion within these areas. There is also a strong association between UFP concentrations and adverse health effects (Pope III, 2002). Previous studies have also shown that dispersion models can be developed to explain UFP concentration levels near major highways and urban areas (Amini et al., 2016; Schulte et al., 2015). Dispersion, deposition, and coagulation can decrease the concentration of UFP but the effects of coagulation and deposition are small within short distances of the source so the main mechanism is dispersion near the highway (Zhang et al., 2004).

a)

b)

Figure 4-3- View of a)barrier vegetation site and b) solid barrier site

UFP concentrations were measured with TSI Condensation Particle Counters (CPCs), Model 3022A. This model can measure concentrations in the range 5×10^3-10^5 particles/cm^3. Raspberry Pie Model 2B computers were configured to serve as data loggers for the CPCs.

Meteorological variables were measured with Campbell Scientific CSAT3 3-D (three dimensional) sonic anemometers. Campbell Scientific CR1000, CR3000, and CR5000 dataloggers were used to record the data at the 1HZ frequency. The sonic anemometers were powered with deep cycle marine batteries. The traffic flow in each lane of the freeway was obtained from the CalTrans Performance Measurements System (www.pems.dot.ca.gov). Cars and trucks are treated separately in the data.

One CPC was located at each one of the downwind sampling locations, east of highway 99. CPCs were installed inside two cars and powered with deep cycle marine batteries. Both cars were parked at 4 m distance behind the barrier, one downwind of the solid barrier, and the other downwind of the barrier with vegetation. CPCs were interchanged each day to avoid instrumental error. Another set of anemometer and CPC was located at west side of the freeway at a local resident house next to the highway 99. One sonic anemometer was located at this location to measure temperature and wind velocities. An extra anemometer was used as a backup unit at the same location. Since the wind was blowing from the southwest most of the time, measurements at this location are

considered as background. The anemometers were installed on a pole at 5 m above ground level (AGL).

The measurements were conducted on 21st, 22nd, 25th, 26th, 27th, 28th, and 30th of June 2016. The selected measurement period was 12:00–18:00 hours, during which time the wind blew primarily from the southwest. Since the highway is north-south, the wind that is perpendicular to the road is westerly. To avoid the effects of the interference between the two sections of the highway on downwind concentrations, we focused on data from June 25th, 26th, and 27th, when the wind was westerly most of the time. A sonic anemometer was installed at each of the downwind sampling locations to measure the effects of the solid and the wall-vegetation barriers on wind characteristics and turbulence levels. The sonic anemometers were installed on poles at 2.5 m above the ground and at 4 m downwind of the barrier sections.

Table 4-1 shows the time and date that each instrument was operational. Upwind sonic anemometers and CPC functioned throughout the measurement period. The data collection on July 27th and 28th were shortened due to malfunction of the downwind CPCs.

Table 4-1- Overview of the dates and time of measurement.

Day #	Date	Downwind anemometers start time	Downwind anemometers stop time	Downwind CPCs start time	Downwind CPCs stop time
1	6/21/2016	---	---	14:00	16:30
2	6/22/2016	---	---	13:00	15:00
3	6/25/2016	11:30	17:30	13:00	17:30
4	6/26/2016	11:30	16:00	11:45	16:00
5	6/27/2016	12:45	17:00	16:00	17:00
6	6/28/2016	10:45	14:30	12:30	14:30
7	6/30/2016	---	---	14:30	16:30

4.3 Results

The data was filtered to focus on wind directions within 45° of perpendicular to the freeway at both sections (cross-road winds) to best capture the effects of the barriers. The freeway direction at the solid barrier section is 270° true to the north, and at the vegetation-solid barrier section is 254° true to the north. Thus, our analysis was confined to data collected when the wind direction was within $259° \pm 34°$ true to the north. The wind direction was obtained from the upwind 3-D sonic anemometer. The air quality data, micrometeorological data, and traffic data were averaged over 15-min periods for analysis.

Figure 4-4 shows the average wind pattern during the measurement period. The winds were light before noon with an average below 1 m/s. Stronger winds occurred during the afternoon from 2 PM to 6 PM when most of our measurement was made.

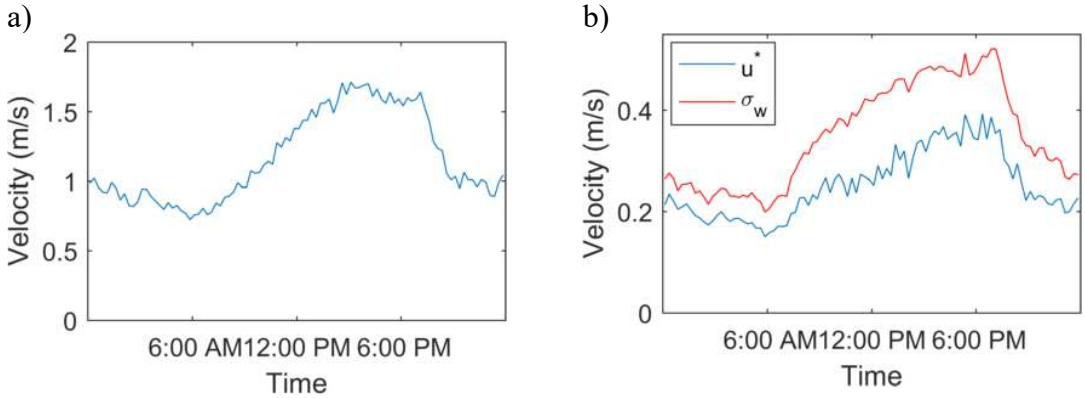

Figure 4-4- a) Average wind velocity, b) friction velocity (u^*) and vertical velocity (σ_w) fluctuations from upwind sonic anemometer for the period of measurement.

Measured concentrations near freeways depend on several variables, such as wind speed, flow turbulence, traffic activity, wind direction(M. G. Snyder et al., 2013), and the effect of the obstacles on these parameters. All the parameters except the effects of the obstacles are measured by the upwind sonic anemometer. Therefore, we should investigate the turbulence data and the effects of each configuration on the flow field to analyze the UFP concentration data.

4.3.1 Concentration measurement

The time series of 1-min averaged UFP concentrations during June 25th and 26th of the sampling campaign are shown in Figure 4-5. The background concentrations do not vary significantly and they are of the order of 5000 #/cm^3, which indicates that freeway

emissions have little impact on the upwind receptor. On the other hand, the downwind UFP concentrations at both sites show significant variations, with spikes reaching 6×10^4 #/cm^3.

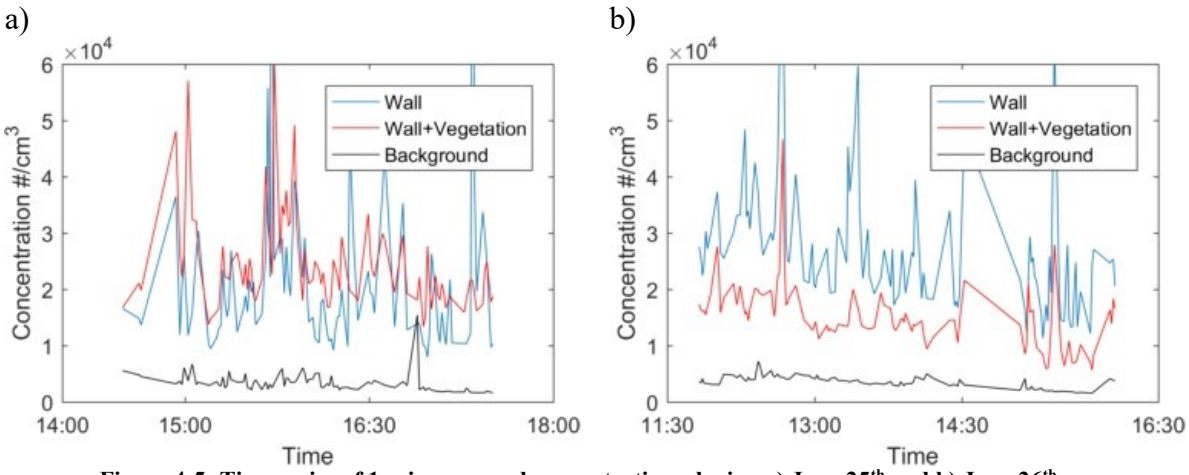

Figure 4-5- Time series of 1-min averaged concentrations during a) June 25th and b) June 26th.

The background concentrations were subtracted from the measured downwind concentrations to estimate the impact of the highway on downwind concentration. Figure 4-6 compares the UFP concentrations behind the solid barrier and wall-vegetation barrier for the entire sampling period in terms of the ratio of the measured concentrations. The trees behind the solid barrier result in smaller downwind concentrations relative to those behind the solid barrier more than 60% of the time. There is no trend in this ratio with upwind direction. On an average, the concentration behind the wall-vegetation barrier is 0.87 times the average concentration behind the wall. The median of the ratios is 0.66.

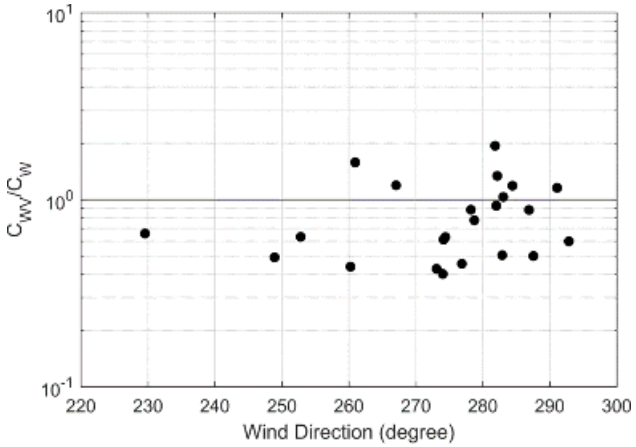

Figure 4-6- Ratio of behind wall-vegetation (C_{WV}) to behind wall (C_W) concentrations under cross-road winds.

Figure 4-7 suggests that the vegetation increases concentrations relative to those behind the wall without vegetation as the wind speed and σ_w increase; the ratio becomes larger than unity indicating that at some point the reduction in turbulence levels by the vegetation might negate the effect of the increased vertical dispersion associated with the lofting of the plume.

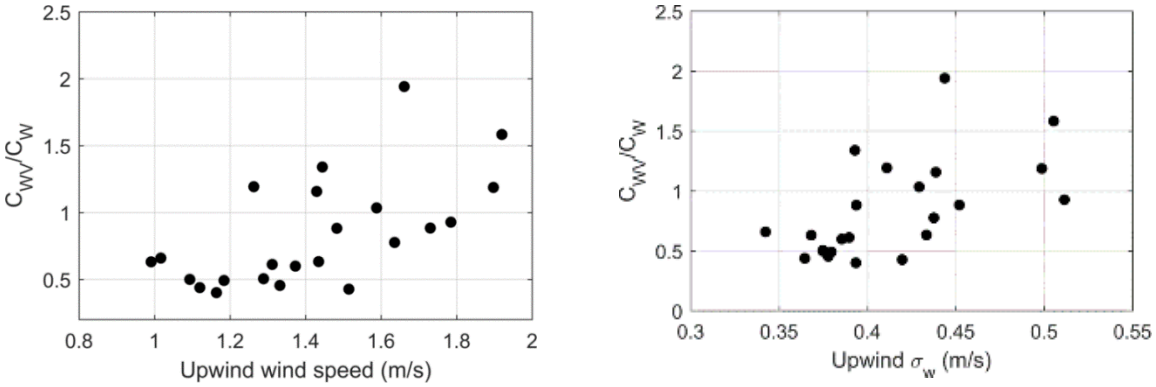

Figure 4-7- Variation of the ratio of behind wall-vegetation (C_{WV}) to behind wall (C_W) concentrations with upwind wind speed and σ_w.

4.4 Turbulence measurement

As discussed in the introduction section, adding vegetation to a flat roadway is expected to decrease downwind wind speed and turbulence levels. To examine the effects of adding vegetation to a solid barrier on downwind wind speed and turbulence, the ratio of vertical velocity fluctuations behind the wall-vegetation barrier to behind wall is shown in Figure 4-8-a. This figure indicates that adding vegetation to a solid barrier results in lower vertical velocity fluctuation, σ_w, for almost the entire sampling period. Its value is on average 0.8 times the corresponding values behind the wall, respectively. The relationship between upwind σ_w and the reduction in the turbulence behind the two walls is indicated by Figure 4-8-b. The trend in the points suggests that as the upwind turbulence increases, the vegetation increases its impact on reducing turbulence relative to that behind the wall. This supports our hypothesis that there is a point beyond which vegetation

reduces the mitigating effect of a solid wall. We cannot draw definite conclusions about when this crossover occurs without more data.

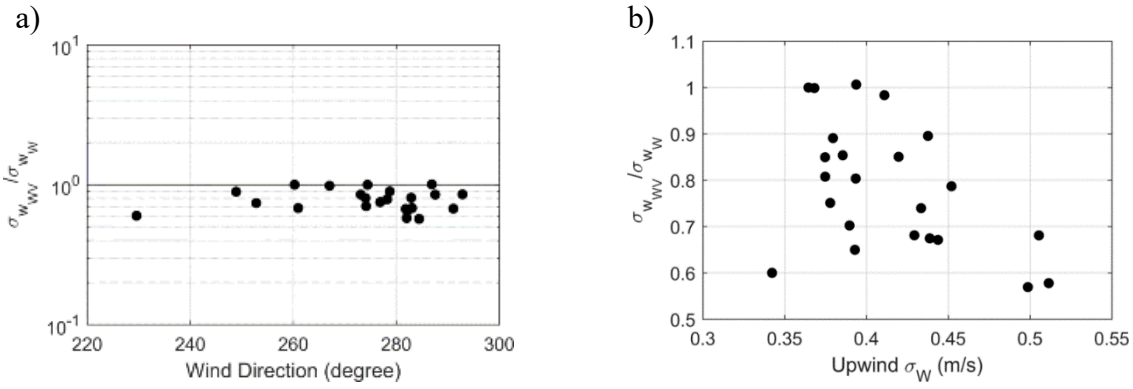

Figure 4-8- Ratio of behind wall-vegetation ($\sigma_{W_{WV}}$) to behind the wall (σ_{W_W}) vertical velocity fluctuations. b) Variation of the ratio of vertical velocity fluctuations measured downwind of the two walls as a function of upwind σ_w.

4.5 Framework of model

4.5.1 Solid barrier model

The concentration behind the barrier is assumed to be well-mixed from the surface to the barrier height. This represents the mixing induced by recirculation in the wake of the barrier. Above the barrier height, a Gaussian distribution is considered for the concentration. The model assumes that the maximum concentration occurs above barrier height at $H_p = H + \frac{\sigma_{z_B}}{2}$ where σ_{z_B} is the vertical plume spread right behind the barrier. An entrainment factor, f_m, is used to reduce the entrainment into the barrier wake during

unstable conditions to ensure that the model can describe the data from the Idaho Falls experiment(Finn et al., 2010). The entrainment factor is parameterized as Amini et al. (2016):

$$f_m = f_c + (1 - f_c)\left(1 - \exp\left(-\frac{x}{L_s}\right)\right) \tag{4-1}$$

Then the surface concentration is given by:

$$C_s = \frac{\frac{q}{\cos\theta} f_m}{f_m U(H).H.[\exp(-p_1^2) + \exp(-p_2^2)] + U(\bar{z})\sqrt{\frac{\pi}{2}}\sigma_z.[2 - \mathrm{erf}(p_1) - \mathrm{erf}(p_2)] \times [\exp(-p_1^2) + \exp(-p_2^2)]} \tag{4-2}$$

where q is the emission rate per length of the line source, U is the wind speed at half of the barrier height, θ is the wind angle from the perpendicular direction to the road, H_w is the height of the wall, σ_z is the vertical plume spread, and $U(\bar{z})$ is the wind speed evaluated at effective plume centerline. $U(H)$ is the velocity at barrier height, $p_1 = (H - H_p)/\sqrt{2}\sigma_z$, $p_2 = (H + H_p)/\sqrt{2}\sigma_z$. This model was used to predict the concentration behind the barrier next to a highway in Riverside, CA (Amini et al., 2016).

The vertical plume spread is calculated from the following equations (Akula Venkatram et al., 2013):

$$\sigma_z = 0.57\frac{u_*}{U(\bar{z})}x\left(1 + 3\frac{u_*}{U(\bar{z})}\left(\frac{x}{L}\right)^{\frac{2}{3}}\right)^{-1} \quad for\ L > 0.0 \tag{4-3}$$

$$\sigma_z = 0.57 \frac{u_*}{U(\bar{z})} x \left(1 + 1.5 \frac{u_*}{U(\bar{z})} \frac{x}{|L|}\right) \quad for\ L < 0.0$$

4.5.2 Wall-vegetation barrier model

A vegetative barrier affects downwind concentrations through the following mechanisms: 1) it deflects the particles upward and a fraction of the plume is lofted above it, 2) it reduces the turbulence levels behind the barrier which causes less mixing, and 3) a fraction of the particles deposit on the vegetation.

A simple calculation provides useful results about the order of magnitude of the deposition rate of ultrafine particles on the vegetation in the field study. The fraction of the incoming particles passing through the vegetative barrier is given approximately by

$$f = exp\left[-\left(\frac{v_d}{U}.(LAI).\frac{t}{H}\right)\right] \tag{4- 4}$$

where LAI is the leaf area index, U is the overall incoming wind speed, t and H are the thickness and the height of the vegetation, and v_d is the deposition velocity. To find the minimum value for the fraction, we take v_d to be the largest value corresponding to deposition of UFP on pine leaves reported by which is around 4 cm/s (Petroff et al., 2008b). The pine leaf LAI is around 5, and we take U to be 1.5 m/s (the mean wind speed at 5m AGL in our measurement is 1.44 m/s) (Vong et al., 2010). The thickness is taken to be 4 m, and the height to be 15 m. This results in 97% of the particles passing through the barrier.

We can compare this reduction to the reduction by the dispersion and lofting which is caused by a barrier and compare it to a no-barrier case at $x = 4\ m$ distance from

downwind edge of the highway using equation (2). For $W = 42\ m/s, H_w = 5m, u_* = 0.3$, and wind speed $U = 1.5\ m/s$ at the neutral condition, we have a 38% reduction. We conclude that the effect caused by deposition is small compared to the lofting and dispersion effects, which allows us to focus on the impact of dispersion on reducing concentrations downwind of the barrier.

Recall that the vegetation has the following effects on dispersion: 1) it lofts the plume increasing vertical dispersion, and thus decreasing concentrations, 2) it decreases downwind turbulence, which in turn has two opposing effects: it reduces entrainment of plume material into the wake, reducing concentrations close to the wall, but at the same time decreases dispersion of the plume being entrained into the wake. The combination of these effects for vegetation-wall barrier can result in either increasing or decreasing concentrations relative to the solid barrier depending on the distance from the barrier and the upwind meteorology.

As the first step in modeling the complex effects of vegetation, we applied the modified mixed wake model, described by Equations (1) to (2) to interpret the results. We accounted for the effects of vegetation through three modifications: 1) the friction velocity is multiplied by the ratio of vertical velocity fluctuation behind the wall-vegetation, ($\sigma_{w_{wv}}$), to wall barrier, (σ_{w_w}), to model the reduction of turbulence by the vegetation, 2) the entrainment of material into the wake, given by Equation (1) is multiplied by the ratio of turbulent velocities, and 3) the effective height of the wall is increased to account for additional plume lofting induced by the vegetation:

$$C_s \tag{4-5}$$

$$= \frac{\frac{q}{\cos\theta} f_m}{f_m r U(H).H_{wv}.[\exp(-p_1^2) + \exp(-p_2^2)] + U(\bar{z})\sqrt{\frac{\pi}{2}}\sigma_z.[2 - \mathrm{erf}(p_1) - \mathrm{erf}(p_2)]}$$

$$\times [\exp(-p_1^2) + \exp(-p_2^2)]$$

where $H_{wv}$is the equivalent wall-vegetation height and σ_z is calculated using equation (4-3) with changing friction velocity to $u_{*_{WV}} = ru_*$ where $r = \sigma_{w_{wv}}/\sigma_{w_w}$.

4.6 Modeling results

There is a large uncertainty in the UFP emission factor. Different studies have found emission factors of a mixed vehicle fleet to lie in the range 10^{12}~$10^{14}\frac{\#}{km.veh}$ (Kumar et al., 2011). We treat the emission factor as an unknown parameter and its value is obtained by fitting the model estimates to the observations. The emission factor was found using concentrations at the wall section and equation (2). The calculated emission factor, along with concentrations behind wall-vegetation barrier, was utilized to obtain the vegetation equivalent barrier height (equation 4-5).

The number of trucks was included in the traffic data. Trucks are considered Heavy Duty vehicles (HDV) and the rest of the fleet is considered as Light Duty Vehicle (LDV). The emission factor ratio of HDV to LDV calculated using the EMFAC model inventory for $PM_{2.5}$ turns out to be 25 (https://www.arb.ca.gov/emfac).

The effective height of the vegetation-wall barrier was adjusted to ensure that the UFP emission factors behind the two walls were approximately the same. The equivalent barrier height for the wall-vegetation barrier turns out to be 7.5 m. The common emission factor is 2.26×10^{14} which lies within the reported range in the literature (Kumar et al., 2011; Morawska et al., 2008). Analysis of the upwind meteorology indicated that the roughness length is 0.2 m.

Figure 4-9 shows the comparison between modeled and observed values for wall and wall-vegetation barriers. The correlation between model estimates and observed values is small. However, all the model estimates are within the factor of two of the observations at the wall section. For the wall-vegetation barrier, 96% of the estimated concentrations lie within the factor of two of the observed concentrations. The model is able to predict the correct concentration magnitudes.

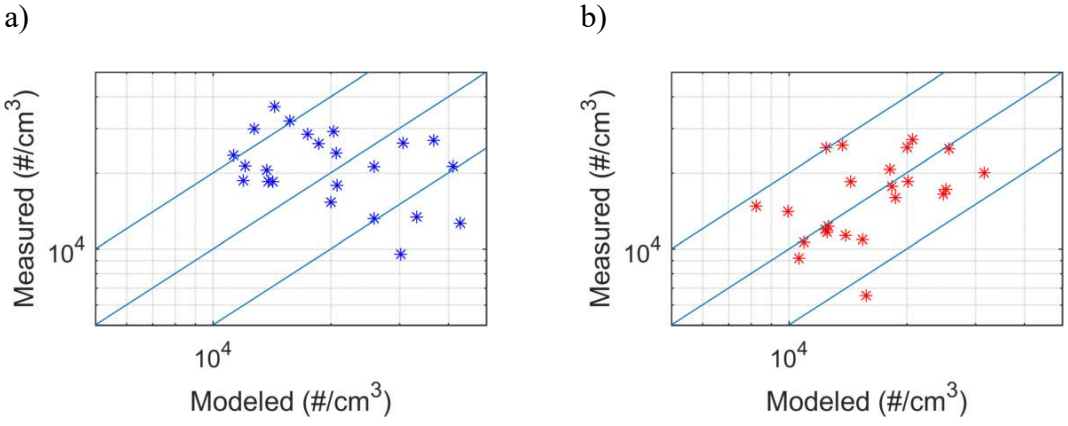

Figure 4-9- Comparison of measured and modeled concentration for a) wall barrier, and b) wall-vegetation barrier.

Figure 4-10 shows the quantile-quantile plot of modeled and measured values in both sections. that the results show that the model provides a good description of the observed concentration distributions behind the two barrier sections.

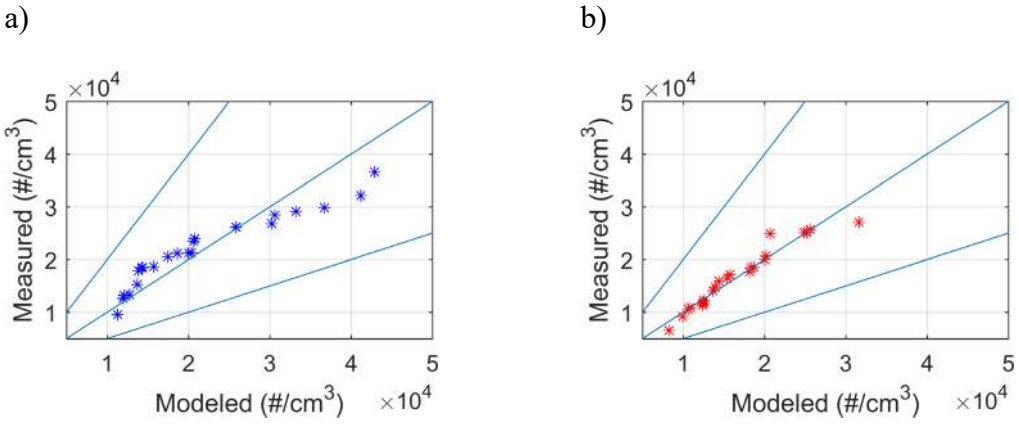

Figure 4-10- Quantile-quantile plot of measured and modeled values of a) wall barrier and b) wall-vegetation barrier.

Figure 4-11-a compares the modeled concentration gradients for the wall, vegetation-wall, and no barrier case. Figure 4-11-b shows the concentration ratios of the wall and a wall-vegetation barrier to no barrier case versus downwind distance. The averaged values were used for traffic and meteorological data during days 4, 5, and 6 since the downwind meteorological values were only available for these days. The wind speed is 1.42 m/s, the friction velocity is 0.3 m/s, and the ratio of σ_w ($\frac{\sigma_{w_{wv}}}{\sigma_{w_w}}$) is 0.78.

Both configurations result in reduction of concentrations comparing to those in flat terrain. At $4\,m$ where measurements were made, the wall reduces the concentration by 80% relative to its value without any barrier. The vegetation-wall barrier reduces the

concentration by 85%. The model shows that adding vegetation to a solid barrier reduces concentration.

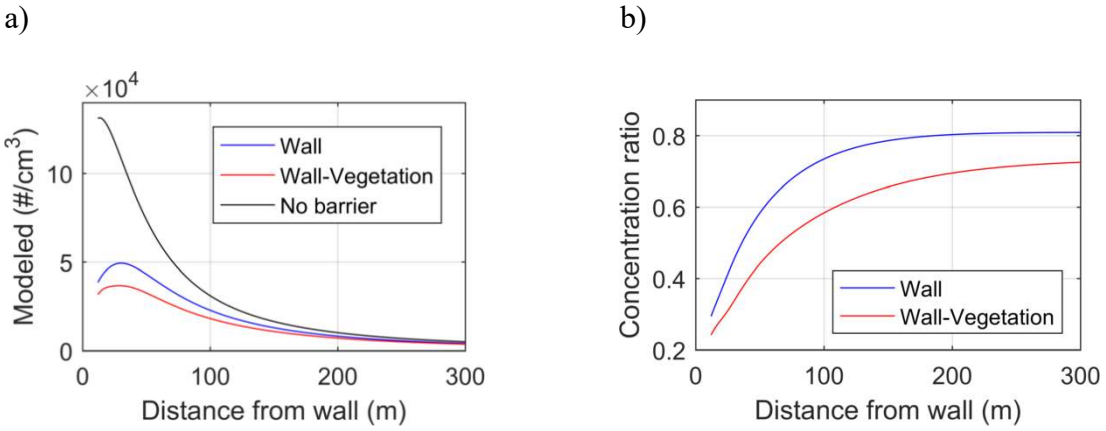

Figure 4-11- a) Concentration gradients predicted by the model for the wall, wall-vegetation, and no barrier cases and b) concentration ratio of wall and wall-vegetation to flat terrain. The traffic and meteorological conditions are the averages of July 25th, 26th,

4.7 Summary and conclusions

We conducted a field study to compare the effects of solid barriers with wall-vegetation barriers on the dispersion of the pollutants. During three days, the concentration and turbulence levels were measured simultaneously downwind of a solid barrier and vegetation-wall barrier in Sacramento, CA next to a congested freeway. Another set of instruments were installed at an upwind location. The main factors for choosing this site was: 1) no major pollution source was present in the area, 2) the solid barrier was uniform and extended for a long distance, 3) the vegetation was uniform in height and type of tree, and 4) we had access to very close distances behind the barriers.

The vegetation was found to reduce the turbulence levels behind barrier compared to the wall barrier. Behind the wall-vegetation barrier vertical velocity fluctuation (σ_w) were measured to be 0.75 of the corresponding values behind the wall barrier. This shows that the vegetation is reduces the turbulence levels consistently. Moreover, we have observed that increasing the upwind turbulence level increases the effect of the vegetation-wall barrier in reducing the downwind turbulence levels relative to the solid barrier. An average reduction in concentration was also observed for the wall-vegetation barrier. The average concentration levels behind the vegetation-wall barrier were 0.87 of the corresponding values behind the wall. Although the observation showed that vegetation behind a solid barrier can cause a reduction in concentrations in general, this was not the case for all of the observed data.

A model was used to evaluate the data from the barrier site. The model was previously used for other field studies (Amini et al., 2016). Due to the uncertainty in the UFP emission factor, we treated the emission factor as an unknown parameter. We used the observed concentrations at the wall site to estimate the emission factor. The emission factor was found to be $2.26 \times 10^{14}\ \#/(km.veh)$. We accounted for the effects of vegetation through three modifications: 1) the friction velocity is multiplied by the ratio of vertical velocity fluctuation, σ_w, behind the vegetation-wall to wall barrier to model the reduction of turbulence by the vegetation, 2) the entrainment of material into the wake is reduced by the ratio of turbulent velocities, and 3) the effective height of the wall is increased to account for additional plume lofting induced by the vegetation.

The evaluation of the model with measurements indicates that over 90% of the model estimates were within a factor of two of the corresponding observations, although the correlation was poor. The distributions of modeled values compared well with that of the observed UFP concentrations. The model shows that the barrier can reduce concentrations near a major line source like a highway compared to the flat train. It also showed that adding vegetation to a solid barrier increases the lofting effect of the barrier which leads to concentration reduction. On the other hand, vegetation decreases the downwind turbulence levels that cause higher concentrations. Our observations indicated that adding vegetation decreases concentration when the turbulence reduction was small which occurred at most of the sampling period. The deposition effects of a vegetation barrier were shown to be negligible.

5 Using Low-Cost Air Quality Sensor Networks to Improve the Spatial and Temporal Resolution of Concentration Maps

5.1 Introduction

Several studies indicate that exposure to fine particulate matter ($PM_{2.5}$) concentrations are associated with cardiovascular diseases (Brook et al., 2017). There is a strong correlation between long-term exposure to fine particulate matter and lung cancer, cardiopulmonary mortality, asthma (Khreis et al., 2017; Pope III, 2002). These results have motivated the expansion of programs to measure $PM_{2.5}$ concentrations in several affected communities.

Moreover, the issue of air quality is also a matter of environmental justice since most of the people who live or work near polluted areas often have low incomes, and are

therefore less able to control their living and working conditions, move away from the polluted areas, and are more at risk of the negative health outcomes associated with exposure to vehicle emissions (Houston et al., 2008; Mitchell and Dorling, 2003).

Most of the monitoring networks currently maintained by State and Federal Agencies do not provide the information at the spatial and temporal resolution required to assess the impact of pollution sources on health. For example, assessing the impact of vehicle emissions on the health of people living next to highways requires a spatial resolution of tens of meters. Because expansion of networks with currently accepted instrumentation is expensive, agencies are considering monitors that are relatively inexpensive but might require calibration against currently used monitors at regular intervals. These monitors, referred to as Low-Cost Air Quality Monitors (LCAQM), can expand the capability of current networks once their accuracy has been evaluated (Mead et al., 2013; E. G. Snyder et al., 2013; White et al., 2012). The USEPA and the South Coast Air Quality Management District (SCAQMD) have established programs to relate measurements from LCAQMs with those from Federal Equivalent Methods (FEM) used in current networks.

Recent development in sensor technology has improved the performance of low-cost sensors (Hagler et al., 2014; Wang et al., 2015). The data gathered by these sensors can enhance the information provided by traditional networks(Castell et al., 2017), and thus provide significant information for air quality management purposes. However, these sensors are usually irregularly spaced and usually concentrated in small areas. They also

require constant service and there are also gaps in their measurement since they are less reliable than regulatory stations. This creates the need to improve the quality of the data gathered by these sensors especially for developing concentration maps.

Several communities have already installed networks of LCAQMs to gauge their usefulness. The Imperial Valley Air Pollution Agency has more than 40 Dylos monitors over the Valley. The relatively high density of the network provides an opportunity to apply methods to increase the spatial and temporal coverage of the network. The Land Use Regression (LUR) is one such method, which achieves this objective by relating measurements to land use factors through linear models (Hoek et al., 2008; Levy et al., 2002; Ryan and LeMasters, 2007). Once the model has been calibrated with measurements, it can be used to estimate concentrations at a location of interest using local land use factors as inputs. However, the LUR model can only provide a static picture of the spatial distribution in that pollutant emissions are not explicitly treated in the model. This means that we cannot estimate the change in the concentration field in response to emission changes.

LUR models have been used widely only because 1) they are based on land use variables, 2) they do not require an understanding of the processes that govern the concentration field and 3) they do not require emission or meteorological inputs. Here, we show how dispersion models can be used to construct the concentration maps that LUR models provide. Because dispersion models relate source strength to air quality they can

be used to predict changes in the concentration field when emissions change(Hoogh et al., 2014).

In this Chapter, we examine the feasibility of using a dispersion model to increase the spatial and temporal resolution of the LCAM network. The approach consists of using the model to estimate the unknown emissions that provide the best fit between model estimates and LCAQM measurements. The residuals between the model estimates and measurements can be then used to create a spatial map at the desired resolution, where the model estimates provide the underlying trend. This approach, which has been illustrated in other previous studies (Pournazeri et al., 2014; Schneider et al., 2017; a Venkatram, 1988), has two advantages: 1) it is based on the governing physics, and 2) it allows the examination of the impact of emission changes on the spatial pattern of concentrations. In this chapter, we apply this approach to interpret the $PM_{2.5}$ concentrations measured by the Dylos network in the Imperial Valley during 2017.

We use the following the steps to apply the dispersion model: 1) Specify sources through their locations and geometry and assign unit emissions to them. Boundaries are treated as lie sources and the entire Valley is modeled as an area source. 2) Construct meteorological inputs for the dispersion model using routine meteorological measurements from an airport located in the valley, 3) Run dispersion model with unit sources and regress model results on measured concentrations to estimate emissions from sources, and 4) Use estimated emissions and meteorological inputs to estimate concentrations at locations of interest.

5.2 Sensor and source locations

Imperial Valley is located in southern California in Imperial County. It is bordered by the Colorado River to the east, the Salton Sea and San Diego County to the west, the US-Mexico Border (Mexicali) to the south, and Riverside County to the North. Most of the land in the Valley is devoted to agricultural activities. According to the California Air Resources Board (CARB), most of the PM emissions in the valley originate from unpaved roads and fugitive windblown dust within the valley (CARB, 2018b). Windblown dust from the desert on the west also makes a contribution to the $PM_{2.5}$ concentrations. Emissions from Mexicali have an impact on concentrations in the southern part of the valley. Historically, the county exceeds California's standards for particulate matter air pollution especially in the southern city of Calexico.

The regulatory air monitoring system in the area consists of 5 FEM stations that measure different gaseous and particle pollutants. Three of these stations measure $PM_{2.5}$. A network of low-cost sensors (IVAN) in Imperial Valley was developed in response to the community's concerns about the air quality and their desire for more local level data (English et al., 2017). This is one of the largest community-based air monitoring networks in the US and is considered the first community-designed network of its size in the world. The network uses modified light-scattering particle counters, DC 1700, manufactured by Dylos Corporation. The particle counter provides four size bin measurements that can be

accessed in real-time through the internet (>0.5um, >1.0 um, >2.5 um, and >10 um) (Carvlin et al., 2017).

The Dylos measurements are well correlated with regulatory ground station sensors. The data, which is displayed online through a website (www.ivan-imperial.org/air), show that, with relative humidity corrections, the $PM_{2.5}$ concentrations from the Dylos instruments can be related to measurements from multiple reference instruments. About 40 of these sensors were operational during most of 2017 (Figure 5-1).

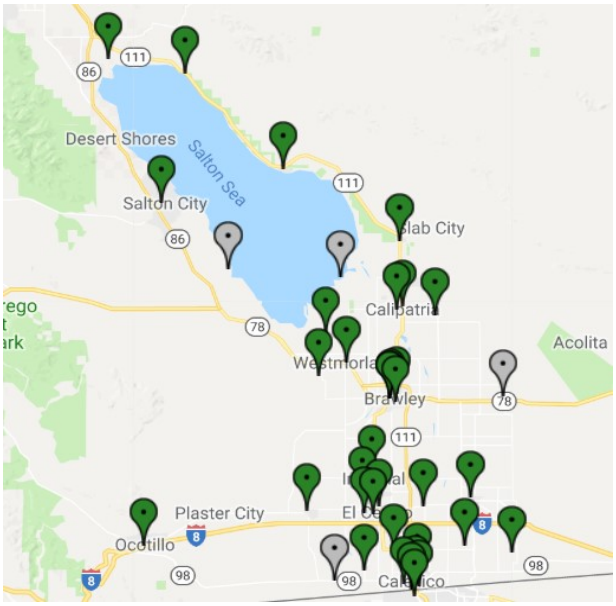

Figure 5-1- Map of low-cost sensors in the Imperial Valley

5.3 Validation of sensor performance

In this section, we investigate the performance of low-cost sensors against regulatory stations to validate the data. Dyloses have been tested by the South Coast Air

Quality Management District. Their study showed that PM measurements from the Dylos sensors are well correlated with measurements with the reference instruments in both field and laboratory studies (http://www.aqmd.gov/aq-spec/product/dc1100-pro).

The comparison shows that the sensor underestimates the values compared to the regulatory station. However, the correlation factor is 0.72 which shows that the measurement is reliable. Correlation factor is also higher than what has been observed for Calexico before (Carvlin et al., 2017). 85 percent of the observations from the low-cost sensors fall within the factor of two of regulatory station observations.

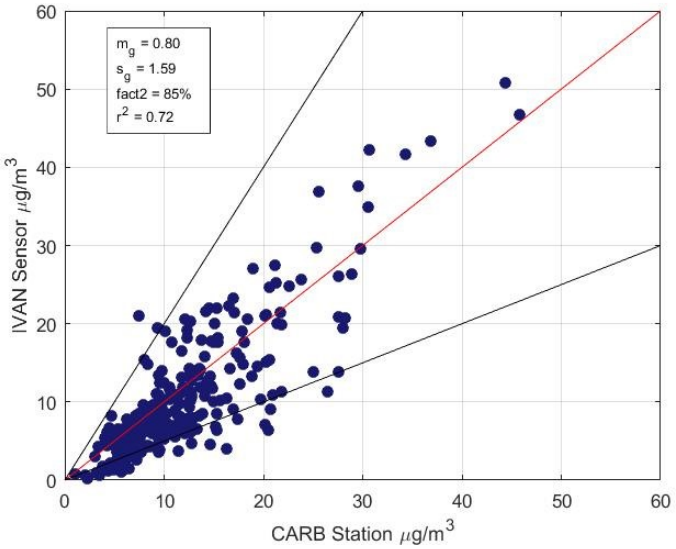

Figure 5-2-Daily averaged concentrations of Sensors compared with regulatory measurements

5.4 Modeling framework

To model the concentrations measured by the sensor network, the potential sources in the area are represented with two types of sources. The agricultural part of the valley was considered as one area source with the initial vertical spread of 2 m. This source represents local area PM sources including unpaved roads, dust from farmlands, and traffic.

Particulate matter can be transported into the valley from across the borders from

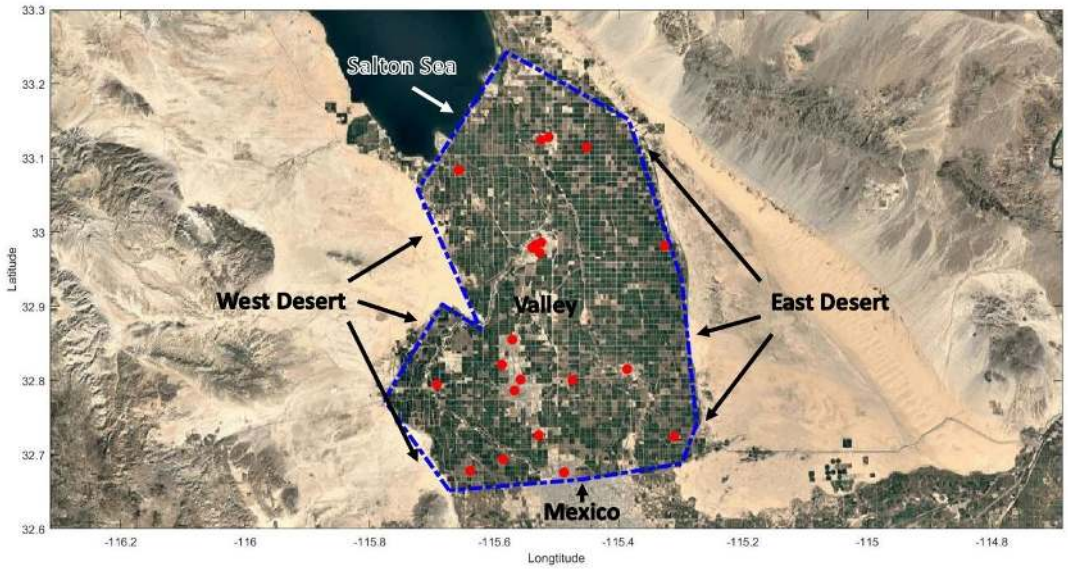

Figure 5-3- Locations of sources used in the dispersion model.

different sources including dust from the deserts and Salton Sea and emissions originating from activities in Mexico. The areas bordering the valley are represented as line sources with an initial vertical spread of 10m, which accounts for the vertical spread of emissions upwind of the borderline sources. We present results from sensitivity studies to examine

the impact of this initial plume spread on estimates of emissions from the line sources. Figure 5-2 shows the map of Imperial Valley and assumed sources in the model.

We use 11 straight lines, laid along the borders of the valley, to represent different source regions that can contribute to the $PM_{2.5}$ concentrations in the Valley. The line sources on the west side of the valley represent the desert, which is referred to as West Desert. The southern edge of the Salton Sea is represented as a separate line source. Line sources on the east represent the East Desert. The line sources on the south side represent emissions from Mexico.

The line sources are modeled using the approach in R-LINE (M. G. Snyder et al., 2013; A. Venkatram et al., 2013). The area source is modeled using the approach in AERMOD (Cimorelli et al., 2005) in which the area integral represented the contributions from sources upwind of a receptor is evaluated with a set of line sources perpendicular to the wind; the number of line sources is determined by the convergence criterion used to evaluate the area integral.

The concentrations from each source were calculated for each location using a unit emission rate. Then the concentrations from different lines are grouped together to represent different sources: West Desert (C_W), Salton Sea (C_S), East Desert (C_E), Mexico (C_M), and Valley (C_V). Then, the emissions from each of the source locations are the non-

negative regression coefficients of the following linear equation that provides the best fit to the observed concentrations, C_{oi}, in the least squares sense

$$C_{oi} = E_w C_{Wi} + E_s C_{Si} + E_E C_{Ei} + E_M C_{Mi} + E_V C_{Vi} + \epsilon_i \quad (5\text{-}1)$$

where *'i'* corresponds to the location of the Dylos sensor, E_W, E_S, E_E, E_M, and E_V are the total emission rates of West Desert, Salton Sea, East Desert, Mexico, and Valley, and ϵ_i is the residual at the receptor.

5.5 Meteorological inputs

The meteorological inputs for the model were derived using the AERMET(Cimorelli et al., 2005) processor from routine measurements made at the Imperial County Airport Meteorological station (KIPL) near El Centro. Hourly data shows that the wind is predominantly from the west and southwest (Figure 5-4). High winds are common during the daytime and low winds usually happen during the night. Most of the low wind speeds happen during the westerly winds. Representing the meteorology over the large area of the valley with measurements from a single station introduces uncertainty in the modeling exercise; it can be improved by using data from multiple stations or outputs from a meteorological model.

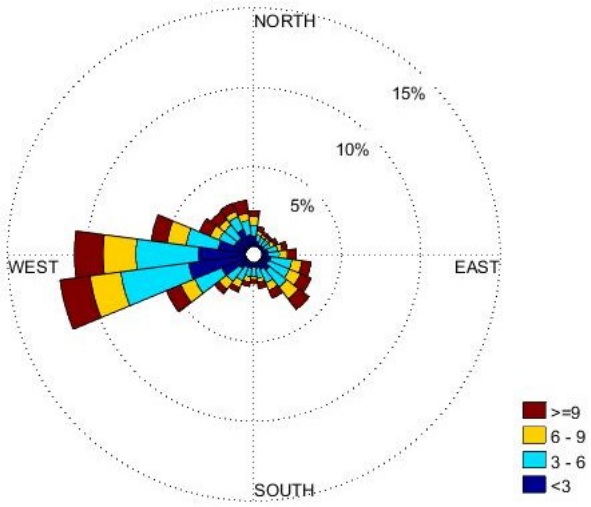

Figure 5-4- Wind rose at KIPL station

5.6 Concentration measurement

The measurements from 36 stations were available during 2017. The sensors that were not running for at least six months of the year were filtered out. Moreover, some of the sensors that were showing high concentration values that were inconsistent with the concentration levels in Calexico were filtered. Figure 5-5 shows the sensor locations with the average annual recorded concentrations which were working for more than 75 percent of the year. Typically, the highest concentrations occur in the southern part of the valley. This is consistent with regulatory reports and measurements (CARB, 2018b; Quintero-NUfiez and Sweedler, 2004).

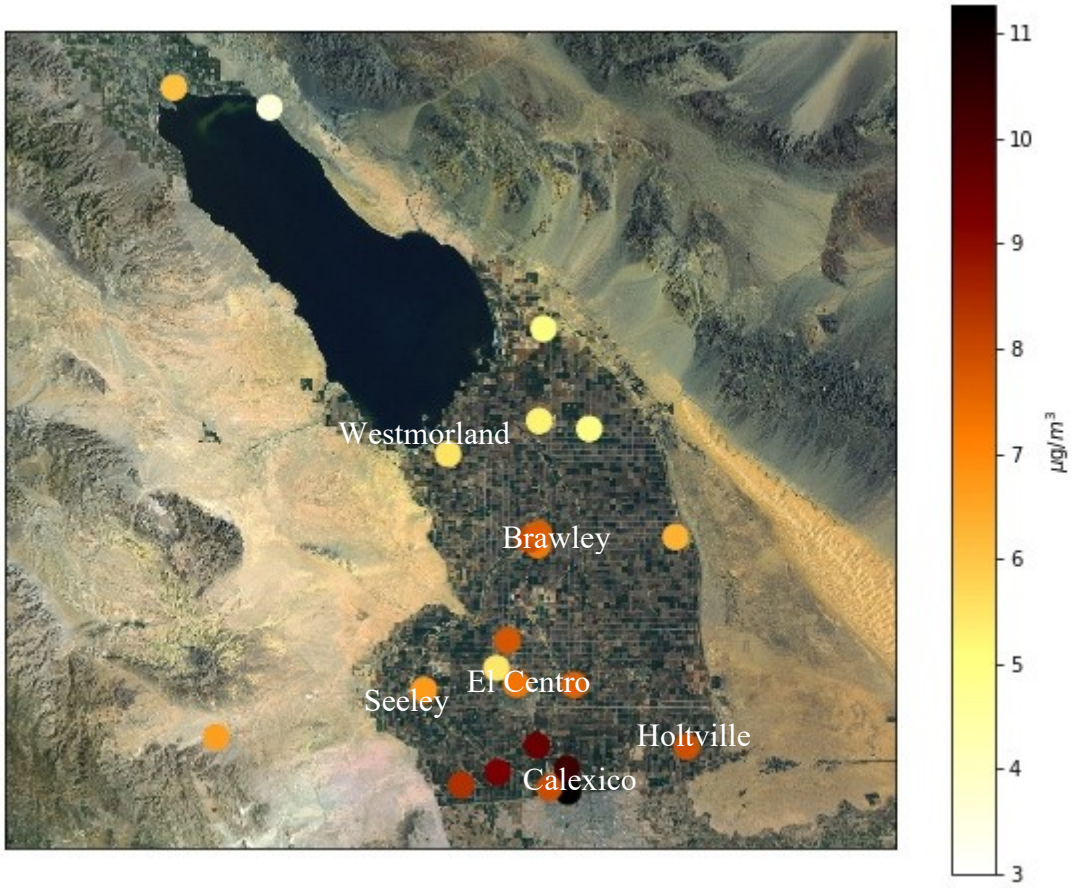

Figure 5-5- The average concentrations for the different sensors in the IVAN system.

5.7 Modeling results

We first considered annually averaged $PM_{2.5}$ concentrations in estimating emissions. The model was fitted to sensor data only if it was operational for at least six months during 2017. This filtering resulted in 21 sensors being considered in the analysis. Only hours with friction velocities above 0.1 m/s were considered to avoid conditions that are considered by AERMET to be calm conditions and have high uncertainty.

We applied the model to the data with three different averaging periods: yearly, monthly, and daily values. For each averaging time, the concentration from each potential source is found for each hour and then averaged for the averaging period. Using these estimates with the averaged observed values in the same period, the best fit line is applied through equation 1 and emission rates are calculated for specific averaging time.

We use two different approaches in periods to calculate the emission rates through regression and compare them with each other to verify the findings. First, we average the annual observation value for each station. Then we calculated the effect of each possible source for unit emission of every hour and average it annually to regress with the calculated annually averaged observation to find the emission rates using equation 5-1.

Figure 5-6-a shows the model performance for annually averaged data. We explore the performance of the model by checking the factor of two percentage and geometric standard deviation (Venkatram, 2008). All of the model estimates fall between the factor of two of the observations, and the geometric standard deviation is s_g=1.15.

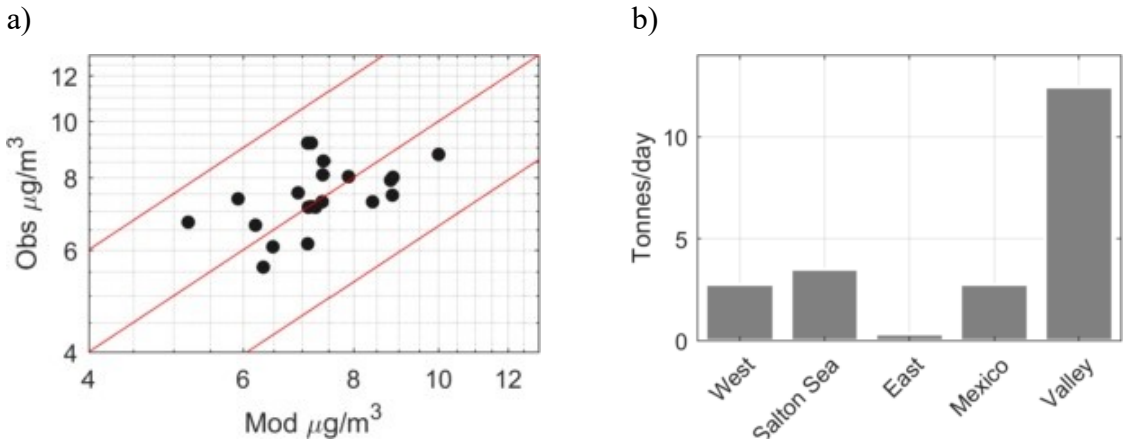

Figure 5-6- a) Model performance for annually averaged data (red lines show factor of 1.5 of observation). b) Emission rates for yearly analysis of model

Figure 5-6-b shows the estimated emission rates from different sources. Based on this model, most of the pollutants are emitted within the valley during the year. California Air Resources Board (CARB, 2018b) estimates the average PM25 emissions to be 11.7 tons per day. Our model estimates it to be 12.4 tons/day. The Salton Sea emits 3.5 tons per day while the west desert emission is 2.8 tons per day. These results indicate that on an annual basis, the observed $PM_{2.5}$ concentrations are dominated by local sources. East Desert has the lowest contribution by emitting 0.34 tons per day for the year. This is mainly because the dominant wind direction was westerly which would bring the pollutants from the Salton Sea and west desert more often. Mexico has also a considerable contribution of 2.8 tons per day.

We use bootstrapping to estimate the 95% confidence intervals for the estimated emissions. The residuals between model estimates and observed $PM_{2.5}$ concentrations are added randomly to model estimates at each receptor to create pseudo-observations which

are then fitted to model estimates to create a distribution of emissions. The 95% confidence interval corresponds to 2.5 and 97.5 percentiles of the distributions. Table 5-1 shows the range of emission rates for different sources. The estimated emissions from the valley have the largest absolute range with 95% confidence interval of 9.0 to 15.3 tons/day.

Table 5-1-Emission rates calculated by the model for yearly averaged observation.

Source	Emission rates (Tons/day)	95% confidence interval (Tons/day)	95% confidence interval range (normalized to the best value)
West Desert	2.8	2.0 – 3.7	0.6
Salton Sea	3.5	1.5 – 5.8	1.2
East Desert	0.3	0.0 – 2.5	8.3
Mexico	2.8	1.6 – 4.1	0.9
Valley	12.4	9.0 – 15.3	0.5

Another way to find the emission rates is based on the monthly averaged values. We calculated the hourly contribution of unit emission from each source at every station and averaged these contributions for each month. We regressed these calculated values with monthly averaged observation and use all of these monthly values to estimate the

emission rates. Figure 5-7 shows the performance of the model for monthly averaged data. 92 percent of model estimates fall in the factor of two of observed values.

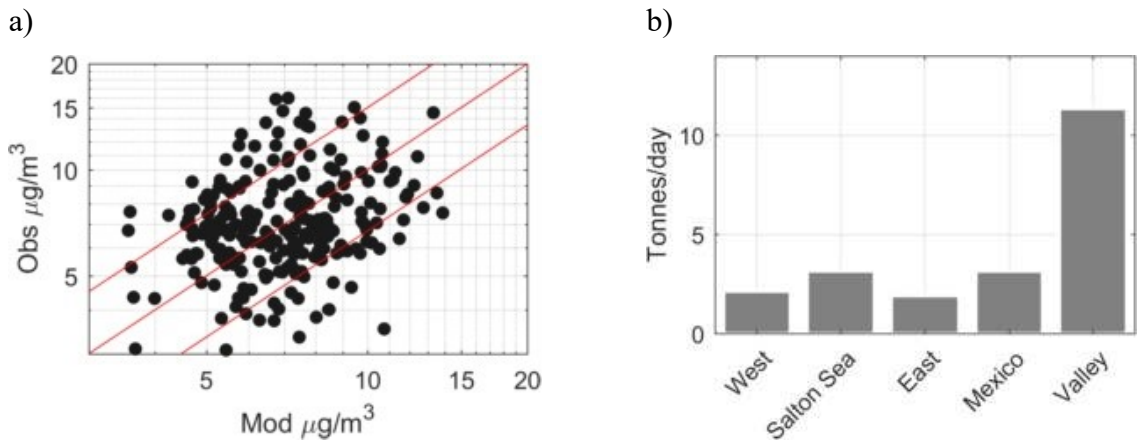

Figure 5-7- Model performance for monthly averaged data (red lines show factor of 1.5 of observation). b) Emission factors for monthly analysis of model

The results derived from monthly averaged concentrations are different from those from the annually averaged concentrations; however, they show similar trends and the values for emission rates are close to the estimates from annually averaged data. The Valley still has the highest emission rates with 11.4 tons per day, the Salton Sea emits 3.2 tons per day and west desert emits 2.1 tons per day. The estimates for Mexico is 3.2 tons per day and higher than the previous estimates from the model. East desert still has the lowest emission rate, 1.9 tons per day, but higher than the previous estimates.

Bootstrapping is applied to these results to calculate the uncertainty in the estimated emissions. The 95% percent confidence interval for annual emission rate is smaller using monthly averaged observations showing more accurate estimates in Table 5-2. For

example, the range for valley emission rates is 4.9 tons per day (9.0 – 13.9 tons per day) which is smaller than the 6.3 tons per day range calculated for the emission rate using annual averaged model. The normalized range of estimates has also been decreased for all of the emission rates in Table 5-2 compared to table 5-1. This is expected since we are using more points in our regression analysis which decreases the degree of freedom and increases the accuracy.

Table 5-2- Emission rates calculated by the model for using monthly averaged observations

Source	Emission rates (Tons/day)	95% confidence interval (Tons/day)	95% confidence interval range (normalized to the best value)
West Desert	2.1	1.5 – 2.8	0.6
Salton Sea	3.2	1.7- 4.9	1.0
East Desert	1.9	0.6 – 3.3	1.4
Mexico	3.2	2.1 – 4.3	0.7
Valley	11.4	9.0 – 13.9	0.4

Figure 5-8 shows the performance of the model for four sensors at different locations assuming constant emission rates of Table 5-2 throughout the year. Most of the values fall in the factor of two of observations.

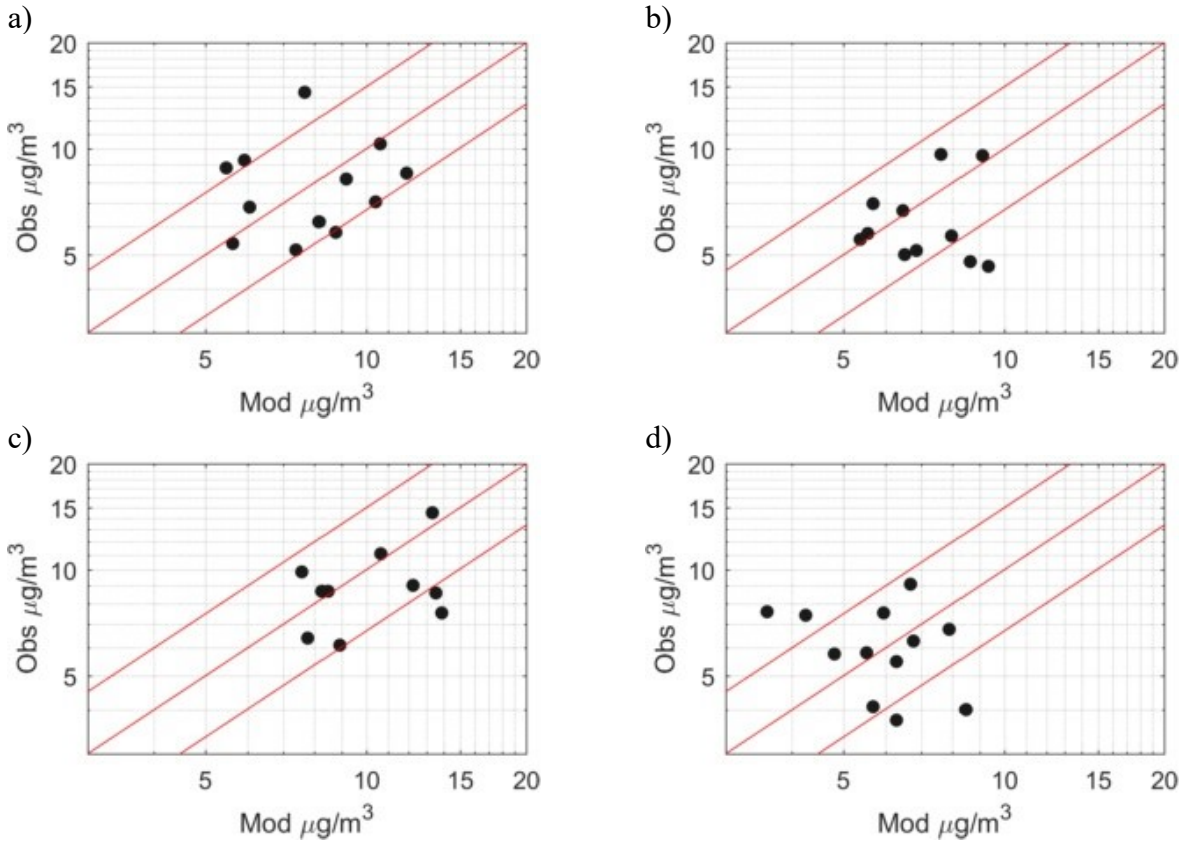

Figure 5-8- Model performance for different sensors for monthly average data at a) Brawley, b) El Centro, and c) Calexico, and d)Westmorland

To explore the model performance and the emission rates throughout the year, we ran the model for monthly averaged of data separately and found the emission rate independently for each month. We only considered sensors that had at least 100 hours each month. Table 5-3 shows the model performance correlation coefficient for monthly averaged data.

Table 5-3- Emission Rates and model coefficient factor for different months

Month	Emission Rate (Tons per day)					Correlation Coefficient Factor (r^2)
	West Desert	Salton Sea	East Desert	Mexico	Valley	
January	2.8	1.1	0	1.9	7.9	0.55
February	2.8	5.1	0	4.5	10.2	0.13
March	2.5	5.2	0	4.0	4.4	0.12
April	3.6	4.4	3.7	3.1	11.2	0.13
May	5.4	7.8	0.9	2.8	12.5	0.55
June	4.1	9.5	1.5	4.9	15.1	0.26
July	3.4	1.4	1.8	3.4	10.6	0.29
August	3.4	8.7	1.0	3.1	4.3	0.34
September	1.9	2.7	7.6	1.2	6.8	0.35
October	2.6	2.7	1.6	4.5	11.2	0.47
November	1.4	1.2	2.8	4.4	8.8	0.18
December	2.3	2.6	0	10.5	27.0	0.28

All of the observations fall in the factor of two of the observations for all of the months. The correlation coefficient can be as high as 0.55 (for January and May), while low correlations occur for a few months. Low correlations are usually associated with small variances in observed concentrations. The largest concentration variance occurs in December when the concentration varies between 7 μ/gm^3. to 25 μ/gm^3. Moreover, this month has the highest concentration levels.

Table 5-3 also shows the emission rates for different months of the year calculated by the model. The Valley is the main source of particulate matters during the year. The largest emissions come during December (27 tons per day from the Valley) when the highest concentrations happen. East Desert has usually the lowest values during the year with very high fluctuations from 0 to 7.6 tons per day. The Salton Sea is also one of the major sources of emission especially during June (9.5 tons per day) and August (8.7 tons per day). Mexico emits large amounts of emission during December (10.5 tons per day). The highest contribution of West desert happens during May when it is 5.4 tons per day.

5.8 Sensitivity of the model to σ_{z0}

Here we look at the sensitivity of the model to the initial vertical plume spread, σ_{z0} of the border line sources. This value is assumed to be 10m for the model. Figure 5-9 shows the change in emission rates with different initial plume spreads. Increasing the initial plume height reduces the emission rates coming from the valley and increases the emission rates from other sources. This is expected since increasing the initial plume spread increases the dispersion from the sources around the valley and decreases the concentrations. This will result in higher emission rates for these sources to account for the increased dispersion.

These results indicate that the emissions estimated by fitting model estimates to corresponding measurements depend on the parameters of the dispersion model. However, most of the pollution in the area originate from the Valley for different vertical plume

spreads. East Desert also contributes the least to the pollution regardless of the initial

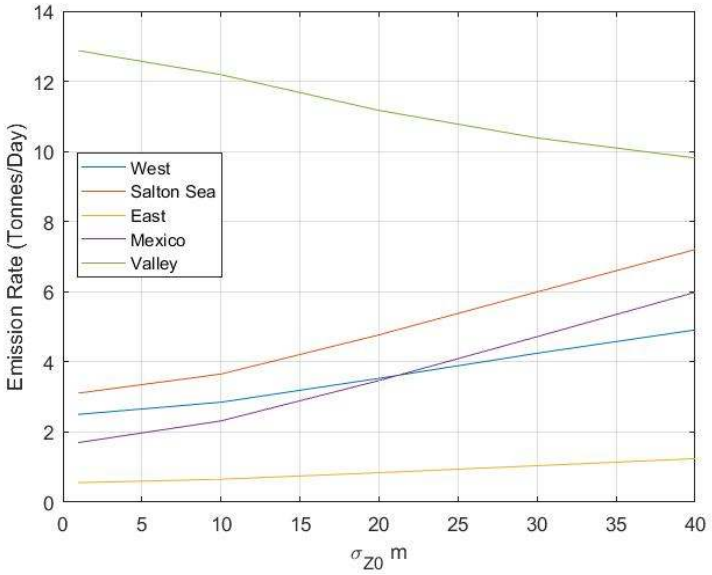

Figure 5-9-Monthly emission rates of different sources at different initial plume spread

vertical plume spread. These results can be used for emission control to mitigate the PM problem in the Valley.

5.9 Using Residual Kriging to improve concentration maps

Accurate concentration maps are needed to estimate exposure to air pollution in epidemiological studies. regulatory monitors usually have a low spatial and temporal resolution which makes it difficult to use it for community-scale assessment and research. Low-cost environmental sensors networks can provide additional air pollution data and capture the spatial variation more thoroughly. These networks can increase the resolution of ground station data, provide timely information about toxic gases, and detect the local air pollution hot spots (Jiao et al., 2016; Yi et al., 2015). This information can also provide

planners with initial data to detect the communities most impacted by air pollution and part of the solution to State Bill 617 (CARB, 2018a; SCAQMD, 2018).

As indicated earlier, LUR has been used to provide the spatial resolution required for exposure assessment. As an alternative that offers the advantages mentioned earlier, we propose a method that combines dispersion modeling with Kriging to construct spatially resolved concentration maps(Venkatram, 1988, Schneider et al., 2017). Kriging has been used commonly to interpolate observations at different locations and create maps in a variety of applications (Matheron, 1971). Simple kriging includes calculating the concentration at each point by the sum of a spatially constant mean and a local fluctuation which is assumed to be spatial isotropic and homogeneous. This might not be true everywhere since the source strength and the dispersion of pollutants are dependent on locations and meteorology.

Simple kriging assumes that the concentration estimate at one location, Z_o(x), is a linear combination of the observations:

$$Z_o(x) = \sum_{j=1}^{N} \lambda_j Z_j \tag{5-2}$$

Where Z_j are the observations at different points and λ_j are the weights assigned to each observation and is calculated based on the distance of the observation to the point x based on the following set of equations:

$$\sum_{i=1}^{N} \lambda_i \gamma_{ij} = \gamma_{io} \tag{5-3}$$

$$\sum_{j=1}^{N} \lambda_i = 1$$

where γ_{ij} is called the semi-variogram, an ensemble-averaged quantity.

$$\gamma_{ij} = < \left(Z_i - Z_j\right)^2 > /2 \tag{5-4}$$

We estimate the semi-variogram using a function of the separation distance ($h = |X_i - X_j|$) by assuming a constant trend is valid for all of the points. Different assumptions are made for this function (Gilbert and Simpson, 1985). Here we use a spherical assumption for finding the semi-variogram:

$$\gamma_{ij}(h) = C_s \left[\frac{3}{2}\frac{h}{a} - \frac{1}{2}\left(\frac{h}{a}\right)^3\right] \quad for\ h < a \tag{5-5}$$

$$= C_s \qquad for\ h > a$$

where C_s is the sill and a is the range in the variogram.

Simple kriging is not likely to be valid for concentration fields since it is only based on the distance from observation points and the underlying spatial structure that is governed by local emission sources and meteorology is ignored. Dispersion models link concentration fields directly to emissions and meteorology and include the underlying trend of the concentration field. So we can use model estimates to estimate the underlying structure in the concentration filed. Similar approaches have been used to produce finer

resolution concentration maps for different pollutants (Pournazeri et al., 2014; Schneider et al., 2017).

We can take the following steps to produce the residual kriging concentration maps:

1- Using dispersion models to estimate the concentration at monitoring stations and calculate the residuals between model and observation.
2- Use kriging to find a map of residuals at all of the grids.
3- Estimate concentrations at all grids in the study domain.
4- Add residuals to the model estimates to create concentration maps.

Figure 5-10-a shows the concentration map based on simple Kriging. The map shows reasonable spatial variation at the regions with a higher density of sensors. However, the regions close to emission sources like the West Desert, where there are a very small number of sensors, we do not observe any variation for $PM_{2.5}$ concentration.

To improve the results of a simple Kriging, we can use a dispersion model to account for spatial changes and account for the difference between the model and observed values by Kriging the residuals and adding them to the model estimates. Figure 5-10-b shows the concentration map produced by this technique. More changes can be seen spatially near the emission sources, like the Desert or the Mexican border. This allows us to see the variation at a smaller scale.

a)

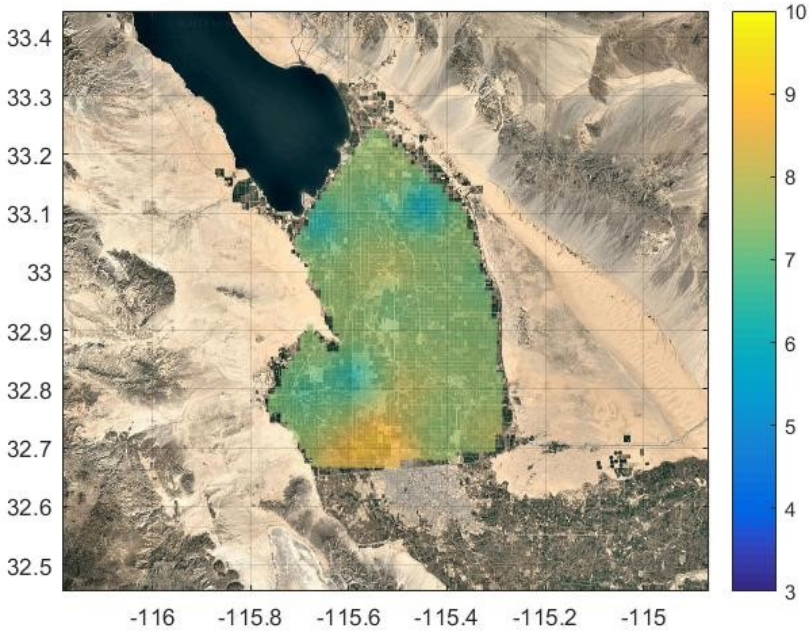

b)

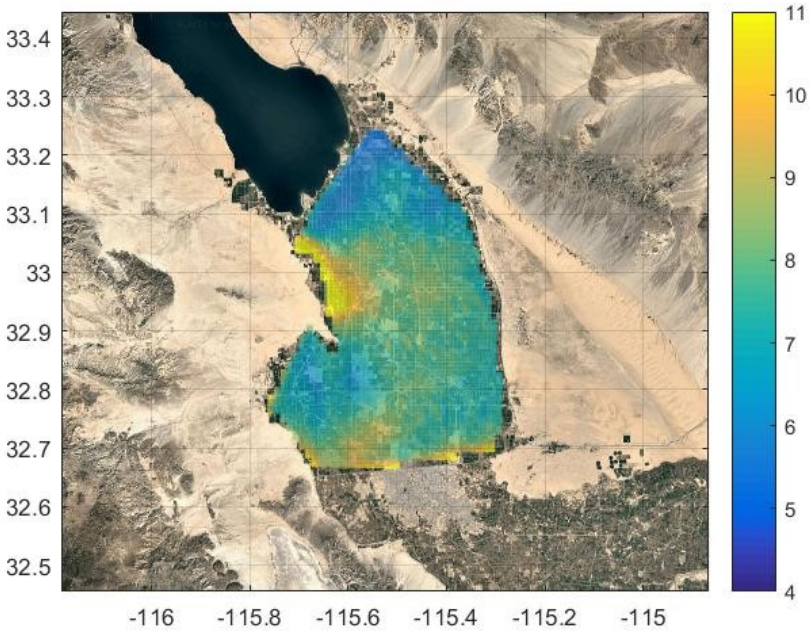

Figure 5-10- Yearly averaged $PM2.5$ concentration maps by a) simple kriging and b)residual kriging

The results from residual Kriging result in a larger variation of concentrations as seen in Figure 5-11. This shows that this approach considers the effect of local emission sources and calculates the change in the concentration fields at a smaller scale in a more realistic manner.

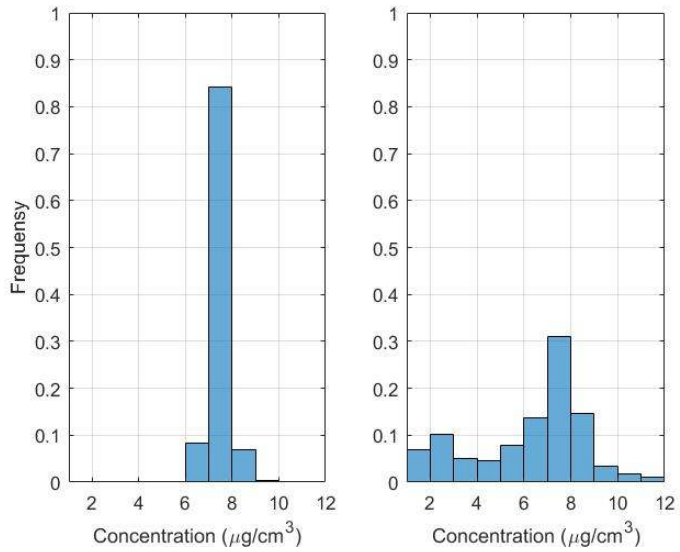

Figure 5-11- Concentration distribution in the area calculated by a) Simple kriging and b) Residual Kriging.

To validate the results from residual kriging, we use a leave-one-out cross-validation technique. We leave out a location from the observations and compare the interpolated value with the observed value. We expect to improve the interpolation results by using residual Kriging compared to simple Kriging specifically for locations with a low density of sensors. This is because at these locations we do not have any close observation if we leave the sensor out so the estimating emission structure will be helpful in estimating the concentration value.

Figure 5-12 shows the interpolation results for simple and residual Kriging compared to each other at different locations. The monthly average model with monthly average emission rate was used. Residual kriging improved the correlation coefficient from 0.05 to 0.31 at Westmorland, 0.57 to 0.62 at Seeley, and 0.77 to 0.92 at Holtville compared to simple kriging. The enhancement for areas with concentrated sensors, such as Brawley, was negligible or non-existent. This is because in the denser sensor areas the observations from sensors are close to each other and can predict each sensor's observations well with simple kriging.

a)

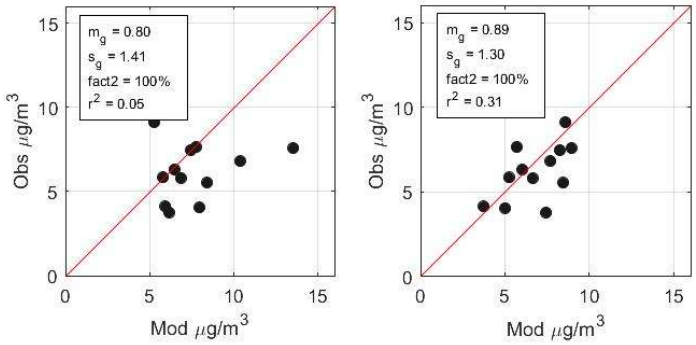

b)

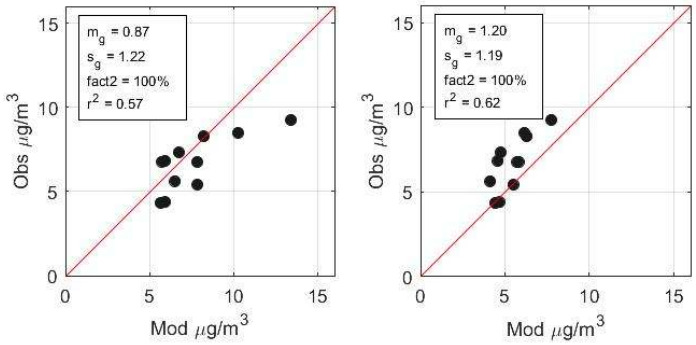

c)

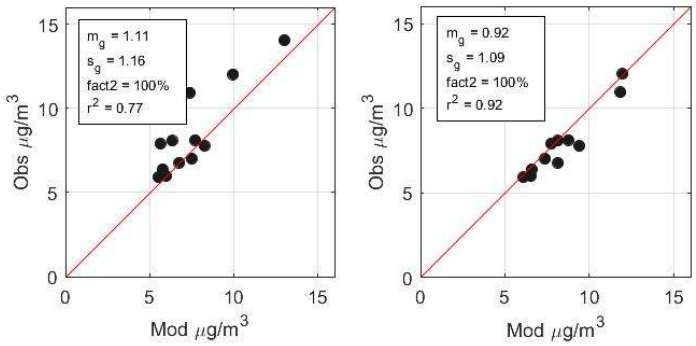

Figure 5-12- Cross-validation of using Simple kriging model (left) and residual kriging model (right) at a)Westmorland, b) Seeley, and c) Holtville.

5.10 Sensitivity analysis of kriging maps

Here we analyze the sensitivity of kriging maps with different ranges in equation 5-5. The range determines the distance over which concentrations are correlated spatially. The maps created in previous sections used a range of 10 km in the kriging algorithm. Figure 5-13 shows the concentration maps and distribution using simple kriging for two different ranges. Decreasing the range reduces the effective radius of influence of each sensor in the final map and most of the values are estimated by using the combined average concentration on the map. The histogram shows that the concentration interpolated by kriging in most of the locations are equal to the average concentration of all of the receptors and the variation of concentrations is small. Setting the range to 20 km increases the influence of each sensor which causes more variation in the concentration over the area. This can be observed in the histogram which shows a wider range of concentration.

a)

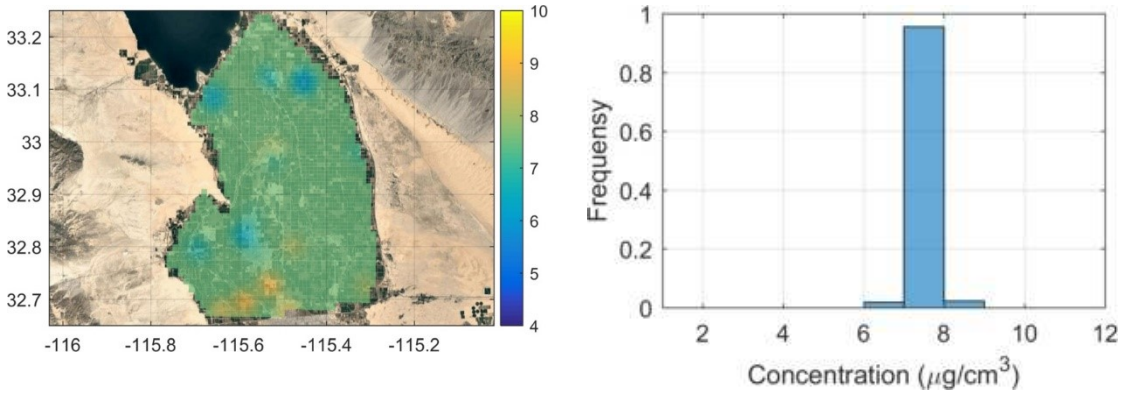

b)

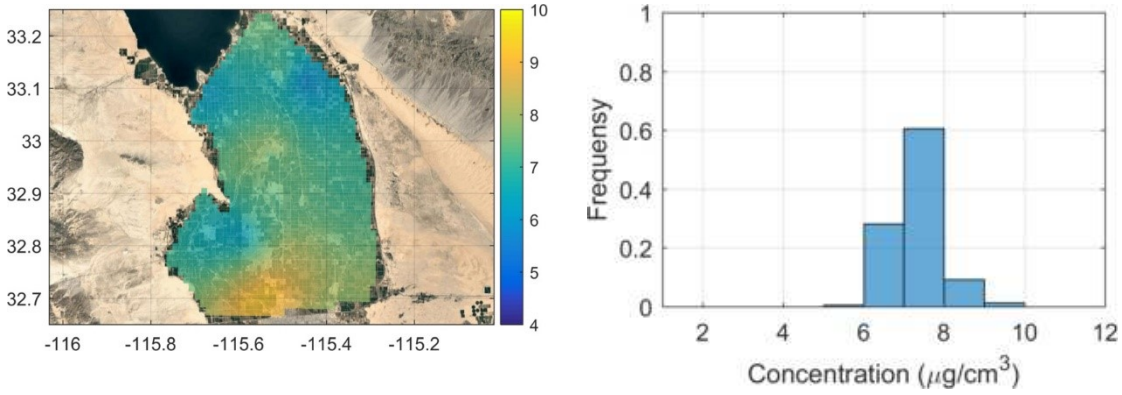

Figure 5-13- Maps (left) and concentration distribution (right) using simple kriging with a) range=5 km and b) range=20 km.

Figure 5-14 shows the results from residual kriging using 5 km and 20 km range. The maps are close to each other and 10 km range map (Figure 5-11-b). This shows that residual kriging is less sensitive to the range of variograms. Histograms change small and the estimated concentration levels at different locations are close to each other using different ranges in residual kriging. This is mainly because the model is responsible for

creating most of the map and the measurement adjust it for local sources using the observations.

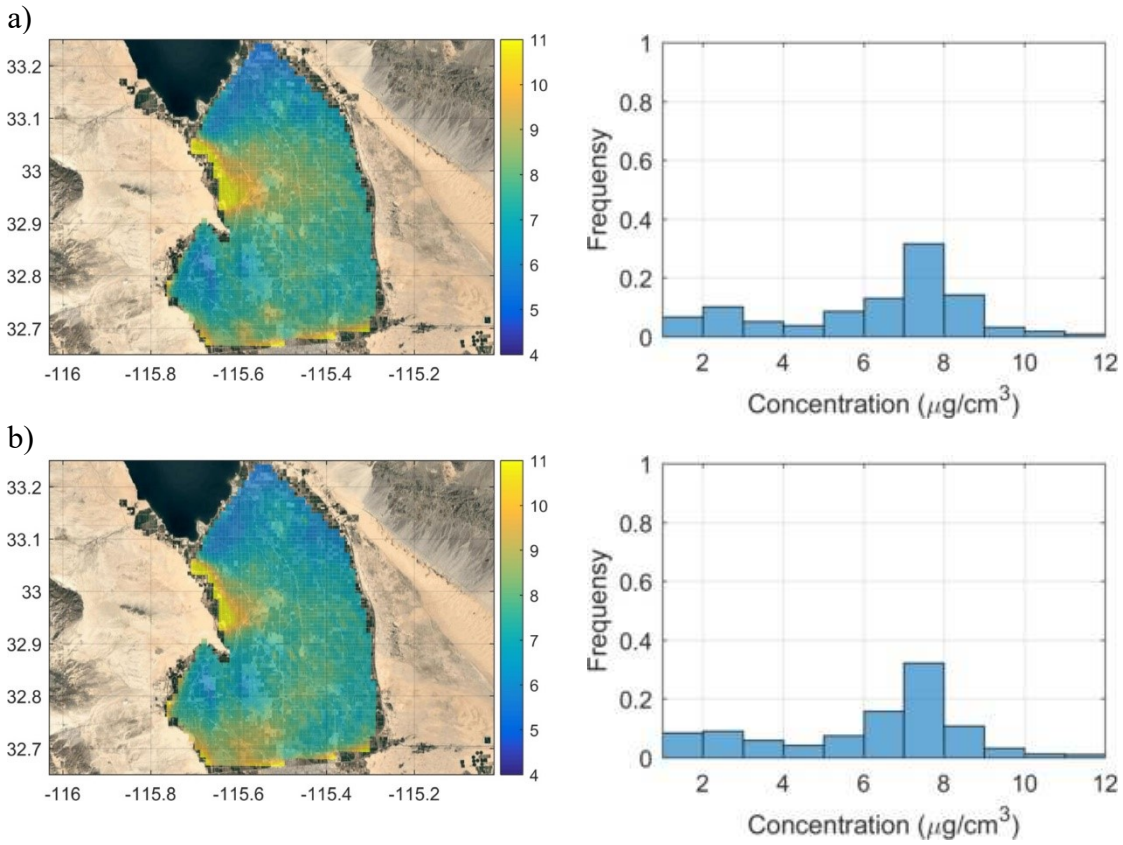

Figure 5-14- Maps (left) and concentration distribution (right) using residual kriging with a) range=5 km and b) range=20 km.

5.11 Summary and conclusions

In this chapter, we analyzed the data provided by a low-cost sensor network in Imperial Valley California. Imperial Valley is among the most polluted districts in the US in particulate matter pollution. $PM_{2.5}$ data measured from the network during 2017 was used to analyze the concentration levels at different locations and times.

A dispersion model was used to describe the concentration levels measured by the low-cost network using the meteorological data gathered by an airport wind station to derive input variables. By fitting the modeled to measured $PM_{2.5}$ concentrations we estimated the emission rates from possible sources in and outside of the Valley. Our interpretation of the data indicates that concentrations within the Imperial Valley are dominated by emissions within the Valley, which has an average emission rate of 11 to 13 tons per day which is consistent with the earlier estimates from CARB of 11.7 tons per day. The rest of the emissions originate from the Salton Sea, Mexico, and West Desert. The desert on the east of the Valley has the lowest contribution to the concentrations mainly because westerly winds were dominant.

Model results were combined with observed values to create fine resolution concentration maps by using residual kriging. We verified this technique and showed that it can improve the accuracy of common interpolation techniques, such as simple kriging. These maps can be very helpful for community-scale air quality assessments.

6 Summary and Conclusions

Exposure to elevated air pollutant concentrations causes numerous adverse health effects including asthma, birth and development effects, premature mortality, and lung cancer. The highest air pollution levels occur in large urban areas, where transportation makes the major contribution to pollutant emissions. Air pollution dispersion models are the link that connects emission sources with concentration levels using the meteorological and geographical parameters. Dispersion models are necessary tools for devising mitigating strategies.

Most air pollution mitigation plans emphasize technologies and policies to reduce emissions from transportation. In recent years, roadway design is suggested as a potential solution to mitigate near-road pollution. Downwind roadside barriers have been proved to enhance the near-road air quality by enhancing the turbulence and dispersion. Similar effects have been also observed for depressed and elevated roads. Vegetation also has been suggested as a mitigation strategy.

Flat terrain roads, which are usually the only case investigated in the current dispersion models, are rarely a real-world situation. Most of the roads have more complicated configurations and road-side structures built in for different applications.

Dispersion models are needed to explain the effect of different roadside configurations to help city planners and policymakers in air quality management policies. Chapters 2, 3, and 4 investigate the effect of roadside structures on dispersions of traffic-produced pollution.

The effects of an upwind solid barrier on near-road and on-road air quality were investigated by analyzing wind tunnel data in chapter 2. The results were used to develop a dispersion model to consider the effect of an upwind roadside barrier on the dispersion of pollutants combined with a downwind barrier. In chapter 3, a field study was conducted to examine the applicability of previously developed models to real-world measurement. In chapter 4, I investigated the effect of vegetation and solid wall combinations.

Air pollution exposure assessment needs estimating the spatial and temporal patterns of pollution concentration over the regions of interest. Traditionally, regulatory sensors have been used for this purpose because of their accuracy and reliability. However, these sensors are usually located far from each other and cannot produce fine resolution concentration maps needed for policymakers and researches. Low-cost sensors have been suggested in recent years to fill these gaps. In chapter 5, I have used dispersion models combined with the data from low-cost sensors to produce accurate temporal and spatial maps of concentrations. Moreover, I estimated emission rates from potential sources in the area of interest.

6.1 The Effect of Upwind Barriers on Near-Road Air Quality

Presence of a solid barrier at the upwind edge of the road will enhance the air quality at the downwind side of the highway. The barrier will create a recirculation zone that can cover a portion of the highway with the winds in the opposite direction of the air flow carrying the pollutants towards the wall. The barrier also acts as a source of turbulence enhancing vertical dispersion. We implemented these effects into a dispersion model to explain the concentration gradients.

The model assumes a single line source located at the barrier location to represent all of the sources covered in the recirculation zone. The initial vertical plume spread is considered to be 1/4 of barrier height to represent the increased vertical plume spread. The model was then combined with the mixed-wake model for the downwind barrier, to simulate the situation with two barriers on both sides of the highway. The models were evaluated with data from the EPA wind tunnel study data and showed generally good agreement with measured values.

The presence of an upwind barrier results in a reduction of downwind concentrations relative to the no barrier case. The effect of the barrier increases with the barrier heights and it can be as large as a downwind barrier.

Barriers on both sides of the highway result in a larger concentration reduction than either an upwind or a downwind barrier, but it is not the sum of the reductions caused by the two barriers by themselves. The effect of barrier becomes smaller at further distances

and beyond 10 barrier heights distance downwind of the two barriers, the reductions caused by the three configurations are similar.

A tentative model was also developed to find the concentration field on the roadway in presence of an upwind barrier. The model is developed based on the observation that the wind flow is blowing towards the wall on the roadway and pushes the pollutants to the barrier.

6.2 The Effect of Downwind Barriers on Near-Road Air Quality

A field study was conducted near a highway in Riverside, California to find the effect of downwind barrier on near-road air quality. The data from six days of the measurement was analyzed with two different dispersion models. The first model is a simplified version of the model presented in Schulte et al. (2014), which was referred to as the Simple Barrier Model. The second model was modified to account for reduced entrainment in the immediate wake of the barrier during unstable conditions. This was based on the observations from a previous fields study that the downwind barrier enhances the dispersion more than predicted by the models during unstable conditions (Finn et al., 2010; Schulte et al., 2014).

UFP was considered as the tracer gas in this study. The models were able to estimate the concentrations well. UFP emission factor is highly uncertain and was treated as unknown. Emission factors were calculated by fitting model estimates to measured values. The emission factors resulting from the simple barrier model is $10.3 \pm 2.39 \times 10^{13}$ #/(veh.km) (95%) and that from the modified mixed wake model is $7.04 \pm 1.49 \times 10^{13}$ #/(veh.km) (95%). The estimates were well within the range of literature.

Both models provide adequate estimates of the magnitude and the spatial variation of concentrations; the modified mixed wake model has a smaller bias. The models predict that a 4 m barrier results in a 30-45% reduction in average concentration within 40 m (10H)

of the barrier, relative to the no-barrier site. The effect of the barrier is smaller for shorter barrier heights. The average concentration reduction within 40 m is 13-20% for a 2m barrier. The good performance of the simple barrier model reinforces the conclusion from Schulte et al. (2014) that the presence of the barrier is equivalent to shifting the line sources on the road upwind by a distance of about $HU(H/2)/u_*$.

6.3 Using Vegetation to Enhance the Impact of Solid Barriers on Near-road Air Pollution

A study was conducted to find the effect of vegetation with solid wall barrier on the dispersion of traffic produced pollutants. UFP concentration and turbulence levels were measured simultaneously downwind of a solid barrier and vegetation-wall barrier in Sacramento, CA next to a congested freeway.

The vegetation acted as a sink for turbulence. Behind the wall-vegetation barrier vertical velocity fluctuation (σ_w) were measured to be 0.75 of the corresponding values behind the wall barrier. This shows that the vegetation reduces the turbulence levels consistently. We also observed that increasing the upwind turbulence level increases the effect of the vegetation-wall barrier in reducing the downwind turbulence levels relative to the solid barrier.

The effect of vegetation on concentration was uncertain. The observation showed that vegetation behind a solid barrier can cause a reduction in concentrations in general. However, this was not the case for all of the observed data and the vegetation increased concentrations relative to those behind the wall without vegetation as the wind speed and σ_w increased. The average concentration levels behind the vegetation-wall barrier were 0.87 of the corresponding values behind the wall.

A model developed by Amini et al., (2016) was used to analyze the data. Due to the uncertainty in the UFP emission factor, we treated the emission factor as an unknown parameter. The observation at the wall site was used to estimate the emission factor. The model was modified to account for the effects of vegetation by using these assumptions: 1) the friction velocity is multiplied by the ratio of vertical velocity fluctuation, σ_w, behind the vegetation-wall to wall barrier to model the reduction of turbulence by the vegetation, 2) the entrainment of material into the wake is reduced by the ratio of turbulent velocities, and 3) the effective height of the wall is increased to account for additional plume lofting induced by the vegetation. The evaluation of the model with measurements indicates that over 90% of the model estimates were within a factor of two of the corresponding observations, although the correlation was poor. The model showed that the barrier can reduce concentrations near a major line source like a highway compared to the flat train. It also showed that adding vegetation to a solid barrier increases the lofting effect of the barrier which leads to concentration reduction. The deposition effects of a vegetation barrier were shown to be negligible.

6.4 Using Low-Cost Air Quality Sensor Networks to Improve the Spatial and Temporal Resolution of Concentration Maps

The data from a low-cost sensor network in Imperial Valley was analyzed. The sensors measured $PM_{2.5}$ concentrations for over 20 locations across the valley. The observations were consistent with the measurements from regulatory stations in the area. The data from the low-cost sensor network was used to construct spatial and temporal maps of concentration levels using a simple kriging interpolation method which calculates the weighted averaged concentration based on the distance from each observation. However, this method is not reliable for the locations far from observations and lacks the resolution needed for air quality management policies. To increase the resolution of concentration maps, dispersion models were used in the following steps.

First, the location of potential sources in the area was estimated based on the geographical features of the valley. Then, the emission rates for each one of these sources were calculated by regressing a dispersion model estimates and measured values. A concentration map was created using these emission rates and the model. The residuals between the observation and predictions were kriged and added to the concentration maps to produce high-resolution concentration fields. A leave-one-out cross-validation technique showed that this residual kriging method will improve the performance of the simple kriging and creates more accurate concentration maps.

Our interpretation of the data also indicated that concentrations within the Imperial Valley are dominated by the emissions originated from the valley, which has an average emission rate of 11 to 13 tons per day. This is consistent with the earlier estimates from CARB of 11.7 tons per day. The rest of the emissions originated from the Salton Sea, Mexico, and West Desert. The desert on the east of the Valley has the lowest contribution to the concentrations mainly because westerly winds were dominant.

References

Ahangar, F.E., Heist, D., Perry, S., Venkatram, A., 2017. Reduction of air pollution levels downwind of a road with an upwind noise barrier. Atmos. Environ. doi:10.1016/j.atmosenv.2017.02.001

Alley, E.R., Stevens, L.B., Cleland, W.L., 1998. Air quality control handbook. McGraw-Hill.

Amini, S., 2018. The Development and Application of Models for Dispersion of Roadway Emissions: The Effects of Roadway Configurations on Near Road Concentrations of Vehicle Emissions and Increasing the Spatial Resolution of Satellite-Derived PM2. 5 Maps.

Amini, S., Ahangar, F.E., Heist, D.K., Perry, S.G., Venkatram, A., 2018. Modeling dispersion of emissions from depressed roadways. Atmos. Environ. 186. doi:10.1016/j.atmosenv.2018.04.058

Amini, S., Ahangar, F.E., Schulte, N., Venkatram, A., 2016. Using models to interpret the impact of roadside barriers on near-road air quality. Atmos. Environ. 138, 55–64. doi:10.1016/j.atmosenv.2016.05.001

Anderson, J.O., Thundiyil, J.G., Stolbach, A., 2012. Clearing the Air: A Review of the Effects of Particulate Matter Air Pollution on Human Health. J. Med. Toxicol. doi:10.1007/s13181-011-0203-1

Baldauf, R., Thoma, E., Hays, M., Shores, R., Kinsey, J., Gullett, B., Kimbrough, S., Isakov, V., Long, T., Snow, R., Khlystov, A., Weinstein, J., Chen, F.-L., Seila, R., Olson, D., Gilmour, I., Cho, S.-H., Watkins, N., Rowley, P., Bang, J., 2008. Traffic and meteorological impacts on near-road air quality: summary of methods and trends from the Raleigh Near-Road Study. J. Air Waste Manag. Assoc. 58, 865–878.

Baldauf, R., Thoma, E., Khlystov, A., Isakov, V., Bowker, G., Long, T., Snow, R., 2008. Impacts of noise barriers on near-road air quality. Atmos. Environ. 42, 7502–7507.

Baldauf, R.W., Isakov, V., Deshmukh, P., Venkatram, A., Yang, B., Zhang, K.M., 2016. Influence of solid noise barriers on near-road and on-road air quality. Atmos. Environ. 129, 265–276.

Becker, S., Lienhart, H., Durst, F., 2002. Flow around three-dimensional obstacles in boundary layers. J. Wind Eng. Ind. Aerodyn. 90, 265–279.

Beelen, R., Hoek, G., van Den Brandt, P.A., Goldbohm, R.A., Fischer, P., Schouten, L.J., Jerrett, M., Hughes, E., Armstrong, B., Brunekreef, B., 2007. Long-term effects of traffic-related air pollution on mortality in a Dutch cohort (NLCS-AIR study). Environ. Health Perspect. 116, 196–202.

Benson, P.E., 1992. A review of the development and application of the CALINE3 and 4 models. Atmos. Environ. Part B, Urban Atmos. doi:10.1016/0957-1272(92)90013-I

Berkowicz, R., 2000. OSPM - A Parameterised Street Pollution Model. Environ. Monit. Assess. 65, 323–331. doi:10.1023/A:1006448321977

Bowker, G.E., Baldauf, R., Isakov, V., Khlystov, A., Petersen, W., 2007. The effects of roadside structures on the transport and dispersion of ultrafine particles from highways. Atmos. Environ. 41, 8128–8139.

Brauer, M., Hoek, G., Van Vliet, P., Meliefste, K., Fischer, P.H., Wijga, A., Koopman, L.P., Neijens, H.J., Gerritsen, J., Kerkhof, M., Heinrich, J., Bellander, T., Brunekreef, B., 2002. Air pollution from traffic and the development of respiratory infections and asthmatic and allergic symptoms in children. Am. J. Respir. Crit. Care Med. 166, 1092–1098.

Brook, R.D., Newby, D.E., Rajagopalan, S., 2017. The global threat of outdoor ambient air pollution to cardiovascular health: time for intervention. JAMA Cardiol. 2, 353–354.

CARB, 2018a. Community Air Protection Program Framework CONCEPT PAPER.

CARB, 2018b. Clean Air Act Section 179B Technical Demonstration Imperial County PM2.5 Nonattainment Area.

Carvlin, G.N., Lugo, H., Olmedo, L., Bejarano, E., Wilkie, A., Meltzer, D., Wong, M., King, G., Northcross, A., Jerrett, M., 2017. Development and field validation of a community-engaged particulate matter air quality monitoring network in Imperial, California, USA. J. Air Waste Manage. Assoc. 67, 1342–1352.

Castell, N., Dauge, F.R., Schneider, P., Vogt, M., Lerner, U., Fishbain, B., Broday, D., Bartonova, A., 2017. Can commercial low-cost sensor platforms contribute to air

quality monitoring and exposure estimates? Environ. Int. 99, 293–302. doi:https://doi.org/10.1016/j.envint.2016.12.007

Chang, J.C., Hanna, S.R., 2004. Air quality model performance evaluation. Meteorol. Atmos. Phys. 87, 167–196.

Chen, H., Bai, S., Eisinger, D., Niemeier, D., Claggett, M., 2009. Predicting near-road PM2. 5 concentrations: comparative assessment of CALINE4, CAL3QHC, and AERMOD. Transp. Res. Rec. J. Transp. Res. Board 26–37.

Cimorelli, A.J., Perry, S.G., Venkatram, A., Weil, J.C., Paine, R.J., Wilson, R.B., Lee, R.F., Peters, W.D., Brode, R.W., 2005. AERMOD: A Dispersion Model for Industrial Source Applications. Part I: General Model Formulation and Boundary Layer Characterization. J. Appl. Meteorol. 44, 682–693. doi:10.1175/JAM2227.1

Dockery, D.W., Pope, C.A., Xu, X., Spengler, J.D., Ware, J.H., Fay, M.E., Ferris Jr, B.G., Speizer, F.E., 1993. An association between air pollution and mortality in six US cities. N. Engl. J. Med. 329, 1753–1759.

Enayati Ahangar, F., Amini, S., Venkatram, A., 2017. Using Vegetation to Enhance the Impact of Solid Barriers on Near-road Air Pollution, in: A&WMA's 110th Annual Conference & Exhibition. A&WMA's 110th Annual Conference & Exhibition, Pittsburgh.

English, P.B., Olmedo, L., Bejarano, E., Lugo, H., Murillo, E., Seto, E., Wong, M., King, G., Wilkie, A., Meltzer, D., 2017. The Imperial County Community Air Monitoring

Network: a model for community-based environmental monitoring for public health action. Environ. Health Perspect. 125.

Finn, D., Clawson, K.L., Carter, R.G., Rich, J.D., Eckman, R.M., Perry, S.G., Isakov, V., Heist, D.K., 2010. Tracer studies to characterize the effects of roadside noise barriers on near-road pollutant dispersion under varying atmospheric stability conditions. Atmos. Environ. 44, 204–214.

Gallagher, J., Baldauf, R., Fuller, C.H., Kumar, P., Gill, L.W., McNabola, A., 2015. Passive methods for improving air quality in the built environment: A review of porous and solid barriers. Atmos. Environ.

Gehring, U., Wijga, A.H., Brauer, M., Fischer, P., de Jongste, J.C., Kerkhof, M., Oldenwening, M., Smit, H.A., Brunekreef, B., 2010. Traffic-related air pollution and the development of asthma and allergies during the first 8 years of life. Am J Respir Crit Care Med 181, 596–603. doi:10.1164/rccm.200906-0858OC

Ghasemian, M., Amini, S., Princevac, M., 2017. The influence of roadside solid and vegetation barriers on near-road air quality. Atmos. Environ. 170, 108–117.

Gidhagen, L., Johansson, C., Langner, J., Foltescu, V.L., 2005. Urban scale modeling of particle number concentration in Stockholm. Atmos. Environ. 39, 1711–1725. doi:10.1016/j.atmosenv.2004.11.042

Gilbert, R.O., Simpson, J.C., 1985. Kriging for estimating spatial pattern of contaminants: Potential and problems. Environ. Monit. Assess. 5, 113–135.

doi:10.1007/BF00395842

Hagler, G.S.W., Lin, M.Y., Khlystov, A., Baldauf, R.W., Isakov, V., Faircloth, J., Jackson, L.E., 2012. Field investigation of roadside vegetative and structural barrier impact on near-road ultrafine particle concentrations under a variety of wind conditions. Sci. Total Environ. 419, 7–15.

Hagler, G.S.W., Solomon, P.A., Hunt, S.W., 2014. New technology for low-cost, real-time air monitoring. EM Air Waste Manag. Assoc. Mag. Environ. Manag. Air Waste Manag. Assoc. Pittsburgh, PA, USA.

Hagler, G.S.W., Tang, W., Freeman, M.J., Heist, D.K., Perry, S.G., Vette, A.F., 2011. Model evaluation of roadside barrier impact on near-road air pollution. Atmos. Environ. 45, 2522–2530. doi:10.1016/j.atmosenv.2011.02.030

HEI, 2010. Traffic-Related Air Pollution: A Critical Review of the Literature on Emissions, Exposure, and Health Effects.

Heist, D., Isakov, V., Perry, S., Snyder, M., Venkatram, A., Hood, C., Stocker, J., Carruthers, D., Arunachalam, S., Owen, R.C., 2013. Estimating near-road pollutant dispersion: A model inter-comparison. Transp. Res. Part D Transp. Environ. 25, 93–105.

Heist, D.K., Perry, S.G., Brixey, L.A., 2009. A wind tunnel study of the effect of roadway configurations on the dispersion of traffic-related pollution. Atmos. Environ. 43, 5101–5111.

Hitchins, J., Morawska, L., Wolff, R., Gilbert, D., 2000. Concentrations of submicrometre particles from vehicle emissions near a major road. Atmos. Environ. 34, 51–59. doi:10.1016/S1352-2310(99)00304-0

Hoek, G., Beelen, R., De Hoogh, K., Vienneau, D., Gulliver, J., Fischer, P., Briggs, D., 2008. A review of land-use regression models to assess spatial variation of outdoor air pollution. Atmos. Environ. 42, 7561–7578.

Hoek, G., Brunekreef, B., Goldbohm, S., Fischer, P., van den Brandt, P.A., 2002. Association between mortality and indicators of traffic-related air pollution in the Netherlands: a cohort study. Lancet 360, 1203–1209. doi:10.1016/S0140-6736(02)11280-3

Hoogh, K. De, Korek, M., Vienneau, D., Keuken, M., Kukkonen, J., Nieuwenhuijsen, M.J., Badaloni, C., Beelen, R., Bolignano, A., Cesaroni, G., Cirach, M., Cyrys, J., Douros, J., Eeftens, M., Forastiere, F., Forsberg, B., Fuks, K., Gehring, U., Gryparis, A., Gulliver, J., Hansell, A.L., Hoffmann, B., Johansson, C., Jonkers, S., Kangas, L., Katsouyanni, K., Künzli, N., Lanki, T., Memmesheimer, M., Moussiopoulos, N., Modig, L., Pershagen, G., Probst-hensch, N., Schindler, C., Schikowski, T., Sugiri, D., Teixidó, O., Tsai, M., Yli-tuomi, T., Brunekreef, B., Hoek, G., Bellander, T., 2014. Comparing land use regression and dispersion modelling to assess residential exposure to ambient air pollution for epidemiological studies. Environ. Int. 73, 382–392. doi:10.1016/j.envint.2014.08.011

Hooghwerff, J., Tollenaar, C.C., van der Heijden, W.J., 2010. In-situ air quality measurements on existing and innovative noise barriers, in: Brebbia, C.A., Longhurst, J.W.S. (Eds.), Air Pollution XVIII. WIT Press, Kos, Greece, pp. 129–139. doi:10.2495/AIR100121

Houston, D., Krudysz, M., Winer, A., 2008. Diesel truck traffic in low-income and minority communities adjacent to ports: environmental justice implications of near-roadway land use conflicts. Transp. Res. Rec. 2067, 38–46.

Huan, L., Kebin, H., 2012. Traffic optimization: a new way for air pollution control in China's urban areas.

Irwin, H.P.A.H., 1981. The design of spires for wind simulation. J. Wind Eng. Ind. Aerodyn. 7, 361–366. doi:10.1016/0167-6105(81)90058-1

James Gauderman, W., McConnell, R.O.B., Gilliland, F., London, S., Thomas, D., Avol, E., Vora, H., Berhane, K., Rappaport, E.B., Lurmann, F., 2000. Association between air pollution and lung function growth in southern California children. Am. J. Respir. Crit. Care Med. 162, 1383–1390.

Jiao, W., Hagler, G., Williams, R., Sharpe, R., Brown, R., Garver, D., Judge, R., Caudill, M., Rickard, J., Davis, M., 2016. Community Air Sensor Network (CAIRSENSE) project: evaluation of low-cost sensor performance in a suburban environment in the southeastern United States. Atmos. Meas. Tech. 9, 5281–5292.

Khreis, H., Kelly, C., Tate, J., Parslow, R., Lucas, K., Nieuwenhuijsen, M., 2017.

Exposure to traffic-related air pollution and risk of development of childhood asthma: a systematic review and meta-analysis. Environ. Int. 100, 1–31.

Kim, J.J., Smorodinsky, S., Ostro, B., Lipsett, M., Singer, B.C., Hogdson, A.T., 2002. Traffic-related Air Pollution and Respiratory Health: the East Bay Children's Respiratory Health Study. Epidemiology 13, S100.

Kittelson, D.B., Watts, W.F., Johnson, J.P., Remerowki, M.L., Ische, E.E., Oberdorster, G., Gelein, R.A., Elder, A., Hopke, P.K., Kim, E., Zhao, W., Zhou, L., Jeong, C.H., 2004. On-road exposure to highway aerosols. 1. Aerosol and gas measurements. Inhal. Toxicol. 16, 31–39.

Kumar, P., Ketzel, M., Vardoulakis, S., Pirjola, L., Britter, R., 2011. Dynamics and dispersion modelling of nanoparticles from road traffic in the urban atmospheric environment-A review. J. Aerosol Sci. 42, 580–603.

Kumar, P., Morawska, L., Martani, C., Biskos, G., Neophytou, M., Di Sabatino, S., Bell, M., Norford, L., Britter, R., 2015. The rise of low-cost sensing for managing air pollution in cities. Environ. Int. 75, 199–205. doi:https://doi.org/10.1016/j.envint.2014.11.019

Lee, E.S., Ranasinghe, D.R., Ahangar, F.E., Amini, S., Mara, S., Choi, W., Paulson, S., Zhu, Y., 2018. Field evaluation of vegetation and noise barriers for mitigation of near-freeway air pollution under variable wind conditions. Atmos. Environ. 175. doi:10.1016/j.atmosenv.2017.11.060

Levy, J.I., Wolff, S.K., Evans, J.S., Hoek, G., Beelen, R., De Hoogh, K., Vienneau, D., Gulliver, J., Fischer, P., Briggs, D., 2002. A review of land-use regression models to assess spatial variation of outdoor air pollution. Risk Anal. An Int. J. 42, 895–904.

Li, T.-T., Bai, Y.-H., Liu, Z.-R., Liu, J.-F., Zhang, G.-S., Li, J.-L., 2006. Air quality in passenger cars of the ground railway transit system in Beijing, China. Sci. Total Environ. 367, 89–95.

Matheron, G., 1971. The Theory of Regionalized Variables and Its Application, Cahiers du Centre de morphologie mathematique. Centre de morphologie mathematique, Eisle National Superieure des Mines de Paris.

McNaughton, K.G., 1988. 1. Effects of windbreaks on turbulent transport and microclimate. Agric. Ecosyst. Environ. 22–23, 17–39. doi:10.1016/0167-8809(88)90006-0

Mead, M.I., Popoola, O.A.M., Stewart, G.B., Landshoff, P., Calleja, M., Hayes, M., Baldovi, J.J., McLeod, M.W., Hodgson, T.F., Dicks, J., Lewis, A., Cohen, J., Baron, R., Saffell, J.R., Jones, R.L., 2013. The use of electrochemical sensors for monitoring urban air quality in low-cost, high-density networks. Atmos. Environ. 70, 186–203. doi:https://doi.org/10.1016/j.atmosenv.2012.11.060

Mitchell, G., Dorling, D., 2003. An environmental justice analysis of British air quality. Environ. Plan. A 35, 909–929.

Monzón de Cáceres, A., 1994. Traffic control systems to alleviate congestion and air

pollution. Sci. Total Environ. 146–147, 45–50. doi:https://doi.org/10.1016/0048-9697(94)90218-6

Morawska, L., Ristovski, Z., Jayaratne, E.R., Keogh, D.U., Ling, X., 2008. Ambient nano and ultrafine particles from motor vehicle emissions: Characteristics, ambient processing and implications on human exposure. Atmos. Environ.

Ning, Z., Hudda, N., Daher, N., Kam, W., Herner, J., Kozawa, K., Mara, S., Sioutas, C., 2010. Impact of roadside noise barriers on particle size distributions and pollutants concentrations near freeways. Atmos. Environ. 44, 3118–3127. doi:10.1016/j.atmosenv.2010.05.033

Oberdörster, G., 2000. Pulmonary effects of inhaled ultrafine particles. Int. Arch. Occup. Environ. Health 74, 1–8.

Paulson, S.E., Zhu, Y., Venkatram, A., Lee, E.S., Ranasinghe, D.R., Enayati Ahangar, F., Amini, S., Frausto-Vicencio, I., Choi, W., Sum, W., 2017. Effectiveness of sound wall-vegetation combination barriers as near-roadway pollutant mitigation strategies.

Perry, S.G., 1992. CTDMPLUS: A dispersion model for sources near complex topography. Part I: Technical formulations. J. Appl. Meteorol. 31, 633–645.

Petroff, A., Mailliat, A., Amielh, M., Anselmet, F., 2008a. Aerosol dry deposition on vegetative canopies. Part I: Review of present knowledge. Atmos. Environ. 42, 3625–3653. doi:10.1016/j.atmosenv.2007.09.043

Petroff, A., Mailliat, A., Amielh, M., Anselmet, F., 2008b. Aerosol dry deposition on vegetative canopies. Part II: A new modelling approach and applications. Atmos. Environ. 42, 3654–3683.

Pope III, C.A., 2002. Lung Cancer, Cardiopulmonary Mortality, and Long-term Exposure to Fine Particulate Air Pollution. JAMA J. Am. Med. Assoc. doi:10.1001/jama.287.9.1132

Pope III, C.A., Dockery, D.W., 2006. Health effects of fine particulate air pollution: lines that connect. J. Air Waste Manage. Assoc. 56, 709–742.

Pournazeri, S., Princevac, M., 2015. Sound wall barriers: Near roadway dispersion under neutrally stratified boundary layer. Transp. Res. Part D Transp. Environ. doi:10.1016/j.trd.2015.09.025

Pournazeri, S., Tan, S., Schulte, N., Jing, Q., Venkatram, A., 2014. A computationally efficient model for estimating background concentrations of NOx, NO2, and O3. Environ. Model. Softw. 52. doi:10.1016/j.envsoft.2013.10.018

Quintero-NUfiez, M., Sweedler, A., 2004. Air quality evaluation in the Mexicali and Imperial Valleys as an element for an Outreach Program. Imp. Val. Dev. Environ. US-Mexican Bord. Reg. 263.

Ryan, P.H., LeMasters, G.K., 2007. A review of land-use regression models for characterizing intraurban air pollution exposure. Inhal. Toxicol. 19, 127–133.

Samet, J.M., Dominici, F., Curriero, F.C., Coursac, I., Zeger, S.L., 2000. Fine particulate air pollution and mortality in 20 US cities, 1987–1994. N. Engl. J. Med. 343, 1742–1749.

SCAQMD, 2018. Community Recommendations for AB 617 Implementation.

Schneider, P., Castell, N., Vogt, M., Dauge, F.R., Lahoz, W.A., Bartonova, A., 2017. Mapping urban air quality in near real-time using observations from low-cost sensors and model information. Environ. Int. 106, 234–247.

Schulman, L.L., Strimaitis, D.G., Scire, J.S., 2000. Development and evaluation of the PRIME plume rise and building downwash model. J. Air Waste Manage. Assoc. 50, 378–390.

Schulte, N., 2015. The Impact of Roadside Barriers and Buildings on Near Road Concentrations of Vehicle Emissions. University of California, Riverside.

Schulte, N., Amini, S., Ahangar, F.E., Venkatram, A., 2017. The impact of road structures and buildings on urban air quality, in: HARMO 2017 - 18th International Conference on Harmonisation within Atmospheric Dispersion Modelling for Regulatory Purposes, Proceedings.

Schulte, N., Snyder, M., Isakov, V., Heist, D., Venkatram, A., 2014. Effects of solid barriers on dispersion of roadway emissions. Atmos. Environ. 97. doi:10.1016/j.atmosenv.2014.08.026

Schulte, N., Tan, S., Venkatram, A., 2015. The ratio of effective building height to street width governs dispersion of local vehicle emissions. Atmos. Environ. 112, 54–63. doi:10.1016/j.atmosenv.2015.03.061

Setälä, H., Viippola, V., Rantalainen, A.-L., Pennanen, A., Yli-Pelkonen, V., 2013. Does urban vegetation mitigate air pollution in northern conditions? Environ. Pollut. 183, 104–12. doi:10.1016/j.envpol.2012.11.010

Snyder, E.G., Watkins, T.H., Solomon, P.A., Thoma, E.D., Williams, R.W., Hagler, G.S.W., Shelow, D., Hindin, D.A., Kilaru, V.J., Preuss, P.W., 2013. The changing paradigm of air pollution monitoring.

Snyder, M.G., Venkatram, A., Heist, D.K., Perry, S.G., Petersen, W.B., Isakov, V., 2013. RLINE: A line source dispersion model for near-surface releases. Atmos. Environ. 77, 748–756. doi:10.1016/j.atmosenv.2013.05.074

Snyder, W.H., 1979. The EPA meteorological wind tunnel: its design, construction and operating characteristics. US Environmental Protection Agency, Office of Research and Development, Environmental Sciences Research Laboratory.

Steffens, J.T., Heist, D.K., Perry, S.G., Isakov, V., Baldauf, R.W., Zhang, K.M., 2014. Effects of roadway configurations on near-road air quality and the implications on roadway designs. Atmos. Environ. 94, 74–85. doi:10.1016/j.atmosenv.2014.05.015

Steffens, J.T., Wang, Y.J., Zhang, K.M., 2012. Exploration of effects of a vegetation barrier on particle size distributions in a near-road environment. Atmos. Environ. 50,

120–128.

Tong, Z., Baldauf, R.W., Isakov, V., Deshmukh, P., Max Zhang, K., 2016. Roadside vegetation barrier designs to mitigate near-road air pollution impacts. Sci. Total Environ. 541, 920–7. doi:10.1016/j.scitotenv.2015.09.067

Tong, Z., Whitlow, T.H., MacRae, P.F., Landers, A.J., Harada, Y., 2015. Quantifying the effect of vegetation on near-road air quality using brief campaigns. Environ. Pollut. 201, 141–149. doi:10.1016/j.envpol.2015.02.026

US EPA, 2004. User's guide for the AMS/EPA regulatory model—AERMOD.

Venkatram, a, 1988. on the Use of Kriging in the Spatial-Analysis of Acid Precipitation Data. Atmos. Environ. 22, 1963–1975. doi:10.1016/0004-6981(88)90086-8

Venkatram, A., 2013. Dispersion Modeling. Handb. Environ. Fluid Dyn. 2, 333–344. doi:10.1002/9781118723098

Venkatram, A., 2008. Computing and displaying model performance statistics. Atmos. Environ. 42, 6862–6868.

Venkatram, A., 1988. On the use of kriging in the spatial analysis of acid precipitation data. Atmos. Environ. 22, 1963–1975.

Venkatram, A., Horst, T.W., 2006. Approximating dispersion from a finite line source. Atmos. Environ. 40, 2401–2408.

Venkatram, A., Schulte, N., 2018. Urban Transportation and Air Pollution. Elsevier

Science.

Venkatram, A., Snyder, M.G., Heist, D.K., Perry, S.G., Petersen, W.B., Isakov, V., 2013. Re-formulation of plume spread for near-surface dispersion. Atmos. Environ. 77, 846–855.

Venkatram, A., Snyder, M.G., Heist, D.K., Perry, S.G., Petersen, W.B., Isakov, V., 2013. Re-formulation of plume spread for near-surface dispersion. Atmos. Environ. 77. doi:10.1016/j.atmosenv.2013.05.073

Vong, R.J., Vong, I.J., Vickers, D., Covert, D.S., 2010. Size-dependent aerosol deposition velocities during BEARPEX'07. Atmos. Chem. Phys. 10, 5749–5758. doi:10.5194/acp-10-5749-2010

Vos, P.E.J., Maiheu, B., Vankerkom, J., Janssen, S., 2013. Improving local air quality in cities: To tree or not to tree? Environ. Pollut. 183, 113–122. doi:10.1016/j.envpol.2012.10.021

Wang, H., Takle, E.S., 1995. A numerical simulation of boundary-layer flows near shelterbelts. Boundary-Layer Meteorol. 75, 141–173. doi:10.1007/BF00721047

Wang, Y., Li, J., Jing, H., Zhang, Q., Jiang, J., Biswas, P., 2015. Laboratory evaluation and calibration of three low-cost particle sensors for particulate matter measurement. Aerosol Sci. Technol. 49, 1063–1077.

White, R.M., Paprotny, I., Doering, F., Cascio, W.E., Solomon, P.A., Gundel, L.A., 2012.

Sensors and'apps' for community-based: Atmospheric monitoring. EM Air Waste Manag. Assoc. Mag. Environ. Manag. 36–40.

World Health Organization, 2006. Health risks of particulate matter from long-range transboundary air pollution. Pollut. Atmos. 169. doi:10.3787/j.issn.1000-0976.2017.07.006

Yi, W.Y., Lo, K.M., Mak, T., Leung, K.S., Leung, Y., Meng, M.L., 2015. A survey of wireless sensor network based air pollution monitoring systems. Sensors 15, 31392–31427.

Zhang, K.M., Wexler, A.S., 2004. Evolution of particle number distribution near roadways—Part I: analysis of aerosol dynamics and its implications for engine emission measurement. Atmos. Environ. 38, 6643–6653. doi:10.1016/j.atmosenv.2004.06.043

Zhang, K.M., Wexler, A.S., Zhu, Y.F., Hinds, W.C., Sioutas, C., 2004. Evolution of particle number distribution near roadways. Part II: The "Road-to-Ambient" process. Atmos. Environ. 38, 6655–6665.